TECHNISCHE UNIVERSITÄT MÜNCHEN

Lehrstuhl für Entwicklungsgenetik

The role of ERK/MAPK signalling in emotional behaviour – studies on *Braf* knockout and gain-of-function mutant mice

Benedikt Wefers

Content

1 Zusammenfassung

Der ERK/MAPK-Signalweg (extracellular signal-regulated kinase/mitogen-activated protein kinase pathway) ist ein konservierter Signaltransduktionsweg, welcher in einer Vielzahl von Zelltypen extrazelluläre Signale überträgt. Seine Aktivierung wurde mit verschiedenen zellulären Prozessen wie Zellproliferation, Zelldifferenzierung, Neuronenentwicklung und der Fähigkeit des Lernens und des Gedächtnisses in Verbindung gebracht. Zudem wurde der ERK/MAPK-Signalweg in den letzten Jahren mit Emotionsverhalten und der Entstehung von Affektstörungen assoziiert.

Um die Funktion des ERK/MAPK-Signalwegs für das Emotionsverhalten zu bestimmen, habe ich nichtinduzierbare und induzierbare konditionale *Braf*-Knockout-Mäuse untersucht, deren ERK/MAPK-Signalübertragung in den Neuronen des Vorderhirns unterbrochen ist. Die Verhaltensanalysen dieser *Braf*-Mutanten zeigten, dass die ERK/MAPK-Signalübertragung eine entscheidende Rolle für das Angst- und Depressionsverhalten spielt. Außerdem konnte ich durch den Vergleich von Mutanten, bei denen das *Braf*-Gen entweder während der juvenilen oder der adulten Lebensphase induzierbar inaktiviert wurde, unterschiedliche Einflüsse des ERK/MAPK-Signals auf das Emotionsverhalten in den beiden Zeiträumen beschreiben.

Der Verlust der ERK/MAPK-Signalübertragung während der juvenilen Phase führt in adulten Mutanten zu stark verringertem Angstverhalten, zu einer verminderten Komplexität hippocampaler Neuronen sowie zu Änderungen der mRNA-Expression von 150 Genen. In Mutanten, in denen das BRAF-Protein erst in der adulten Phase inaktiviert wird, wurde hingegen normales Angstverhalten, aber auch ein gesteigertes depressionsähnliches Verhalten beobachtet. Neben diesen Einflüssen auf das Emotionsverhalten haben meine Analysen außerdem eine regulatorische Funktion des ERK/MAPK-Signalwegs auf die circadianen Rhythmen aufgedeckt.

Um den Effekt einer Gain-of-Function-Mutation des ERK/MAPK-Signalwegs auf das Emotionsverhalten zu untersuchen, wurde eine vorderhirnspezifische $Braf^{V600E}$ Knock-In-Mauslinie verwendet. Da aber sowohl der juvenil als auch

der adult induzierte Knock-In zu schneller Letalität führte, konnten die geplanten Verhaltensuntersuchungen nicht durchgeführt werden.

Zusammengefasst tragen diese Ergebnisse über die Funktionen und die Mechanismen des ERK/MAPK-Signalwegs im Hinblick auf Angst und Depression zum Verständnis bei der Entstehung von Affektstörungen bei und können dadurch die Entwicklung von neuartigen therapeutischen Medikamenten ermöglichen.

2 Summary

The extracellular signal-regulated kinase/mitogen-activated protein kinase (ERK/MAPK) pathway is a conserved signalling pathway that mediates extracellular signals in many cell types. Its function has been linked to various cellular processes, like proliferation, differentiation, neuronal development, and learning and memory. In recent years, ERK/MAPK signalling has been also implicated into emotional behaviour and the development of mood disorders.

To unravel the roles of ERK/MAPK signalling in emotional behaviour, I analysed conditional, non-inducible, and inducible knockout mice for the *Braf* gene, to interfere with the ERK/MAPK signalling pathway in forebrain neurons. The behavioural analyses of these *Braf* mutants revealed that ERK/MAPK signalling plays a decisive role in anxiety and depression-like behaviour. Moreover, by comparison of mutants that lost ERK/MAPK activity during either the juvenile or the adult life phase, I was able to identify distinct influences of these two periods on emotions.

The juvenile depletion of ERK/MAPK signalling results in the disregulation of the expression of 150 genes. This in turn affects the dendritogenesis of the maturing hippocampal neurons, leading to a reduction of the complexity of the neuronal network. Consequently, due to the postnatal loss of the ERK/MAPK signal, a reduction in anxiety was found. In contrast, mutants with a late depletion of BRAF during adulthood showed normal anxiety levels, but increased depression-like behaviour. Besides its effects on emotions, my studies also revealed a regulatory function of the ERK/MAPK signalling on circadian activity.

For the analysis of the gain-of-function mutation of the ERK/MAPK pathway on emotional behaviour, a forebrain-specific Braf^{V600E} knockin mouse line was used. However, as both the postnatal and the adult knockin were lethal, further behavioural analyses were precluded.

Taken together, these results on the roles and mechanisms of ERK/MAPK signalling in anxiety and depression contribute to the understanding of the development of mood disorders and may further enable the design of new therapeutic drugs.

3 Introduction

3.1 The ERK/MAPK signalling pathway

The extracellular signal-regulated kinase/mitogen-activated protein kinase (ERK/MAPK) signalling pathway is an evolutionary conserved signal transduction pathway (for a review, see Rubinfeld and Seger, 2005). It mediates the transmission of extracellular signals from membrane-bound receptors to cytoplasmic and nuclear effectors. These receptors, mostly receptor tyrosine kinases (RTK) or G protein-coupled receptors (GPCR), are activated by their ligands (e.g. mitogens, growth factors, chemokines, and hormones), which trigger the recruitment of adaptor proteins, like growth factor receptor bound protein 2 (GRB2) (Fig. 1, left) and protein tyrosine phosphatase, non-receptor type 11 (PTPN11). The adaptors then activate a small GTPase of the RAS family, which in turn activates the ERK cascade.
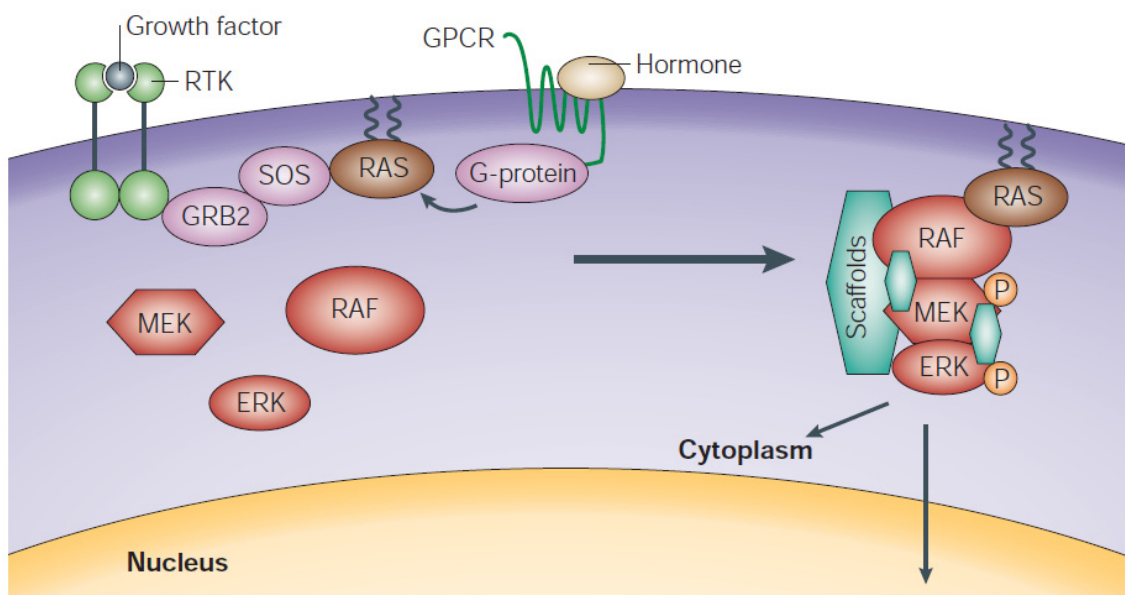
Fig. 1: Schematic representation of the ERK/MAPK signalling pathway
The pathway consists of a linear cascade of the kinases BRAF, MEK1/2, and ERK1/2. They are recruited by scaffold proteins and activated by the small GTPase RAS. Activated ERK either translocates into the nucleus to regulate gene expression or remains in the cytoplasm where it directly interacts with other signalling pathways. Adapted from Wellbrock et al. (2004).

The ERK cascade consists of three levels of subsequent serine/threonine protein kinases: a RAF (rat fibrosarcoma) kinase, two MEK (MAP kinase/ERK

kinase) kinases, and two ERK (extracellular signal-regulated kinase) kinases. Upon activation of RAS, the ERK cascade members are recruited by scaffold proteins and the RAF protein activates its downstream targets MEK1 and MEK2 by phosphorylation. Then, MEK1/2 in turn phosphorylate ERK1 and ERK2, which either finally translocate into the nucleus or directly phosphorylate other proteins in the cytoplasm (Fig. 1, right). In the nucleus, ERK1/2 activate mainly MSK1/2 (mitogen- and stress-activated protein kinase-1 and -2), which in turn activate the transcription factor CREB1 (cAMP-responsive element binding-protein 1) and ELK1 (ETS domain-containing protein Elk-1), a transcription factor of the ternary complex, which regulates the expression of serum response element (SRE)-containing genes.

3.1.1 The RAF family

In mammalian cells, three RAF isoforms are known: ARAF, BRAF, and CRAF (also called RAF-1), which differ in their regional distribution. ARAF is expressed ubiquitously in all organs except the brain (Morice et al., 1999; Storm et al., 1990) with the highest expression levels found in the urogenital organs. Similarly, CRAF is also ubiquitously expressed in all organs, but including the brain, and most abundantly in the cerebellum and the striated muscles (Storm et al., 1990). In contrast, BRAF is expressed at higher levels only in neuronal tissues and in testes, and at low levels in a wide range of other tissues. All three RAF proteins share a common architecture with two conserved regions at the N-terminus and a conserved kinase domain at the C-terminus. In Fig. 2, a schematic illustration of the BRAF protein is shown.

Fig. 2: Schematic representation of the protein structure of BRAF
Blue and black rectangles indicate alternating exons (white numbers). Lengths are true to scale. Orange rectangles indicate important functional domains. RBD: Ras-binding domain

In previous publications, it was shown that BRAF phosphorylates MEK1 and MEK2 more efficiently than either do ARAF or CRAF (Marais et al., 1997) and that BRAF stimulates the activation of ERK kinases in a more robust and faster

way than ARAF or CRAF (Pritchard et al., 1995). Due to these observations, Wellbrock et al. (2004) proposed that BRAF acts as the major MEK activator, whereas ARAF and CRAF fine-tune the levels and duration of ERK activity. Furthermore, in embryonic fibroblasts from Braf$^{-/-}$ mice, ERK activation was strongly diminished, whereas in Araf$^{-/-}$ and Craf$^{-/-}$ mice, ERK activation was not significantly altered (Wojnowski et al., 2000). For these reasons, and as the aim of this thesis was to investigate the different roles of the ERK/MAPK pathway, the *Braf* knockout was chosen to obtain a sustained inactivation of the ERK activity.

As already mentioned above, BRAF is expressed at high levels in all brain regions of adult mice. It is found in the soma, axons, and dendrites of all neurons and in some, but not all, glial cells with a rostro-caudal decreasing gradient of expression (Morice et al., 1999). The murine *Braf* gene is located on chromosome 6, consists of 22 exons (Fig. 2), and is subject to alternative splicing, and so gives rise to more than ten different proteins that show characteristic expression patterns (Barnier et al., 1995). The BRAF proteins vary in size from 69 to 99 kDa, but all isoforms share a common Ras-binding domain (RBD) and a kinase domain for the specific phosphorylation of their downstream targets MEK1/2 (Fig. 2).

3.1.2 General roles of ERK/MAPK signalling

The ERK/MAPK signalling pathway was initially implicated in cell growth by transmitting and controlling mitogenic signals. Meanwhile, it is known that the activation of the ERK cascade is also important for many other physiological processes in proliferating cells, like differentiation, development, stress response, learning and memory, and morphological determination.

Genetic studies in mice have shown that functional ERK/MAPK signalling is essential for embryonic development. Knockout mice of *Braf* or *Craf* die *in utero* between embryonic day (E) 10.5 and E12.5 or between E11.5 and E13.5, respectively (Mikula et al., 2001; Wojnowski et al., 1997). *Araf* knockouts survive to birth but die 7-21 days later due to neurological and intestinal abnormalities (Pritchard et al., 1996). In addition, targeted knockouts of *Erk2* (Hatano et al., 2003; Saba-El-Leil et al., 2003; Yao et al., 2003) and *Mek1* (Giroux et al., 1999) show embryonic lethality caused by an impaired placental development.

In human cancers, the role of the ERK/MAPK signalling in cell proliferation and apoptosis becomes apparent. In about 15 % of human cancers, members of the *Ras* family are mutated (see review Malumbres and Barbacid, 2003). In addition, in ~7 % of all human cancer samples and in ~70 % of malignant melanomas, *Braf* mutations were found (Davies et al., 2002). The most common *Braf* mutation, which is present in >90 % of cases, is the valine-to-glutamate substitution at position 600 (V600E) that leads to an overactive kinase function of BRAF.

Besides cancer, mutations in the members of the ERK/MAPK pathway were also found to cause other human diseases. The neuro-cardio-facial-cutaneous (NCFC) or RAS/MAPK syndromes are all caused by mutations of members of the *Ras*, *Raf,* or *Mek* family (Aoki et al., 2008; Bentires-Alj et al., 2006). Typical symptoms of these diseases are facial dysmorphisms, abnormalities of heart and skin, mental retardation, and a higher predisposition to cancer.

3.1.3 ERK/MAPK signalling in the central nervous system

In the cells of the central nervous system (CNS), the ERK/MAPK signalling pathway plays specialised roles in cellular processes like long-term potentiation, long-term depression, synaptogenesis, neuronal differentiation, and circadian rhythms.

In an *Erk1* knockout model, Mazzucchelli et al. (2002) demonstrated the role of the ERK/MAPK signalling in striatal-mediated learning and memory. Moreover, the forebrain-specific conditional knockout of *Braf* revealed its effects on hippocampal long-term potentiation and hippocampus-dependent learning (Chen et al., 2006a). An important cellular process that mediates long-term potentiation and depression is the re-organisation of synapses. By means of electrophysiological analyses, the ERK/MAPK pathway was implicated in the activity-dependent formation of dendritic filopodia (Wu et al., 2001).

In recent publications, the influence of ERK/MAPK signalling on neuronal differentiation was shown. Using conditional *Braf* knockouts specific for the dorsal root ganglion neurons, Zhong et al. (2007) observed impaired neuronal maturation and axonal growth. In an epiblast-restricted *Braf* knockout model, the essential role of ERK/MAPK signalling in CNS myelination and oligodendrocyte

differentiation was found (Galabova-Kovacs et al., 2008). Furthermore, the depletion of ERK2 specifically in neuronal progenitor cells led to a reduction in cortical neurogenesis and thereby to an impaired associative learning (Samuels et al., 2008).

In the circadian clock, the ERK/MAPK pathway is also known to be a key component of the circadian feedback loop, not only in the suprachiasmatic nucleus (SCN), but also in extra-SCN regions (for a review, see Coogan and Piggins, 2004). Dependent on the current light phase, levels of phosphorylated ERK1/2 (pERK1/2) continuously cycle and regulate the gene expression of other key components of the circadian clock, like *Per1*, *Per2*, and *Bmal1* (Akashi et al., 2008).

Besides the molecular mechanisms that are regulated or mediated by the ERK/MAPK signalling pathway, during the last decade emerging evidence suggests that this pathway is also involved in the establishment of anxiety and depression (for a review, see Coyle and Duman, 2003). Activation of ERK/MAPK signalling was found in human patients treated with different mood stabilizers like lithium (Einat et al., 2003; Kopnisky et al., 2003) or valproic acid (Einat et al., 2003; Hao et al., 2004). In addition, antidepressants like fluoxetine and imipramine affect the ERK/MAPK activity; however, the effects observed in previous studies are inconsistent (Fumagalli et al., 2005; Tiraboschi et al., 2004). Moreover, in post-mortem brains of patients suffering from depression, decreased levels of pERK1/2 were found (D'Sa and Duman, 2002). Finally, Engel et al. (2009) observed in *Erk1* knockout mice a behavioural excitement profile similar to that induced by psychostimulants. Nevertheless, up to now, little is known about the concrete role of ERK/MAPK signalling in emotional behaviour in respect to involved brain regions, crucial phases of life, activators, and downstream effects.

3.2 Anxiety and mood disorders

Mental disorders represent some of the most common health problems world-wide. The "German Health Interview and Examination Survey" from 1998 revealed that about one third of adult Germans between 18 and 65 years suffer from one or more mental disorders once in life. Among those, only 36 % receive a medical treatment (Wittchen and Jacobi, 2001). Moreover, pharmacological compounds available for the treatment of mood disorders are not effective in every patient and display various side effects.

Affective mental disorders are classified into mood disorders including bipolar disorders (characterised by abnormally high or pressured mood states) and depressive disorders (including major depression disorder), and into anxiety disorders (e.g. phobias, generalised anxiety disorder, and post-traumatic stress disorder). Environmental factors, like stress and emotional disturbances strongly influence these diseases; however, they are also based on a genetic predisposition (Hettema et al., 2001; Sklar, 2002). The genetic basis of mental disorders can be studied using appropriate genetic mouse models (for a review, see Cryan and Holmes, 2005). For the analysis of these mouse models, various behavioural paradigms have been developed. While the measurement of anxiety behaviour in mice is comparable to anxiety in humans, the study of mood disorders in rodents is more difficult. Due to the complex phenotype and the heterogeneity of this disease, the analysis of the entire phenotypic spectrum in one behavioural paradigm is not possible. Thus, the analysis of single behavioural and physiological aspects – the so-called endophenotypes – is necessary (Hasler et al., 2004).

Anxiety is a natural mood condition, which differs from fear by the fact that it can also occur without a triggering stimulus. It becomes pathological if this state permanently remains even without any cause of danger. The Diagnostic and Statistical Manual of Mental Disorders, 4th Edition (DSM-IV, American Psychiatric Association, 1994), distinguishes between specific phobias, generalized anxiety disorder, social anxiety disorder, panic disorder, agoraphobia, obsessive-compulsive disorder, and post-traumatic stress disorder, which all vary

in their underlying stimulus. Hence, discrimination of the different forms of anxiety in mice is readily possible by the use of specific behaviour tests.

In contrast to anxiety disease, mood disorders are more heterogeneous, classified into depressive disorders, bipolar disorders, and substance-induced mood disorders. Coinciding endophenotypes of major depression and the depressive episode of bipolar disorder have been described, e.g. anhedonia, changes in appetite or weight, insomnia, loss of energy, feelings of worthlessness and guilt, and recurrent thoughts of death or suicidal ideation, plans, or attempts (American Psychiatric Association, 1994).

Mood and anxiety disorders exhibit a high comorbidity, i.e. patients diagnosed with one of the two diseases are likely to suffer also from the other disease during their lifetime, and medications often act on both diseases simultaneously (Jacobi et al., 2004; Williamson et al., 2005). About 14 % of the European population are affected with one or both disorders within their lifetime. The incidence to contract mental disorders is higher in women than in men, as well as the chance of comorbidity and to respond differently in some medications (Gorman, 2006). Hence, it is important to distinguish between genders in the analysis of mouse models for emotional behaviour.

3.3 The Braf^flox mouse line

3.3.1 General description and previous findings

For the conditional knockout of *Braf*, I used the Braf^flox mouse line that was generated in Alcino Silva's group (Chen et al., 2006a). In this mouse line, exon 14 of the *Braf* gene, which is the first exon encoding for the kinase domain of BRAF, is flanked by two Cre recombinase recognition sites (loxP sites, Fig. 3 a). This "floxed" allele encodes for the active, wild-type BRAF protein that can be inactivated by Cre-mediated recombination. Thereby, exon 14 is excised ("deleted" allele, Braf$^\Delta$), which leads to a frame shift in the coding sequence, resulting in a kinase-deficient, non-functional BRAF protein. For the detection of the different *Braf* alleles, a PCR genotyping assay was used (see materials and methods sections 6.6.6.1 and 7.1.2.2). In Fig. 3 b, exemplary PCR genotyping results from the three different *Braf* alleles are shown, detecting a 413-bp band from the Braf^flox, a 357-bp band from the wild-type *Braf*, and a 282-bp band from the Cre recombined Braf$^\Delta$ allele.
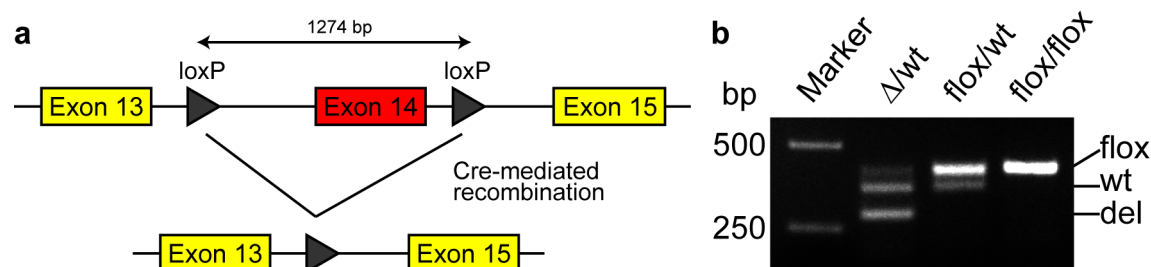
Fig. 3: Scheme of the modified Braf^flox allele
a) Exon 14 of the *Braf* gene is flanked by two Cre recombinase recognition sites (loxP sites). Upon Cre-mediated recombination, exon 14 is excised, leading to a shift in the open reading frame and thereby to a kinase deficient, non-functional BRAF protein. **b**) PCR genotyping bands of the different *Braf* alleles (wt: wild-type, 357 bp; flox: floxed, 413 bp; del: deleted, 282 bp)

The Braf^flox mouse line was imported to the Helmholtz Zentrum München by Dr. Christiane Hitz. She generated conditional *Braf* knockouts (Braf^cko) by crossing the Braf^flox line with a transgenic CaMKIIα-Cre line (Minichiello et al., 1999). The CaMKIIα promoter becomes active in all excitatory forebrain neurons shortly after birth. For a detailed characterisation of the expression pattern of the CaMKIIα promoter, see section 4.1.1.

In order to determine the efficiency of the inactivation of *Braf* in conditional mutants, a Western blot analysis of samples from different brain regions was performed by Dr. C. Hitz. As shown in Fig. 4, the BRAF protein was reduced in all forebrain regions of Braf[cko] mutants in comparison to control mice with floxed *Braf* alleles. In olfactory bulbs (OB), hippocampus (HC), striatum (St), and frontal (fCx) and posterior cortex (pCx) of *Braf* conditional knockout mutants, a strong reduction of BRAF was observed. In contrast, in the thalamus (Th), the midbrain (MB), and the cerebellum (CB) only little reduction and in the brainstem (BS) no reduction of BRAF was found.
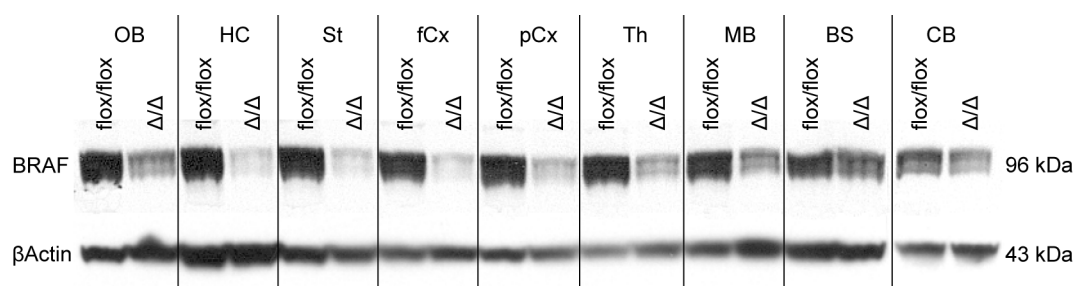
Fig. 4: Western blot analysis of Braf[cko] mice
BRAF protein was reduced in all forebrain regions of homozygous Braf[cko] mice (Δ/Δ) compared to floxed littermates (flox/flox). Strong reduction was observed in olfactory bulbs (OB), hippocampus (HC), striatum (St), and frontal (fCx) and posterior cortex (pCx) and weak reduction in thalamus (Th), midbrain (MB), and cerebellum (CB). No reduction was found in the brainstem (BS). βActin was used as loading control. Experiment was performed by Dr. C. Hitz (Hitz, 2007)

This Western blot analysis demonstrated the efficiency of the conditional *Braf* inactivation using a constitutive Cre transgene under control of the CaMKIIα promoter in adult mice.

3.3.2 *Braf* in emotional behaviour

In order to investigate the role of ERK/MAPK signalling in emotional behaviour in the forebrain of adult mice, Dr. C. Hitz analysed *Braf* conditional knockout mice in several behavioural paradigms. These results are compiled in her PhD thesis (Hitz, 2007), but for the sake of comprehensibility of the following studies, the major findings are briefly summarised below.

Braf conditional knockout mice were tested first in the modified hole board (7.7.2) for a broad assessment of a variety of locomotor, social, memory, and anxiety parameters. Mutants showed no differences in the overall distance trav-

elled and in the number of line crossings, suggesting a normal exploratory phenotype (Fig. 5 a and Table 8, Hitz, 2007). Interestingly, the latency until the mutant animals started their first action was significantly increased (Fig. 5 a). In the object recognition task of the modified hole board, control animals exhibited a normal recognition ability. Mutant animals in contrast were capable of recalling and distinguishing the objects, but displayed a strong neophobia against the unfamiliar object (Table 8).
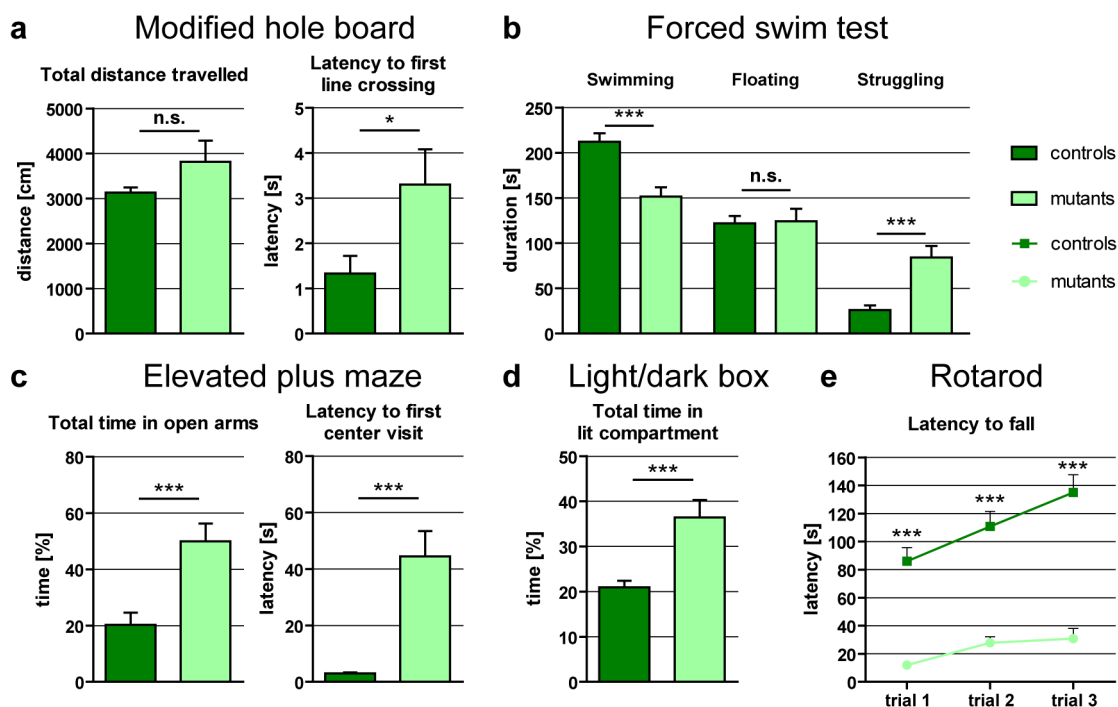
Fig. 5: Behavioural analysis of *Braf* conditional knockout mice
a) Modified hole board: Mutant mice showed no change in overall locomotion (left) and an increased latency to their first action (right). **b**) Forced swim test: Mutant mice showed an altered ratio of active behaviours (Swimming and Struggling) but no change in inactive behaviour (Floating), indicating no effect on depression-like behaviour. **c**) Elevated plus maze: Mutant mice spent significantly more time in the open arms, demonstrating an anxiolytic effect of the knockout (left). The latency to the first action was again highly increased (right). **d**) Light/dark box: Anxiolytic effect of the *Braf* knockout could be seen by increased time spent in the lit compartment. **e**) Accelerating rotarod: *Braf* mutants showed poor performance on the accelerating rotarod and an impaired learning ability between the trials. All experiments were performed by Dr. C. Hitz. (n.s.: not significant, *: $p < 0.05$, ***: $p < 0.001$)

In order to analyse depression-like behaviour, *Braf* conditional knockout mice were tested in the forced swim test (7.7.6). As shown in Fig. 5 b (Hitz, 2007), a change in the ratio of active behaviours was observed. Mutant animals showed significantly less swimming and an increase in struggling. Nevertheless, the to-

tal duration of these active behaviours as well as of inactive behaviour (floating) was not changed between mutants and controls, indicating no overall effect on depression-like behaviour.

In the elevated plus maze (7.7.4), a behavioural paradigm to measure anxiety levels, *Braf* conditional mutants spent approximately 50 % of the time in the open, more aversive arms, whereas controls only spent ~20 % of the time in these compartments (Fig. 5 c, Hitz, 2007). This demonstrated reduced anxiety in the mutants. Similar to the modified hole board, mutant mice showed a strongly increased latency for their first action in the maze (Fig. 5 c).

A second anxiety-related behaviour test, the light/dark box (7.7.5), confirmed the anxiolytic phenotype found in the elevated plus maze. Mutant mice spent significantly more time in the lit compartment of the box compared to controls (Fig. 5 d, Hitz, 2007).

A striking phenotype was observed in the accelerating rotarod (7.7.7). Compared to their floxed littermates, the mutants showed a very poor performance in all three trials of the test (Fig. 5 e, Hitz, 2007). While controls performed well in the test and even improved their ability during the trials, mutants failed already after few seconds and showed only little improvement.

In conclusion, the behavioural analysis performed by Dr. Christiane Hitz revealed reduced anxiety but normal depression-like behaviour in Braf^{cko} mice. Furthermore, the mutant mice showed an increase in the latency of their first action and an impaired motor coordination.

3.4 Objectives of this thesis

Dr. Christiane Hitz demonstrated in her PhD thesis that the inactivation of the ERK/MAPK signalling in the forebrain of mice affects anxiety behaviour (Hitz, 2007). However, the detailed interrelations between the ERK/MAPK signalling and emotional behaviour needed further characterisation. Hence, the objective of this work was to provide a more detailed study of the exact role of the ERK/MAPK signalling pathway in emotional behaviour of mice with respect to the underlying molecular mechanisms, the involved brain regions, and crucial phases of life. For this purpose, I generated and analysed three types of Braf mutants:

   i)   Constitutive, forebrain-specific Braf mutants (Braf^{cko} mice, section 4.1)

In the first step, the phenotype of the *Braf* conditional knockout mice, which were used by Dr. C. Hitz, was characterised further. For this purpose, the mutants were analysed in a broad neurological test battery to determine their general health status, locomotion, anxiety, physiology, and sensory cognition. In addition, a global gene expression analysis was performed to identify candidate genes that are connected to the altered emotional behavioural response of Braf^{cko} mice. Finally, the dendrite growth, spine formation, and the GABAergic signal transmission in the hippocampus of Braf^{cko} mice were determined.

   ii)   Inducible, forebrain-specific *Braf* mutants (Braf^{icko} mice, sections 4.2, 4.3)

To find correlations between emotional behaviour and distinct brain regions, I compared on the one hand the behavioural profiles of two *Braf* knockout mouse lines with similar, forebrain-specific knockout patterns. On the other hand, animals in which the BRAF depletion either was restricted to the dorsal or to the ventral hippocampus, were compared.

To determine the crucial phase of life in which ERK/MAPK signalling plays a role in emotional behaviour, I used an inducible *Braf* knockout mouse line for the characterisation of behavioural phenotypes. The induction of the *Braf* inactivation by tamoxifen was performed either soon after birth or later in adult mice to determine the impact of BRAF deficiency during postnatal brain development.

iii) Conditional *Braf* overactivated mice (Braf^{V600E} mice, section 4.4)

Finally, I used a mouse line with an inducible overactive BRAF kinase mutation (Braf^{V600E}) to determine the impact of overactivated ERK/MAPK signalling on emotional behaviour.

With these experiments, I aimed to gain new insights into the molecular mechanisms that are involved in the ERK/MAPK-dependent regulation of emotional behaviour that ultimately may contribute to develop new approaches for the treatment of anxiety and depression disorders.

4 Results

4.1 Effects of *Braf* knockout in forebrain neurons

4.1.1 Characterisation of the CaMKIIα-Cre mouse line

In order to study the role of the ERK/MAPK signalling pathway in mice, fore-brain-specific *Braf* knockout mice were generated. For this purpose, a trans-genic CaMKIIα-Cre mouse line was chosen that was created by Minichiello et al. (1999) (MGI ID: 2176753, "Tg(Camk2a-cre)159Kln"). This mouse line har-bours a transgenic expression cassette in which an 8.5 kb CaMKIIα promoter fragment is linked with the Cre recombinase coding region (including a nuclear localisation signal and a SV40 polyadenylation signal).

Given that the expression patterns of transgenes depend on a variety of fac-tors, like genetic background and generation number since establishment of the line, the reported spatial and temporal expression pattern of Cre in this mouse line needed to be reconfirmed. Therefore, I characterised the precise Cre activ-ity profile of the CaMKIIα-Cre mouse line that is maintained in the mouse facility of the Institute of Developmental Genetics at the Helmholtz Zentrum München.

For this purpose, CaMKIIα-Cre mice were bred with *Rosa26* Cre reporter mice (Soriano, 1999). This reporter mouse line contains a loxP-flanked stop-cassette followed by the β-galactosidase coding region, inserted into the *Rosa26* locus. Upon Cre-mediated recombination, the stop-cassette is excised leading to the transcription of the β-galactosidase gene.

Double transgenic R26R^{Cre} mice were used for lacZ staining as described (see section 7.6.5). As shown in Fig. 6 a and b, the CaMKIIα-Cre mouse line showed high Cre activity in all forebrain regions: in the olfactory bulb (oB), re-combination occurred in all layers except of the outermost glomerular layer. In the cortex (Cx), the hippocampus (Hc), and the striatum (St), Cre activity was observed in nearly all cells in every subregion with the highest activity in the granular cells of the hippocampus.
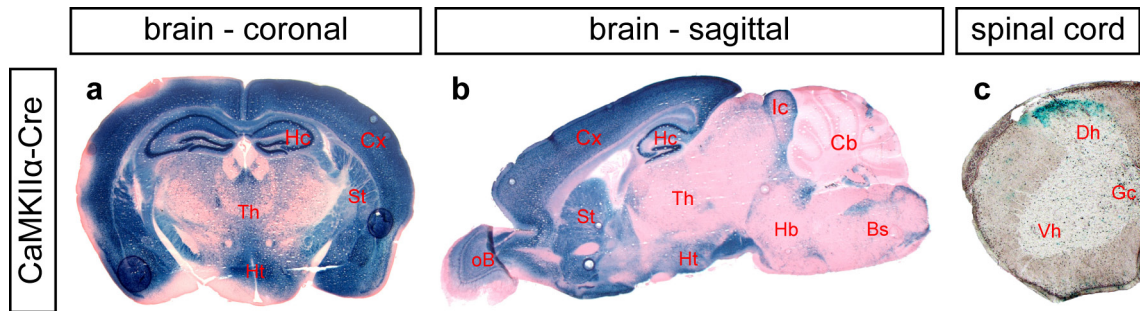
Fig. 6: Expression pattern of the CaMKIIα-Cre mouse line
CaMKIIα-Cre mice were bred with *Rosa26* Cre reporter mice, which show β-galactosidase activity after Cre recombination (blue staining). LacZ staining of coronal (**a**) and sagittal (**b**) sections of the brain and of the spinal cord (**c**) was used for the detection of β-galactosidase. High Cre activity was observed in the olfactory bulb (oB), cortex (Cx), hippocampus (Hc), and striatum (St). Medium activity was found in the hypothalamus (Ht), inferior colliculus (Ic), and the dorsal horn (Dh) and weak to no activity in the thalamus (Th), hindbrain (Hb), brainstem (Bs), cerebellum (Cb), ventral horn (Vh), and gray commissure (Gc).

Besides the strong activity in forebrain regions, the Cre recombinase was expressed also in other regions of the nervous system. Medium activity was observed in the hypothalamus (Ht) and the inferior colliculus (Ic), as well as in the layer I of the dorsal horn (Dh) of the spinal cord (Fig. 6 c). In all other investigated regions – the thalamus (Th), the hindbrain (Hb), the brainstem (Bs), the cerebellum (Cb), and the ventral horn (Vh) and the gray commissure (Gc) of the spinal cord – only weak to no staining was found.

4.1.2   Reduction of BRAF in forebrain neurons

As already shown in section 3.3, *Braf* conditional knockouts were obtained by breeding Braf^{flox} mice with CaMKIIα-Cre mice. In the first mating cycle, homozygous Braf$^{flox/flox}$ mice were bred with heterozygous CaMKIIα-Cre mice to obtain Braf$^{flox/wt;CaMKIIα-Cre}$ mice. In the subsequent mating cycle, these heterozygous mutants were bred with Braf$^{flox/flox}$ mice to obtain homozygous Braf$^{flox/flox;CaMKIIα-Cre}$ mutants (henceforth named as "Braf^{cko}").

As female Braf^{cko} mothers neglect their pubs – leading subsequently to early postnatal lethality – matings of female heterozygous mutants with male homozygous Braf$^{flox/flox}$ mice were used unless otherwise stated. For experiments, homozygous Braf^{cko} animals were used as mutants (also named "mutants" or "Δ/Δ") and homozygous Braf$^{flox/flox}$, which lack the Cre allele, were used as controls (also named "controls" or "flox/flox"). The genetic background of mutants

and controls used in all Braf^cko studies was calculated to a mean value of genetic contribution derived to 93.8 % from C57BL/6J, 6.1 % from FVB and 0.1 % from 129/Sv.

In order to check whether the expression of the Cre recombinase in Braf^cko mice leads to a recombination also *in vivo*, the rearrangement of the *Braf* allele was analysed on the genomic level. The presence of the floxed and the deleted allele was determined in two forebrain regions, the cortex and the hippocampus, as well as in the cerebellum as negative control. DNA samples from heterozygous mutants (n = 2) and floxed controls (n = 2) were analysed by Southern blotting using a specific probe that detects the recombined allele. To obtain the temporal pattern of the recombination, DNA samples were taken at 2, 3, 4, 5, 6, and 8 weeks after birth.

Quantitative analysis of the Southern blot of cortical samples demonstrated that recombination in mutants becomes apparent at the age of 2 weeks and continuously increases until the age of 8 weeks (Fig. 7 a). The highest level of recombination was measured at the age of 8 weeks (36.8 ± 3.8 %), which determines the beginning of adolescence in mice. In contrast, not any recombined *Braf* allele was detected in the controls at any point in time. In the hippocampus, which exhibited high Cre activity in the *Rosa26* reporter assay, recombination in mutants also becomes apparent at the age of 2 weeks and reaches its endpoint between weeks 6 to 8 (Fig. 7 b). In contrast to the cortex, recombination in the hippocampus was completed at the beginning of adolescence with a maximum level of deleted allele of 39.1 ± 3.1 %. In controls, the deleted allele was absent in all measured points in time. Finally, in the cerebellum, not any recombination was measured in the mutants as well as in the controls at all points in time (data not shown).

In order to validate the Southern blot results and to demonstrate the specificity of the Southern blot probe, the recombination was also determined by PCR in a qualitative manner. As already mentioned in section 3.3.1, the three different *Braf* alleles, the wild-type, the floxed, and the deleted allele, result in PCR products of different sizes. Consistent with the results from the Southern blot, the deleted allele could be detected in cortical and hippocampal samples of mu-

tants at all points in time (Fig. 7 c). In DNA samples from floxed controls and from cerebellar samples of mutants, no PCR product for the deleted allele was found at any point in time.
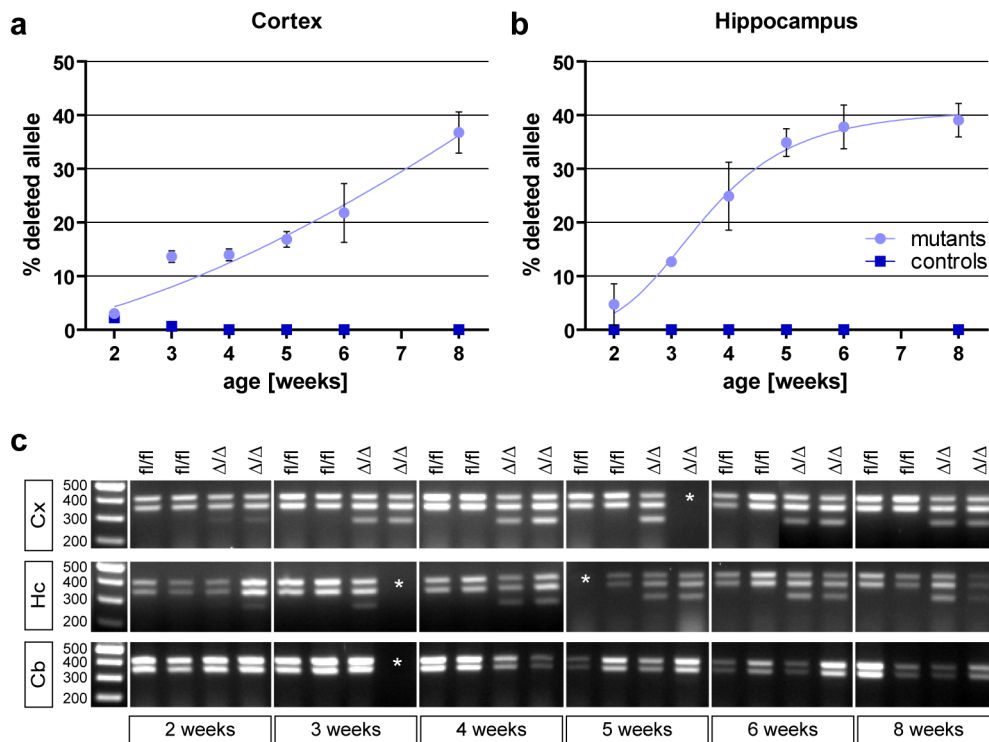
Fig. 7: Recombination of the *Braf* allele in *Braf* conditional knockouts
a,b) Southern blot analysis of cortical (**a**) and hippocampal (**b**) samples from Braf[cko] mice (n = 2) revealed that the Cre-mediated recombination becomes apparent at an age of two weeks and highest levels were found at week 8 in the cortex (**a**) and at week 6-8 in the hippocampus (**b**). Not any recombination was observed in control animals (**a,b**) and in cerebellar samples of mutant mice (data not shown). **c**) Validation of Southern blot results by qualitative PCR (*: no DNA sample for PCR present)

In summary, the results from the Southern blot and the PCR analyses demonstrate that the floxed allele in mutant animals is efficiently recombined. Due to the expression pattern of the Cre recombinase under the control of the CaMKIIα promoter, recombination takes place during postnatal development in all forebrain neurons and some regions of the midbrain.

To characterise further the *Braf* knockout mutation, I studied the depletion of the BRAF protein at the cellular level. To this end, the BRAF protein levels in brains of mutants and controls were determined by immunohistochemistry (IHC). Brains of Braf[cko] mice were dissected, cryosectioned, and immunostained with an antibody specific for the N-terminus of BRAF. As shown in Fig. 8, the

BRAF protein was depleted in the anterior brain regions in all layers of the cortex (fCx) as well as in the whole striatum (St) (a, left panel). In posterior brain regions, BRAF was absent in mutants again in all layers of the cortex (pCx), in the hippocampus (Hc), and the piriform cortex (Pir) (b, right panel). In contrast, BRAF was found ubiquitously in all brain regions of control animals.
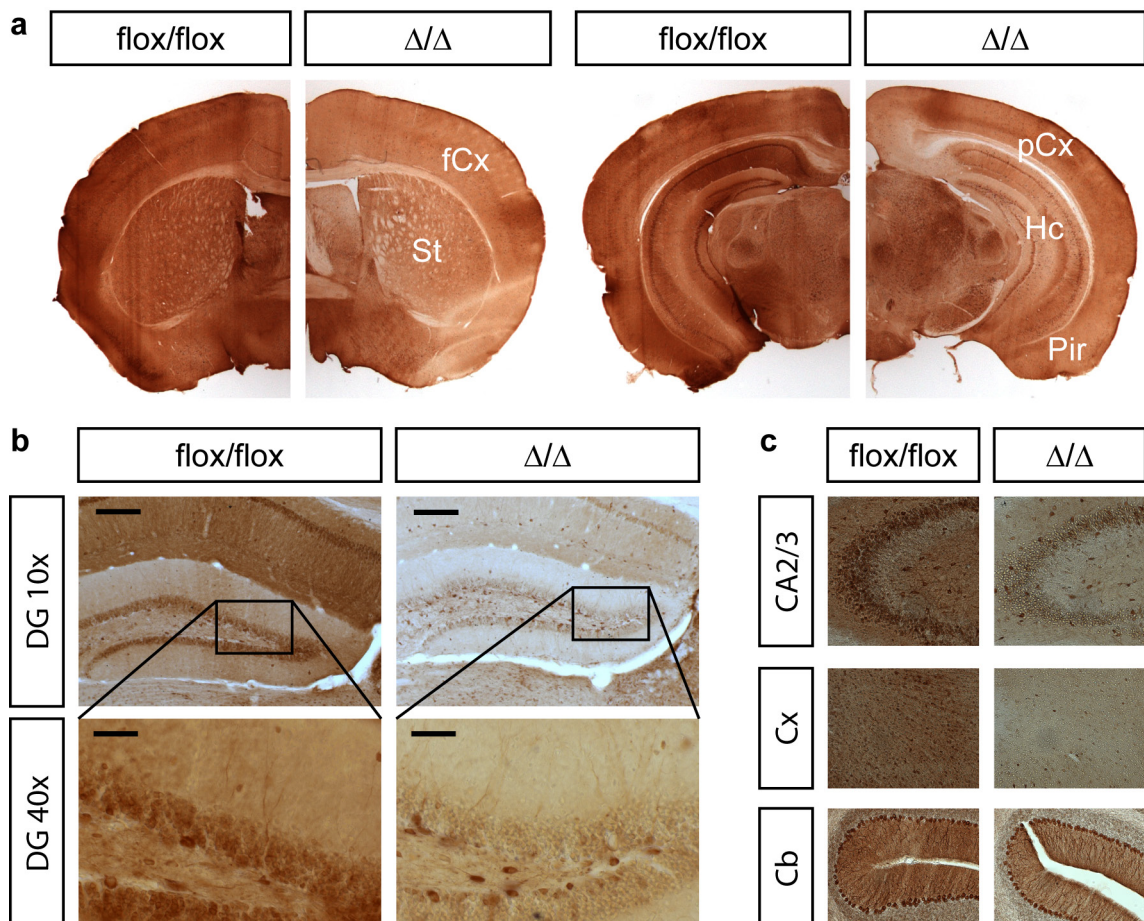
Fig. 8: Immunohistochemistry against BRAF protein
a) IHC staining of anterior (left) and posterior (right) coronal sections revealed BRAF depletion in frontal cortex (fCx), striatum (St), posterior cortex (pCx), hippocampus (Hc), and piriform cortex (Pir) of Braf^{cko} mice (Δ/Δ) but not in controls (flox/flox). **b**) BRAF protein is absent in most, but not all cells in the dentate gyrus (DG, upper panel) of the hippocampus in Braf^{cko} mice. Higher magnification (40x, lower panel) shows BRAF positive cells in the polymorphic layer of the DG. (Scale bar upper panel: 200 µm, lower panel: 50 µm) **c**) BRAF is depleted in the CA2/3 region of the hippocampus (upper panel) and cortex (middle panel) of Braf^{cko} mutants, but not in the cerebellum (lower panel).

In the dentate gyrus (DG) of hippocampi of mutants, BRAF was completely depleted in all cells of the granular layer (Fig. 8 b). However, in the polymorphic layer of the DG, some neurons still expressed BRAF. A double-immunofluorescence analysis using antibodies against BRAF and Parvalbumin

revealed that these cells were mainly GABAergic interneurons (Fig. 9). In the CA2/3 region of the hippocampus and the cortex, the BRAF protein was also absent in most, but not all cells of mutant animals (Fig. 8 c). In the cerebellum, no reduction of BRAF protein was observed in Braf^{cko} mutants.
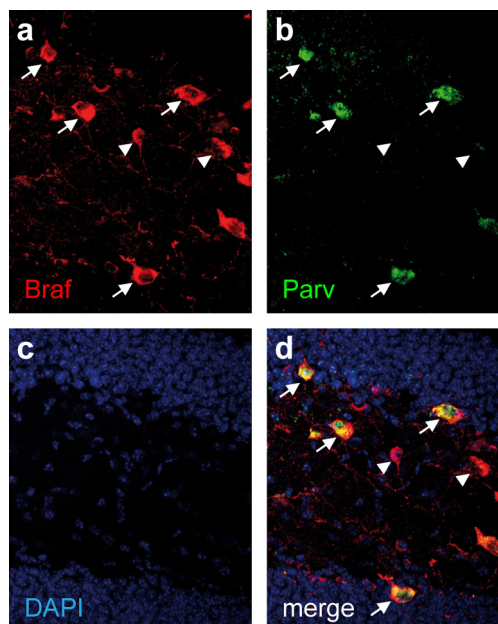
Fig. 9: Immunofluorescence of hippocampal interneurons
IF staining for BRAF protein (**a**) and Parvalbumin (**b**, "Parv"), a marker for GABAergic interneurons, in a hippocampal section of a Braf^{cko} mutant. DAPI was used as nuclear marker (**c**). Overlay of stainings (**d**) revealed mostly Braf^{+}/Parv^{+} interneurons (arrows) as well as Braf^{+}/Parv^{-} cells (arrowheads).

4.1.3 Neurological phenotyping

As already mentioned in section 3.3.2, the *Braf* conditional knockouts were tested by Dr. Christiane Hitz in respect of general locomotion, memory, anxiety, depression-like behaviour, and social interaction and discrimination. For a more general overview about the neurological phenotypes of Braf^{cko} mice, I tested the animals in a neurological test battery (7.7.8). This test battery included various settings to assess general health, basic reflexes, and home cage behaviour. Additionally, anxiety, locomotion, and physiological parameters as well as sensory skills were assessed. All measured parameters are listed in the appendix (9.3.1.7). For the wire test, 10-11 weeks old males and females were used with ten animals per gender and genotype. For all other tests, 9-16 weeks old males and females were used with five animals per gender and genotype.

Braf^{cko} mutants did not show any changes in their general health compared to the controls (for complete results see appendix 9.3.2). All animals appeared to be healthy and had a clean fur without any patches. Animals of both genotypes showed normal behaviour in the home cage and had normal reflexes in response to cage movement, righting, and touch. Nevertheless, 5 out of 10 mutants showed an increased arousal that became manifest in sudden jumping upon animal handling.

In the anxiety-related elevated platform test, the number of head pokes was counted. Male mutants showed less anxiety against high altitude, which became prominent by a significantly increased number of head pokes ($p < 0.01$, Fig. 10 a). Female mutants also tended to showed more head pokes, but the difference was not significant ($p = 0.2$).
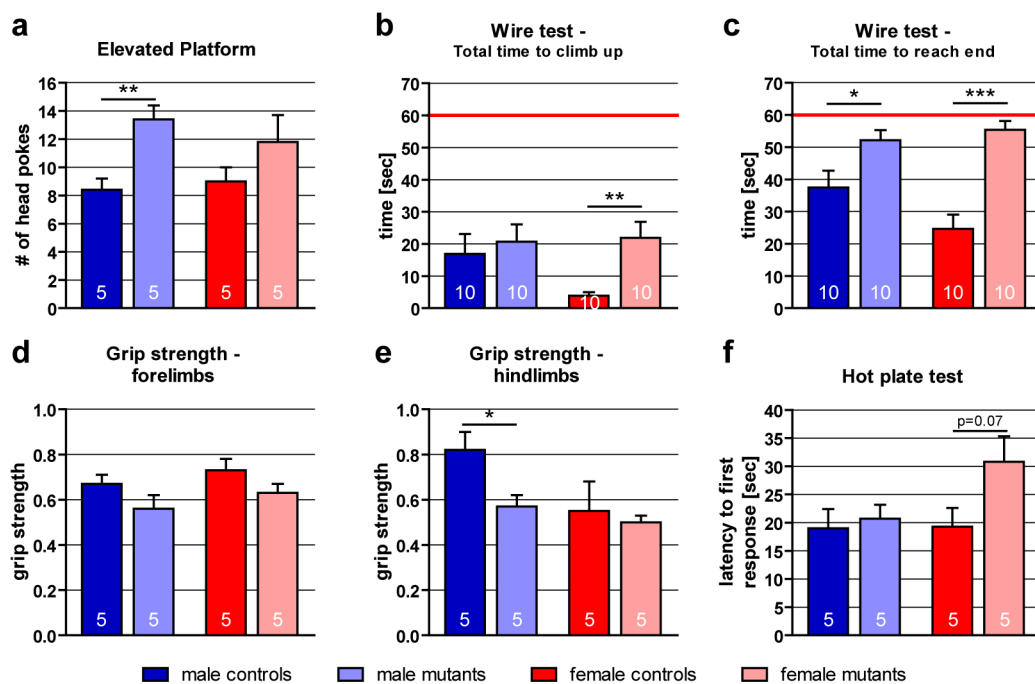
Fig. 10: Results from neurological test battery of *Braf* conditional knockouts
a) Male mutants perform significantly more head pokes in the elevated platform test compared to controls. Female mutants show a similar, but not significant phenotype. **b,c**) Wire test: Female mutants show less climbing ability compared to controls (**b**), whereas no differences were found in males. Mutants of both sexes need significantly longer to complete the test (**c**). **d,e**) Grip strength test: No differences in grip strength in forelimbs in both sexes (**d**). Male, but not female mutants had less grip strength in hindlimbs (**e**). **f**) No significant changes in responses to sensory stimuli were found in both sexes in the hot plate test.
White numerary in bars represents number of animals tested. (*: $p < 0.05$, **: $p < 0.01$, ***: $p < 0.001$)

In the first part of the wire test, in which the animals have to lift themselves to the wire, no differences were found in males (p = 0.7, Fig. 10 b). In contrast, female mutants needed significantly more time than controls to perform this task (p < 0.01). In the second part of the test, in which the animals have to climb along the wire, both sexes showed a decreased performance (Fig. 10 c). Male (p < 0.05) as well as female Braf^{cko} mutants (p < 0.001) needed significantly more time to reach the end compared to controls.

In the grip strength test, no differences were found in the strength of the fore-limbs of males and females (Fig. 10 d). The strength of the hindlimbs was significantly reduced in male (p < 0.05), but not in female mutants (Fig. 10 e).

Finally, the response to sensory stimuli was not changed between mutants and controls of both sexes (Fig. 10 f). Although there was a tendency to an increased latency to the first response in females, the difference did not reach significance (p = 0.07).

In summary, the neurological test battery revealed an overall good neurological condition of the Braf^{cko} mutants. In accordance to the behavioural results from Dr. Christiane Hitz (see section 3.3.2), mutant animals showed a constitutive arousal as well as a reduction in anxiety behaviour. Braf^{cko} mice showed poor performance in the motor coordination task and normal responses to sensory stimulation.

4.1.4   Gene expression analysis

One of the major functions of the ERK/MAPK signalling pathway is the activation of transcription factors by phosphorylation and thereby the regulation of gene expression. In order to identify candidate genes, whose expression is altered due to the loss of ERK/MAPK signalling and which play a role in the regulation of emotional behaviour, a global gene expression study was performed (7.1.3.2) in collaboration with P. Weber (MPI of Psychiatry, Munich).

Hippocampal RNA samples were isolated from five male Braf^{cko} mutants and six male controls (16-21 weeks old) and analysed for differentially expressed genes. For this purpose, microarray chips were used that contain probes for >46,000 different transcripts covering the entire murine transcriptome.

The comparison of the gene expression of mutants and controls revealed 165 differentially expressed transcripts. Of these, 124 transcripts were significantly downregulated ($p < 0.05$) and 41 significantly upregulated ($p < 0.05$). As shown in Table 1, the most significantly regulated genes were cytochrome P450 subtype 26b1, neuropeptide Y, and the serotonin receptor 5B. The complete list with all 165 differentially expressed transcripts can be found in the appendix (9.3.3, Table 6).

Table 1: Differentially regulated genes in microarray analysis of Braf[cko] mice

#	Symbol	Gene name	FC	p-value
1	*Cyp26b1*	cytochrome P450, subtype 26b1	-2.76	0.00001
2	*Npy*	neuropeptide Y	-2.27	0.00001
3	*Htr5b*	5-hydroxytryptamine (serotonin) receptor 5B	-2.37	0.00010
4	*3110047M12Rik*	RIKEN cDNA 3110047M12 gene	-1.81	0.00013
5	*Rnf170*	ring finger protein 170	1.81	0.00013
6	*Efcab6*	EF-hand calcium binding domain 6	-1.82	0.00013
7	*Hcrtr1*	hypocretin (orexin) receptor 1	-1.88	0.00013
8	*Nptx2*	neuronal pentraxin 2	-2.01	0.00013
9	*Etv5*	ets variant gene 5	-1.85	0.00020
10	*Sst*	somatostatin	-1.80	0.00020

only the 10 most significantly regulated genes are listed, FC: fold change, p-value: adjusted p-value

To identify false positive candidates that are not regulated due to the loss of BRAF but due to the presence of the Cre recombinase under the control of the transgenic CaMKIIα expression cassette, a control experiment was performed. CaMKIIα-Cre mice without any floxed allele were compared with littermates of the same genetic background that lack the Cre transgene. Six male CaMKIIα-Cre mice and six male controls (25 weeks old) were analysed using the same microarray assay that was used for the Braf[cko] mice. In total, six transcripts were significantly regulated ($p < 0.05$): zinc finger protein, multitype 2, oxidation resistance 1 (two probes), the Cre transcript (two probes), and 3110047M12Rik (Table 2).

All probes used in the microarrays are known not to have any unspecific binding sites in the mouse genome. Given that the coding sequence of the Cre recombinase is not expressed endogenously in mice, the possibility persisted that any of the probes might bind unexpectedly to the Cre transcript. Therefore,

the sequences of the six detected probes were aligned to the coding sequence of the recombinase using the BLAST algorithm (Altschul et al., 1990). Besides the Cre-specific probes, no other probe showed a homology, which verified the results (data not shown).

Table 2: Differentially regulated genes in microarray analysis of CaMKIIα-Cre mice

#	Symbol	Gene name	FC	p-value
1	Zfpm2	zinc finger protein, multitype 2	-1.8	<0.00001
2	Oxr1	oxidation resistance 1	-2.1	<0.00001
3	Cre	Cre recombinase	1.3	0.00007
4	3110047M12Rik	RIKEN cDNA 3110047M12 gene	-1.9	0.00014
5	Oxr1	oxidation resistance 1	-1.7	0.00035
6	Cre	Cre recombinase	1.6	0.00160

FC: fold change, p-value: adjusted p-value

Comparison of the two microarray studies showed that all six transcripts shown in Table 2 were also significantly regulated in the Braf^{cko} microarray. Therefore, they were considered as false positives and excluded from further analyses. In summary, the microarray studies demonstrated that the ERK/MAPK signalling pathway in the mouse hippocampus regulates the expression of 150 genes. Due to the loss of ERK/MAPK signalling and the resulting distortion of transcription factor regulation 111 genes were downregulated and 39 genes were upregulated.

Microarray assays are known to be error-prone in respect to false positives. Hence, results have to be validated either by *in situ* hybridisation or by quantitative real-time PCR (qPCR). From the 150 regulated genes in Braf^{cko} mutants, thirty-one candidates were chosen and validation was performed using qPCR (7.1.3.3) on new biological replicates of the same sex, genotype, and age as in the microarrays.

As shown in Fig. 11, the microarray results of 26 genes could be validated by qPCR. The expression ratios between microarray and qPCR analysis were comparable in all cases. Two candidates could not be validated because of the lack of suitable primer pairs for the qPCR reaction (hash). In the case of three candidates, the qPCR revealed a false positive result in the microarray (asterisk).

Comparison Microarray vs. qPCR
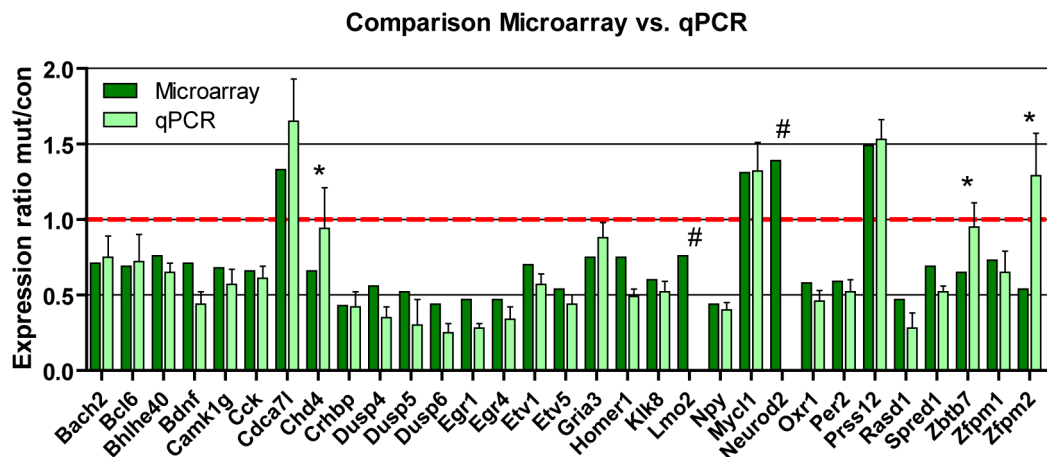
Fig. 11: Comparison between the results from the microarray analysis and the quantitative real-time PCR
The microarray results from 26 of 31 analysed genes were validated by qPCR. Values are shown as expression ratio of mutants compared to controls. *: qPCR disproved result from microarray. #: no qPCR performed due to lack of suitable primer pairs.

The validated candidate genes were then classified in respect to gene ontology and Medical Subject Headings (MeSH) terms. As shown in Table 3, ten genes were found to be transcription factors, seven were immediate early genes, fourteen were behaviour related, four were related to neuronal development, and seven were related to circadian rhythm.

Table 3: Classification of validated, regulated candidate genes

Symbol	Gene name	Microarray ratio	p-value	qPCR validation ratio	s.d.
Transcription factors					
Egr1	early growth response 1, Zif268	0.47	<0.01	0.28	0.03
Egr4	early growth response 4	0.45	<0.01	0.34	0.08
Etv5	ets variant gene 5	0.54	<0.001	0.44	0.06
Per2	period homolog 2 (Drosophila)	0.59	<0.02	0.52	0.08
Etv1	ets variant gene 1	0.70*	<0.05*	0.57	0.07
Bhlhe40	basic helix-loop-helix family, member e40	0.76	<0.02	0.65	0.06
Zfpm1	zinc finger protein, multitype 1	0.73	<0.02	0.65	0.14
Bcl6	B-cell leukemia/lymphoma 6	0.69	<0.05	0.72	0.18
Bach2	BTB and CNC homology 2	0.71	<0.02	0.75	0.14
Mycl1	v-myc myelocytomatosis viral oncogene homolog 1	1.31	<0.05	1.32	0.19
Immediate early genes (IEGs)					
Dusp6	dual specificity phosphatase 6	0.44*	<0.01*	0.25	0.06
Egr1	early growth response 1, Zif268	0.47	<0.01	0.28	0.03
Egr4	early growth response 4	0.45	<0.01	0.34	0.08
Npy	Neuropeptide Y	0.44	<0.001	0.40	0.05
Bdnf	brain-derived neurotrophic factor	0.71	<0.05	0.44	0.08
Camk1g	calcium/calmodulin-dependent protein kinase I gamma	0.68*	<0.02*	0.57	0.10
Cck	cholecystokinin	0.66	<0.01	0.61	0.08
Behaviour related					
Egr1	early growth response 1, Zif268	0.47	<0.01	0.28	0.03
Npy	Neuropeptide Y	0.44	<0.001	0.40	0.05
Crhbp	corticotropin releasing hormone binding protein	0.43	<0.001	0.42	0.10
Bdnf	brain-derived neurotrophic factor	0.71	<0.05	0.44	0.08
Homer1	homer homolog 1 (Drosophila)	0.75	<0.05	0.49	0.05
Spred1	sprouty protein with EVH-1 domain 1, related sequence	0.69	<0.01	0.52	0.04
Klk8	kallikrein related-peptidase 8	0.60	<0.02	0.52	0.07

Per2	period homolog 2 (Drosophila)	0.59	<0.02	0.52	0.08
Etv1	ets variant gene 1	0.70*	<0.05*	0.57	0.07
Camk1g	calcium/calmodulin-dependent protein kinase I gamma	0.68*	<0.02*	0.57	0.10
Cck	cholecystokinin	0.66	<0.01	0.61	0.08
Bhlhe40	basic helix-loop-helix family, member e40	0.76	<0.02	0.65	0.06
Gria3	glutamate receptor, ionotropic, AMPA3 (alpha 3)	0.75	<0.05	0.88	0.10
Prss12	protease, serine, 12 neurotrypsin (motopsin)	1.49*	<0.02*	1.53	0.13
Neuronal development					
Bdnf	brain-derived neurotrophic factor	0.71	<0.05	0.44	0.08
Klk8	kallikrein related-peptidase 8	0.60	<0.02	0.52	0.07
Etv1	ets variant gene 1	0.70*	<0.05*	0.57	0.07
Cck	cholecystokinin	0.66	<0.01	0.61	0.08
Circadian rhythm related					
Dusp6	dual specificity phosphatase 6	0.44*	<0.01*	0.25	0.06
Egr1	early growth response 1, Zif268	0.47	<0.01	0.28	0.03
Rasd1	RAS, dexamethasone-induced 1	0.47	<0.001	0.28	0.10
Bdnf	brain-derived neurotrophic factor	0.71	<0.05	0.44	0.08
Per2	period homolog 2 (Drosophila)	0.59	<0.02	0.52	0.08
Cck	cholecystokinin	0.66	<0.01	0.61	0.08
Bhlhe40	basic helix-loop-helix family, member e40	0.76	<0.02	0.65	0.06

Twenty-two candidate genes were validated by qPCR and classified by gene ontology and MeSH analysis. *: mean values due to multiple transcripts detected in microarray; s.d.: standard deviation

To identify genes that are directly controlled by ERK/MAPK signalling, the promoter regions of all 150 differentially expressed genes were analysed *in silico* for binding sites of the two major ERK-dependent transcription factors CREB1 and ELK1 in collaboration with Dr. J. Hansen and Dr. D. Trümbach (IDG, Helmholtz Zentrum München). Furthermore, the evolutionary conservation of these motifs was analysed (7.1.3.4), as a wide conservation indicates a functional relevance (Cohen et al., 2006) and hence a central function of this gene in neuronal MAPK/ERK signalling.

Table 4: Bioinformatical prediction of CREB1 and ETS/SRF target genes

Gene symbol	Binding site (BS)	# of species	Conserved BS / Module	microarray (fold change)	qPCR (ratio)
Sst	CREB1	10	2	−1.80	n.t.
Nos1	CREB1 CREB1 CREB1 CREB1	8 3 7 4	2 2 1 1	+1.59	n.t.
Gria3	CREB1	8	1	−1.34	0.88
Dusp4	CREB1 ETS/SRF	8 7	1 1	−1.86	0.35
Egr1	CREB1 ETS/SRF	6 4	2 4	−2.13	0.28
D15Wsu169e	CREB1 ETS/SRF	6 2	1 1	−1.29	n.t.
Spata13	CREB1 ETS/SRF	6 2	1 1	+1.50	n.t.
Zfp326	ETS	5	1	−1.36	n.t.

Bdnf (transcript variant 3)	CREB1	4	1	−1.41	0.44
Dusp5	CREB1 ETS/SRF	3 4	1 1	−1.90	0.30
Egr4	CREB1	3	2	−2.24	0.34
Cacna1g	CREB1 ETS/SRF	3 2	1 2	+1.41	n.t.

Twelve differentially expressed genes exhibit CREB1 and/or ETS/SRF binding sites in their promoter regions, which are conserved in up to ten species.

Twelve genes with at least one binding site for CREB1 or ELK1 that were conserved between two or more species were identified (Table 4). The promoters of six of these genes share sequence motifs for both transcription factors, five genes harbour only CREB1 sites, and one gene contains only an ELK1 site. Interestingly, highly conserved CREB1 sites (≥ 4 orthologs) were found in the promoters of the somatostatin (*Sst*), NO synthase 1 (*Nos1*), glutamate receptor 3 (*Gria3*), dual specificity phosphatase 4 (*Dusp4*), early growth response 1 (*Egr1*), *D15Wsu169e*, spermatogenesis associated 13 (*Spata13*), and brain-derived neurotrophic factor transcript variant 3 (*Bdnf*) genes of up to eight mammalian species. Highly conserved ELK1 sites were identified in the promoters of *Dusp4*, *Egr1*, zinc finger protein 326 (*Zfp326*), and dual specificity phosphatase 5 (*Dusp5*). The detailed results of the conservation studies of the promoter regions can be found in the appendix (9.3.3, Table 7).

4.1.5 Home cage behaviour

Besides the experimentally investigated behavioural phenotypes, which were discussed in sections 3.3.2 and 4.1.3, the *Braf* conditional knockout mice also exhibited a striking home cage behaviour. Mutant animals were standing on their hindlimbs in one corner of the home cage and jumped without any escape-searching behaviour for several minutes until exhaustion (data not shown). This stereotypic jumping conduct was observed during the early light phase of normal housing, i.e. during the first hours of the resting phase, and mainly, but not exclusively, in female animals.

In order to rule out whether this jumping stereotypy is linked with the known role of ERK/MAPK signalling in the regulation of the circadian clock, I studied the circadian rhythm of Braf[cko] mice in collaboration with Prof. Dr. T. Roenne-

berg (LMU Munich). Therefore, the home cage activity pattern of ten mutant and ten control Braf[cko] mice (each six males and four females) was recorded for a period of 17 days (7.7.1). Animals were single-caged in a sound and light-insulated room without any disturbances, and the activity was measured using low-profile running wheels in the cages. In order to exclude the external stimulation of circadian rhythms by light, the animals were kept in a 1/23h light/dark condition.
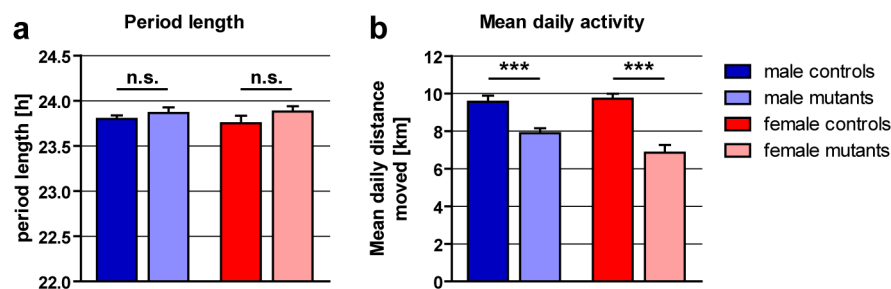
Fig. 12: Voluntary wheel running behaviour in Braf[cko] mice
a) Period length is not altered in mutant males and females. **b**) Mean daily activity is significantly reduced in both genders. (n.s.: not significant, ***: p < 0.001)

As shown in Fig. 12 a, the overall diurnal period length was neither changed in mutant males (23.86 ± 0.06 h) compared to male controls (23.80 ± 0.04 h) nor in mutant females (23.88 ± 0.06 h) compared to female controls (23.75 ± 0.08 h). The detailed periodograms of all subjects can be found in the appendix (Fig. 40, Fig. 41). In contrast, the total distance travelled per day was significantly reduced in mutants of both sexes (Fig. 12 b). Mutant males travelled 7.9 ± 0.3 km (controls: 9.6 ± 0.3 km) and mutant females 6.9 ± 0.4 km (controls: 9.7 ± 0.3 km).

The complete activity patterns of all tested mice are shown in the respective actograms (see appendix, Fig. 36 to Fig. 39). Female mutant #1 died at day 8 of the experiment and was therefore excluded from the analyses of the following days.

The ability to synchronise the circadian clock was not changed due to the depletion of the ERK/MAPK signalling. Four out of ten wild-types and five out of ten mutants achieved synchronisation during the 17 days of the experiment. Whereas the day of synchronisation strongly varied between day 2 and day 13, the synchronisation time was quite consistent (between 2:30 pm and 5:30 pm).

In Fig. 13, two representative cases of synchronised (a,c) and unsynchronised (b,d) animals are shown.
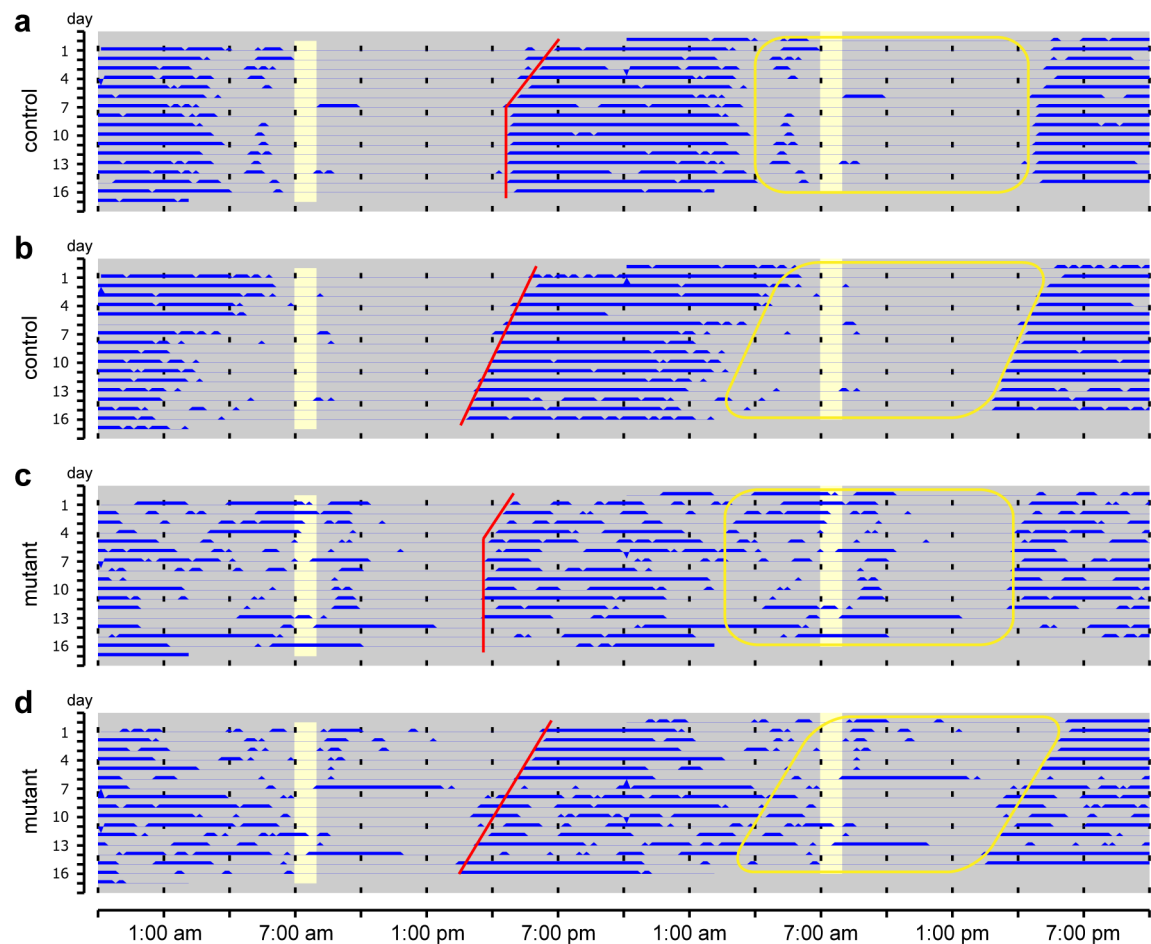
Fig. 13: Actograms of representative Braf^{cko} mice
a,b) control animals, **c,d**) mutant animals (red line: begin of daily activity phase, yellow rectangle: normal daily resting phase)

A striking difference between mutants and controls could be observed in the patterning of the activity. Control animals showed a continuous activity during the active phase for approx. 12 hours without any pauses (Fig. 13 a,b). During the subsequent resting phase, control animals showed only marginal use of the running wheels (yellow rectangles). In contrary, mutants exhibited a much more fragmented activity pattern during the active phase and an obviously increased activity during the resting phase (Fig. 13 c,d).

Quantification of the degree of resting phase activity (in terms of wheel rotations) revealed a significant increase in Braf^{cko} mutants of both sexes (Fig. 14 a; male controls: $5.9 \pm 0.6\,\%$, male mutants: $11.7 \pm 1.4\,\%$, female controls:

9.5 ± 0.8 %, female mutants: 15.0 ± 1.8 %). Moreover, the time being active during the resting phase was also highly increased in males (controls: 13.6 ± 0.6 %, mutants: 20.9 ± 1.2 %) and females (controls: 22.7 ± 1.0 %, mutants: 48.8 ± 1.6 %) (Fig. 14 b).
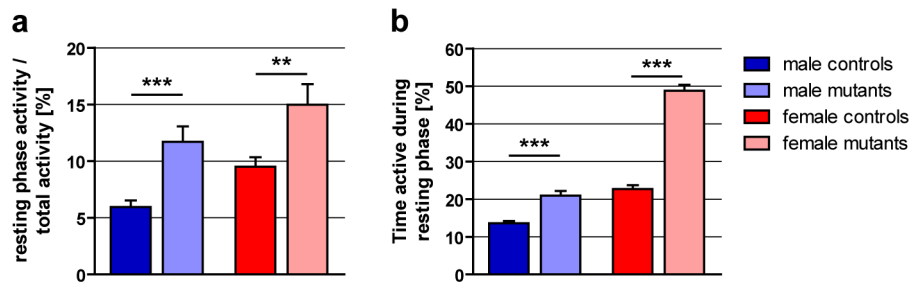
Fig. 14: Resting phase activity of Braf[cko] mice
Ratios of amount of resting phase activity (**a**) and of time of resting phase activity (**b**) are highly increased in mutants of both sexes. (******: $p < 0.01$, *******: $p < 0.001$)

These differences are also evident in the composite graphs of the tested animals (see appendix, Fig. 42 to Fig. 45). Controls show only a single peak during their activity phases and only little activity during the resting phase, whereas several mutants exhibit two distinct peaks with the second one shifted to the resting phase.

In summary, the analysis of voluntary wheel running activity demonstrated, that the inactivation of the ERK/MAPK pathway in the forebrain leads to a deregulation of the activity pattern, but not to a general disturbance or a time shift in circadian rhythm.

4.1.6 Electrophysiological analysis

Since various drugs used for the medication of mood disorders act on the ionotrophic GABA$_A$ receptors in the limbic system, the GABAergic signalling in hippocampal neurons of *Braf* conditional knockout mutants was analysed.

A first experiment was carried out at the Max Planck Institute of Psychiatry in Munich by Dr. Matthias Eder. Coronal brain slices of mutant and control animals were prepared (n = 7-8) and the field potentials in the CA1 region of the hippocampus were recorded after stimulation of the Schaffer collaterals (Fig. 15 a). To elucidate whether the GABAergic signalling in these neurons is altered in Braf[cko] mice, leading to a change in the formation of somatic population spikes

(PS), the GABA$_A$ receptors were inhibited by the competitive antagonist bicu-culline methiodide (BIM). As shown in Fig. 15 b, the normalised PS amplitude increased to a higher extent in mutants compared to controls, suggesting an altered GABAergic response.
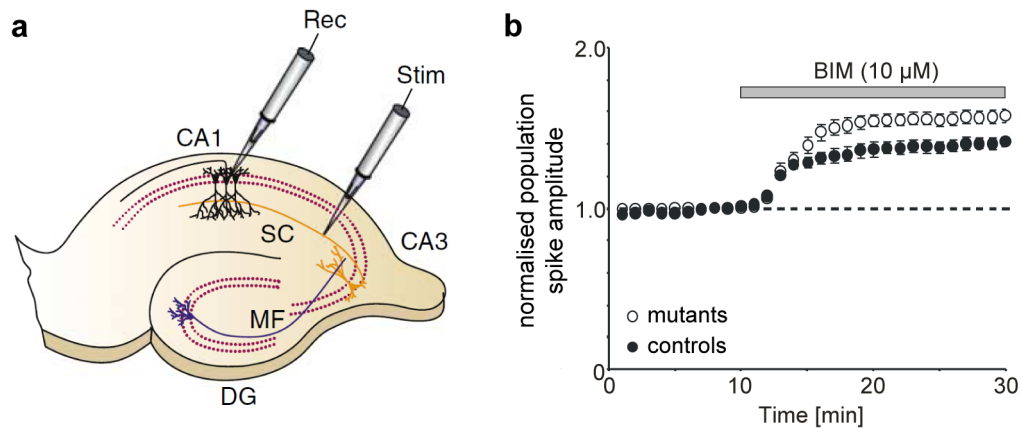
Fig. 15: Preliminary electrophysiological analysis of GABAergic signalling in Braf^{cko} mice
a) Illustration of field potential recordings: stimulation electrode (Stim) was placed in CA1 stratum radiatum, recording electrode (Rec) in CA1 pyramidal cell layer (MF: mossy fiber, SC: Schaffer collateral) (image adapted from Citri and Malenka, 2008). **b**) Extracellular recording of population spikes in CA1 pyramidal cell layer upon GABA$_A$ receptor inhibition with bicuculline (BIM).

In order to validate the first study and to further characterise the GABAergic signalling in Braf^{cko} animals, Prof. Dr. Christian Alzheimer and Dr. Fang Zheng from the Institute of Physiology and Pathophysiology at the University of Erlangen performed more detailed electrophysiological analyses.

The basal transmission and the excitability of the neurons in the CA1 region was not changed in the mutant animals, which was shown by the PS amplitude in response to the stimulus intensity (input-output curve, Fig. 16 a). Interestingly, the repetition of the field potential measurements revealed no alterations (Fig. 16 b), whereas in the first experiment differences between mutants and controls were found (Fig. 15 b). In contrast to the first experiment, picrotoxin was used as GABA$_A$ receptor antagonist instead of bicuculline.
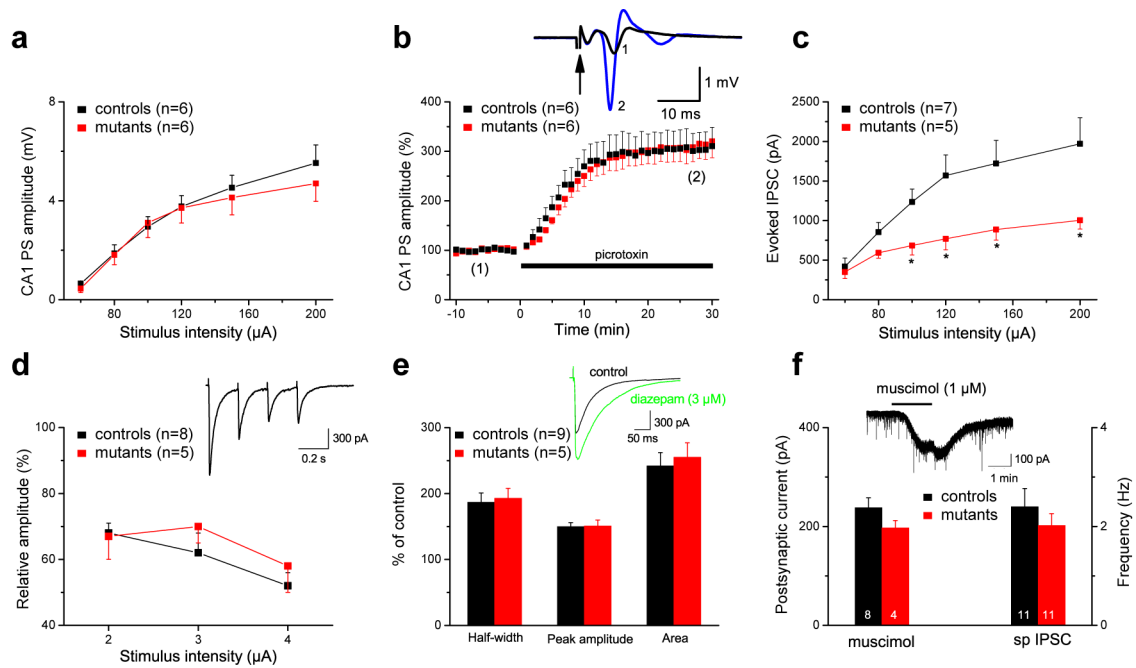
Fig. 16: Detailed electrophysiological analysis of GABAergic signalling in Braf^{cko} mice
a,b) Extracellular recordings. **c-f**) Whole-cell recordings. **a**) Amplitudes of CA1 population spikes. **b**) Population spikes in CA1 pyramidal cell layer evoked by electrical stimulation of the Schaffer collateral/commissural pathway. Effect of application of GABA$_A$ receptor antagonist picrotoxin (100 µM). **c**) Input-output relationship for evoked IPSCs showed reduced response in CA1 pyramidal cells (*: $p < 0.05$). **d**) Depression of evoked IPSCs by repetitive stimulation. **e**) Whole-cell recording of IPSCs from CA1 pyramidal cells: Effect of GABA$_A$ receptor agonist diazepam on evoked IPSCs. **f**) Effect of GABA$_A$ receptor agonist muscimol on evoked IPSCs and measurement of spontaneous IPSCs.

For the specific measurement of the activity and excitability of the GABA$_A$ receptors, whole-cell recordings in the CA1 region were performed. The input-output curve revealed significantly decreased evoked inhibitory postsynaptic currents (IPSCs) in the Braf^{cko} mutants ($p < 0.05$, Fig. 16 c). This difference was enhanced with increasing intensity of the stimulation. The characteristic depression of evoked IPSCs by repetitive stimulation of the GABA$_A$ receptor was not changed as shown in Fig. 16 d. In addition, the effects of the administration of the two GABA$_A$ receptor agonists diazepam (Fig. 16 e) and muscimol (Fig. 16 f, left) were not altered. Finally, the frequency of spontaneous IPSCs in mutants and controls was comparable (Fig. 16 f, right).

To investigate the signalling of the small conductance calcium-activated potassium (SK) channels, the selective SK2 channel blocker apamin was applied to hippocampal slices. This inhibition led to a stronger increase of the PS ampli-

tude of Braf^cko mutants in the CA1 stratum pyramidale (Fig. 17 a). In contrary, apamin had no effect on the field excitatory postsynaptic potentials (fEPSP) in the stratum radiatum in mutants, whereas controls did show an increase in fEPSPs upon inhibition (Fig. 17 b).
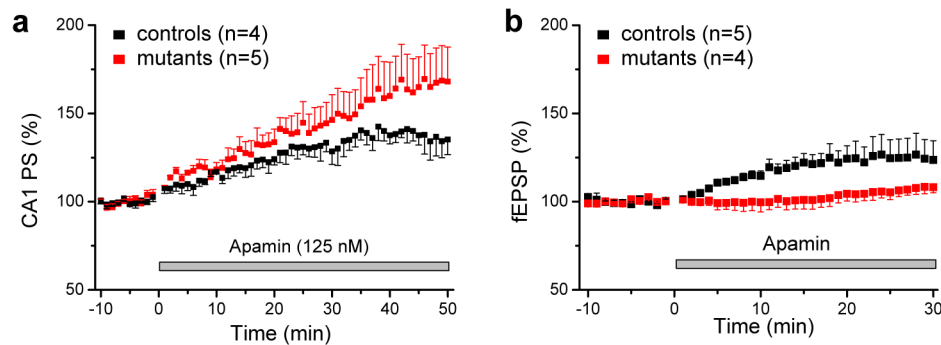
Fig. 17: Electrophysiological analysis of SK2 channel activity in Braf^cko mice
a) Effect of SK2 channel inhibitor apamin on CA1 population spikes. **b**) Effect of SK2 channel inhibitor apamin on field EPSPs in the stratum radiatum.

In summary, the electrophysiological analysis of the hippocampal neurons of Braf^cko mice revealed no changes on the GABAergic transmission and the activity of the GABA$_A$ receptors. However, different responses of the SK2 channels were detected in field potential and single cell measurements.

4.1.7 Neuronal morphology

In several genetic mouse models with altered emotional behaviour, changes in dendritogenesis and spine density were found (Bergami et al., 2008; Chen et al., 2006b; Ma et al., 2008; Scobie et al., 2009). Moreover, as the gene expression analysis identified several candidate genes related to neuronal growth, development, and arborisation, I analysed the neuronal morphology in the *Braf* conditional knockout mutants. Therefore, Golgi stainings of 140 µm thick brain sections of adult mutants and controls were prepared and the dendrites of granular neurons of the dentate gyrus (DG) were then manually traced using the Neurolucida software (MBF Bioscience). Neurons from anterior and posterior regions of the DG were initially analysed separately. Anyhow, as no differences were found between dendrites of the two regions, the results were pooled. In total, 72 neurons of Braf^cko mutants and 138 neurons of controls were traced and analysed.
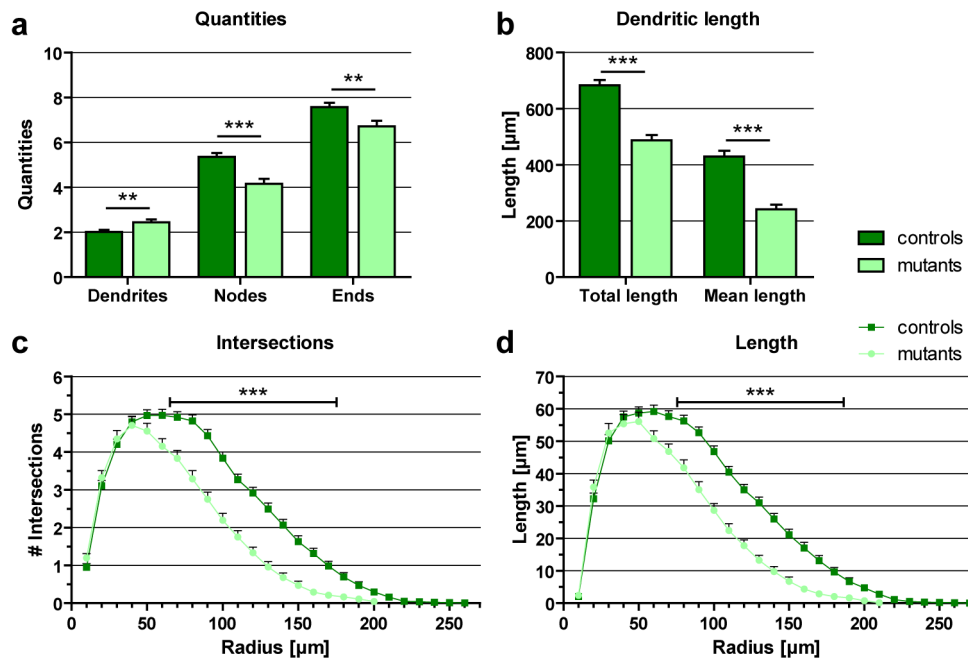
Fig. 18: Neuronal morphology of granular neurons in *Braf* conditional knockouts.
a) Number of dendrites was slightly increased, whereas the numbers of nodes and ends were reduced. **b**) Total and mean length of dendrites were significantly reduced in BRAF deficient mice. (**: $p < 0.01$, ***: $p < 0.001$) **c,d**) Sholl analysis of dendritic branching revealed a significant reduction of number of intersections (**c**) and of dendritic length (**d**) in the distance of 70-170 µm and 80-180 µm from soma, respectively (each $p < 0.001$).

The general analysis of the arborisation of the neuronal dendrites (as shown in Fig. 18 a) revealed a significant increase in the number of primary dendrites in mutants (2.44 ± 0.12) compared to controls (2.01 ± 0.09, $p < 0.01$). In contrast, the quantity of furcations ("nodes") was significantly decreased in mutant animals (4.15 ± 0.22, controls: 5.36 ± 0.17, $p < 0.001$). Consequently, the same was true for the number of terminal dendritic ends (mutants: 6.71 ± 0.25, controls: 7.57 ± 0.19, $p < 0.01$). Measurements of the length of the dendritic processes showed a major reduction in the total length of all dendrites (mutants: 487.2 ± 19.4 µm, controls: 682.9 ± 18.9 µm, $p < 0.001$) as well as in the mean length (mutants: 241.7 ± 16.4 µm, controls: 429.6 ± 20.7 µm, $p < 0.001$) of each primary dendrite (Fig. 18 b).

To characterise further the changes in the arborisation of the dendrites, a Sholl analysis of the tracing data was performed. This analysis describes the number and the length of neurite intersections in relation to their distance from the soma, thereby describing the complexity of the arborisation. In the Braf[cko] mutants, the number of intersections was significantly reduced in a distance of

70-170 µm from the soma (p < 0.001, Fig. 18 c). Consequently, the maximum number of intersections changed from 4.97 at a distance of 60 µm to 4.71 at 40 µm. In addition, the length of the segments was also significantly reduced in a distance of 80-180 µm from the soma (p < 0.001, Fig. 18 d). Analogous to the intersections, the maximum segment length decreased from 59.2 µm at a distance of 60 µm from soma in the controls to 56.1 µm at 50 µm in the mutants.

Analysis of the spine density on primary dendrites of the granular neurons displayed no changes between Braf^{cko} mutants (0.28 ± 0.017 spines/µm) and controls (0.30 ± 0.016 spines/µm, p = 0.36) (Fig. 19 a). In addition, the analysis of the tortuosity, i.e. the distortion of the primary dendrites, did not reveal any significant differences (mutants: 1.106 ± 0.010, controls: 1.097 ± 0.007, p = 0.45) (Fig. 19 b).
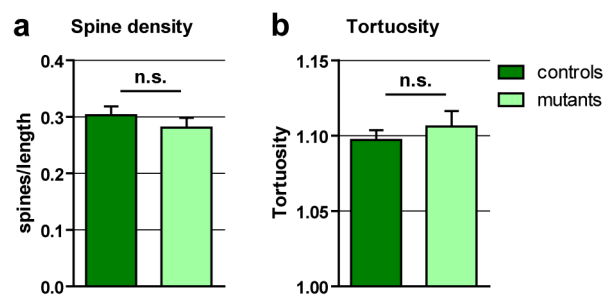
Fig. 19: Spine density and tortuosity of dendrites in Braf^{cko} mice
a) No change in spine density between mutants and controls. **b**) Tortuosity is not altered in Braf^{cko} mutants. (n.s.: not significant)

In summary, the investigation of the neuronal morphology of the granular neurons of the DG uncovered impaired neuronal branching due to the loss of BRAF. The inactivation of the ERK/MAPK signalling leads to a decreased complexity of the dendritic arborisation, whereas the formation of the spines and the dendritic routing are not affected.

4.2 Inactivation of *Braf* during postnatal development

As shown in the preceding sections, the conditional inactivation of *Braf* in fore-brain neurons leads to a variety of phenotypes. The loss of ERK/MAPK signal-ling during postnatal development and adulthood results in changes in hippo-campal gene expression, activity pattern, neuronal morphology, and in a reduc-tion of anxiety behaviour. This latter effect on emotional behaviour may provide new targets for the treatment of mood disorders. However, for the development of efficient drugs, it is important to determine the ontogenic phase at which the ERK/MAPK signalling modifies emotional behaviour.

In order to investigate the role of the ERK/MAPK signalling during the devel-opment of the central nervous system, an inducible Cre transgene was used for the conditional inactivation of *Braf*. For this purpose, the constitutive CaMKIIα-Cre mouse line, in which the Cre recombinase becomes active shortly after birth (see section 4.1.1), was substituted by an inducible CaMKIIα-CreER^{T2} mouse line. The fusion protein CreER^{T2} consists of the Cre recombinase fused to the mutant ligand-binding domain of the human estrogen receptor (ER^{T2}). Heat shock proteins bound to the ER^{T2} block the Cre activity by steric hindrance, leading to an inactive recombinase. In the presence of the synthetic ligand 4-OH-tamoxifen, the heat shock proteins are released and the Cre recombinase becomes active.

4.2.1 Characterisation of the CaMKIIα-CreER^{T2} mouse line

For the inducible inactivation of *Braf*, I used the CaMKIIα-CreER^{T2} mouse line developed by Erdmann et al. (2007) (MGI ID: 3759305, "Tg(Camk2a-cre/ERT2)2Gsc"). Although the CreER^{T2} transgene is expressed from the same promoter as the non-inducible Cre transgene, differences in the expression pat-terns of both are apparent. To confirm the recombinase expression profile of the CaMKIIα-CreER^{T2} transgene, mice were bred with *Rosa26* Cre reporter mice (Soriano, 1999) and the CreER^{T2} recombinase was induced in double trans-genic R26R^{CreER} animals after 3, 6, and 14 weeks of age. Afterwards, brains were stained for β-galactosidase activity as described (see section 7.6.5).

As shown in Fig. 20, the induction of the CreER^{T2} recombinase fusion protein was achieved at all tested points in time. Importantly, the efficiency of induction at three weeks of age (first and second row) was as high as at six weeks (third row) and at adulthood (fourth row). High CreER^{T2} activity was observed in lateral (left and middle column) and medial regions (right column) of the cortex and the hippocampus. In the medial striatum, the hypothalamus, and the midbrain, moderate recombinase activity was found. In all other regions of the brain, the olfactory bulbs, the lateral striatum, the thalamus, the cerebellum, and the brainstem, the CreER^{T2} recombinase was not expressed.
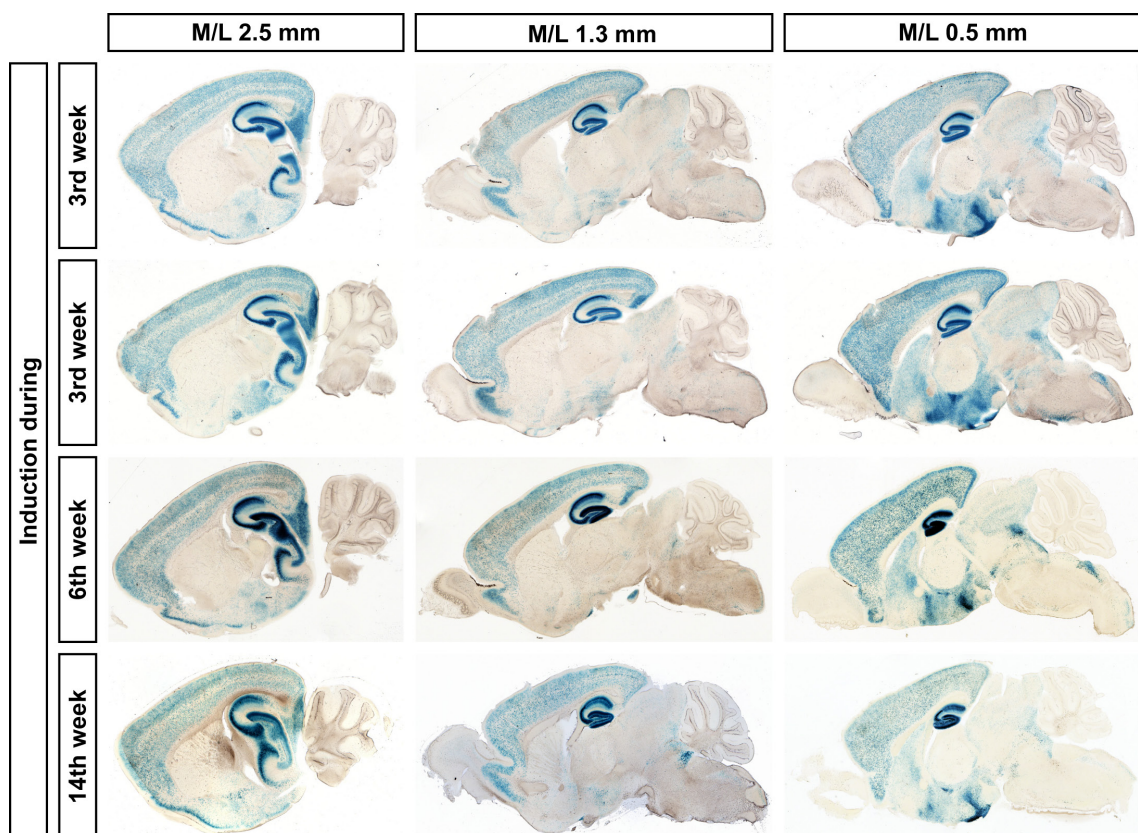
Fig. 20: Expression pattern of the CaMKIIα-CreER^{T2} mouse line
CaMKIIα-CreER^{T2} mice were bred with *Rosa26* Cre reporter mice, which show β-galactosidase activity after Cre recombination (blue staining). Induction with tamoxifen was performed at 3, 6, and 14 weeks of age. LacZ staining of sagittal sections revealed high Cre activity in the cortex and the hippocampus. Medium activity was observed in the medial striatum, hypothalamus, and midbrain and no activity in the olfactory bulbs, lateral striatum, thalamus, cerebellum, and the brainstem.

The Cre activity pattern of the CaMKIIα-CreER^{T2} mouse line is comparable, but not identical to the CaMKIIα-Cre line. In CaMKIIα-CreER^{T2} mice, the Cre recombination efficiency is high in forebrain neurons and almost absent in other

regions. The time-specific inducibility of the recombination process provides a valuable tool for the investigation of developmental gene functions and pheno-types.

4.2.2 Depletion of BRAF in forebrain neurons of Braf^{icko} mice

Inducible *Braf* conditional knockouts were obtained by breeding Braf^{flox} mice with CaMKIIα-CreER^{T2} mice. In the first mating cycle, homozygous Braf$^{flox/flox}$ mice were bred with the heterozygous CaMKIIα-CreER^{T2} mice to obtain Braf$^{flox/wt;CaMKIIα-CreER}$ mice. In the subsequent mating cycle, these heterozygous mutants were bred with Braf$^{flox/flox}$ mice to obtain homozygous Braf$^{flox/flox;CaMKIIα-CreER}$ mutants (henceforth named as "Braf^{icko}").

For the induction of the Cre-recombined *Braf* knockout allele, tamoxifen was either injected intraperitoneally or applied by oral administration of tamoxifen citrate (7.3). Mutant and control subjects were induced either during the 3rd week of life ("early induced Braf^{icko}"), to obtain postnatal *Braf* inactivation comparable to the Braf^{cko} mice, or during the 9th to 10th week of life ("late induced Braf^{icko}") to investigate the acute BRAF deficiency in adult animals. The genetic background of mutants and controls was calculated to a mean value of genetic contribution derived to 93.7 % from C57BL/6J, 6.2 % from FVB and 0.1 % from 129/Sv (early induced Braf^{icko}) and derived to 93.4 % from C57BL/6J, 6.5 % from FVB and 0.1 % from 129/Sv (late induced Braf^{icko}).

To assess whether the induction of Cre recombinase also leads to a depletion of the BRAF protein *in vivo*, the BRAF expression levels were analysed by immunohistochemistry (IHC). Brains of adult early and late induced Braf^{icko} mutants and controls were dissected, cryosectioned, and immunostained with an antibody specific for the N-terminus of the BRAF protein.

In early induced Braf^{icko} mutants, the IHC signal was strongly reduced in all regions of the hippocampus (Fig. 21 b) compared to controls (Fig. 21 a). In addition, BRAF levels were reduced in the cortex and the amygdala, whereas no overt knockout was observed in all other brain regions (data not shown). Comparable results were found in late induced Braf^{icko} animals: BRAF levels were strongly diminished in the hippocampus, cortex, and amygdala of mutants (Fig.

21 d), but not of controls (Fig. 21 c). Again, no reduction was found in other brain regions (data not shown).

early induced Braf^{icko}		late induced Braf^{icko}	
flox/flox	Δ/Δ	flox/flox	Δ/Δ
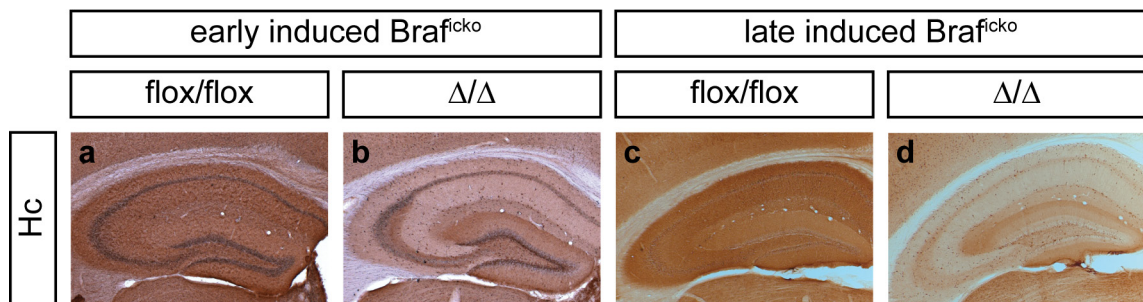
Fig. 21: Immunohistochemistry in Braf^{icko} mice
BRAF-specific IHC staining of hippocampi of early (**b**) and late (**d**) induced mutants revealed reduced protein levels compared to early (**a**) and late (**c**) induced control animals.

In summary, the inducible *Braf* conditional knockouts displayed a strong decrease of BRAF protein in forebrain regions independent on the time of induction. Therefore, the Braf^{icko} mouse line serves as a suitable tool to control the loss of ERK/MAPK signalling during either postnatal development or adulthood and to compare the behaviour of early and late mutants.

4.2.3 Behavioural analysis of Braf^{icko} mutants

In order to determine the role of ERK/MAPK signalling during the postnatal and adult phase, the behaviours of early and late induced Braf^{icko} mice were compared. All experiments were performed in the German Mouse Clinic (GMC) under the supervision of Dr. S. Hölter-Koch.

The group of early induced Braf^{icko} mice consisted of 14 male controls, 6 male mutants, 15 female controls, and 11 female mutants. All animals were 8-16 weeks of age at the beginning of behavioural testing. The group of late induced Braf^{icko} mice consisted of 15 male controls, 16 male mutants, 14 female controls, and 15 female mutants, all at the age of 15-16 weeks. As males and females of the same group and genotype did not show gender-specific differences except of body weight, results of both sexes were pooled for analysis. A summary of results of all measured parameters can be found in the appendix (9.3.4).
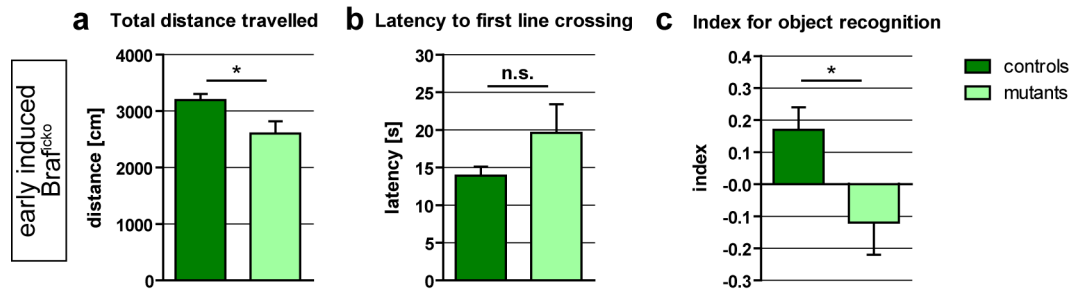
Fig. 22: MHB results of early induced Braf^{icko} mice
a) Early induced Braf^{icko} mutants travelled less compared to controls. **b**) Latency to the first action was increased in mutants but differences failed significance. **c**) Memory was impaired in early induced mutants. (n.s.: not significant, *: p < 0.05)

In the modified hole board, only early induced Braf^{icko} mice were tested. The overall locomotion of mutants was reduced (Fig. 22 a, p < 0.05). The latency to the first action, a phenotype observed in Braf^{cko} mice, was increased in mutants compared to controls, but the difference was not statistically significant (Fig. 22 b, p = 0.16). Comparable to Braf^{cko} mice, also the Braf^{icko} mutants showed an impaired ability in object recognition (Fig. 22 c, p < 0.05).
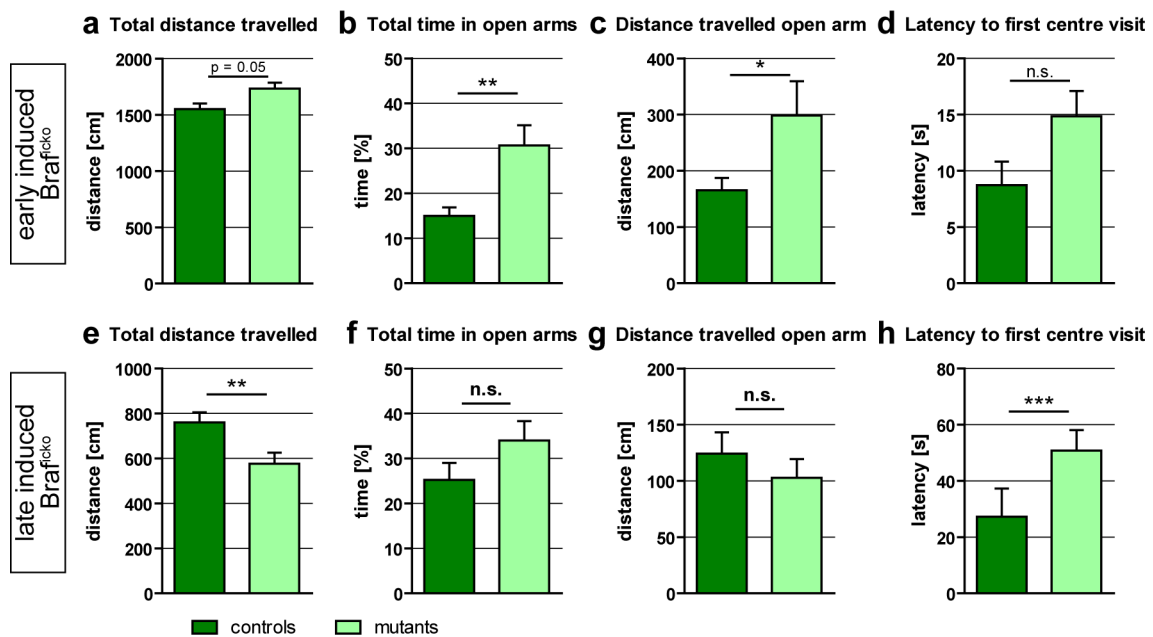
Fig. 23: Comparison of EPM results of Braf^{icko} mice
a-d) Early induced Braf^{icko} mice: Locomotion was slightly increased (**a**), whereas anxiety was reduced in mutants (**b,c**). Latency to first action was increased but difference failed significance (**d**). **e-h**) Late induced Braf^{icko} mice: Locomotor activity was decreased in mutants (**e**). No changes in anxiety behaviour were found (**f,g**), but the latency to first action was strongly increased (**h**). (n.s.: not significant, *: p < 0.05, **: p < 0.01, ***: p < 0.001)

In the elevated plus maze, the locomotion of early induced mutants was slightly increased (Fig. 23 a, p = 0.05), whereas in late induced mutants, a strong reduction was observed (Fig. 23 e, p < 0.01). Anxiety of early induced Braf^{icko} mutants was significantly reduced as animals spent more time (Fig. 23 b, p < 0.01) and travelled farther (Fig. 23 c, p < 0.05) in the aversive open arms of the maze. In contrast, late induced Braf^{icko} mice showed no phenotype in anxiety, as total time (Fig. 23 f, p = 0.12) and total distance travelled in the open arms (Fig. 23 g, p = 0.32) were unchanged. Finally, the latency for the first action was increased in mutants of both groups. In early induced animals the difference failed significance (Fig. 23 d, p = 0.11), whereas in late induced animals the change was highly significant (Fig. 23 h, p < 0.001).
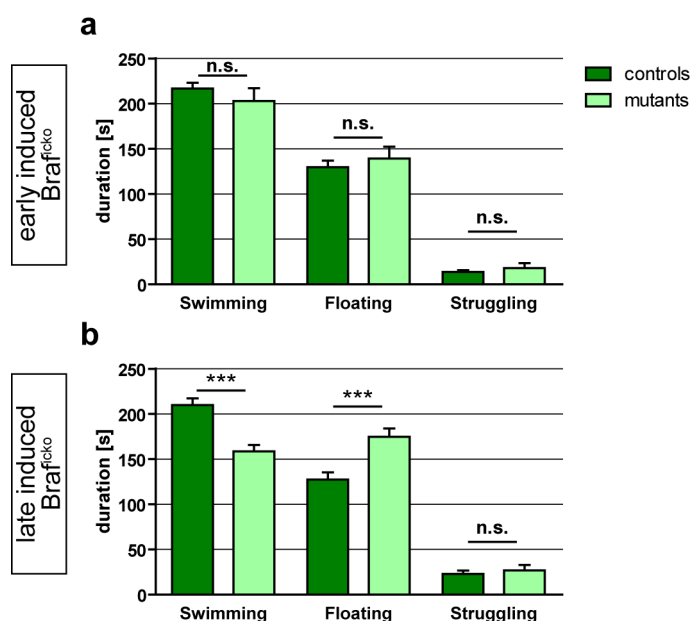
Fig. 24: Comparison of FST results of Braf^{icko} mice
a) Early induced Braf^{icko} mice: all active and inactive behaviours were unaltered between mutants and controls. **b**) Late induced Braf^{icko} mice: More floating and less swimming behaviour demonstrated an increased depression-like behaviour in mutant animals. Struggling was unaltered. (n.s.: not significant, ***: p < 0.001)

In the forced swim test, the early induced Braf^{icko} mice did not show a phenotype (Fig. 24 a). The passive behaviour ("floating") was comparable between mutants and controls (p = 0.74), as well as the two active behaviours swimming (p = 0.61) and struggling (p = 0.62). In contrast, late induced Braf^{icko} mutants showed a significantly increased depression-like behaviour (Fig. 24 b), which was apparent by their floating times (p < 0.001). This resulted in a reduction of

swimming times (p < 0.001), while the duration of escape-searching behaviour was unaltered (p = 0.56).

Since Braf^{cko} mice had a reduced body weight and showed a phenotype in the accelerating rotarod test, the inducible *Braf* conditional knockouts were also tested in this paradigm. Interestingly, body weights were highly increased in mutants of early induced (males and females: p < 0.001) as well as of late induced animals (males: p < 0.05, females: p < 0.001). In addition, body weights showed a high variation e.g. ranging from 21.0 to 47.8 g and from 21.5 to 38.3 g in early and late induced female mutants, respectively.
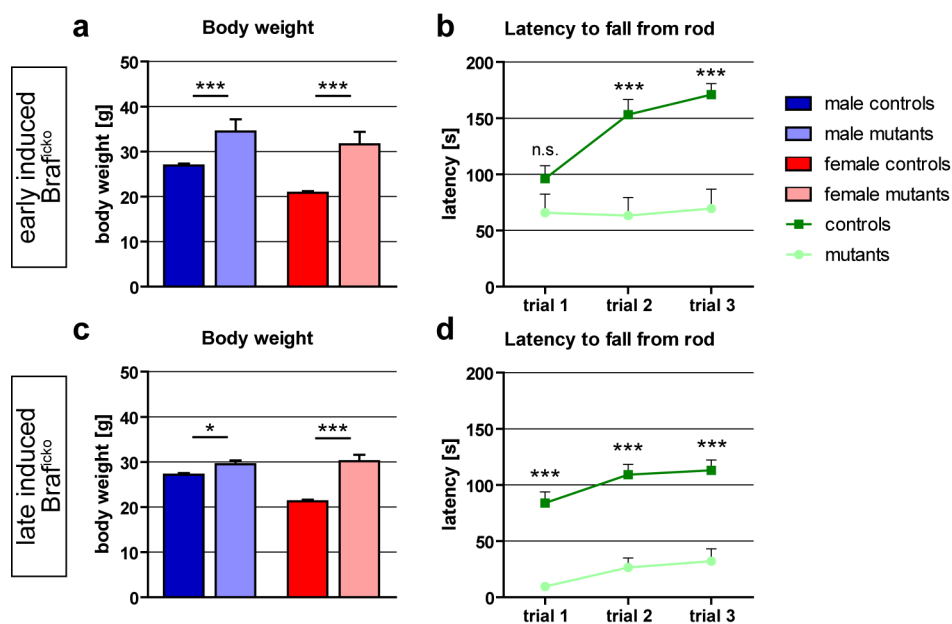
Fig. 25: Comparison of rotarod results of Braf^{icko} mice
Body weight was increased in mutants of both sexes of early as well as of late induced Braf^{icko} mutants (**a,c**). Consequently, motor coordination was impaired in mutants of early and late induced animals (**b,d**). (n.s.: not significant, *: p < 0.05, ***: p < 0.001)

Due to the increased body weight, mutants were not able to perform the accelerating rotarod task properly. As shown in Fig. 25 b and d, the latency to fall from the rod was significantly decreased in mutants of early and late induced Braf^{icko} mice.

4.2.4 Summary of behavioural analysis of Braf^{icko} mice

The comparison of early and late induced Braf^{icko} mice revealed effects of the loss of ERK/MAPK signalling on physiology and emotional behaviour. In both

groups, the conditional inactivation of *Braf* led to a strong increase in body weight of most, but not all mutants. This weight gain likely resulted in a decreased exploratory behaviour in the modified hole board and the elevated plus maze, and in a poor performance in the rotarod. Interestingly, the early induction of the *Braf* knockout led to a decrease in anxiety-related behaviour. Depression-like behaviour instead was not affected. In contrast, the late induction of the *Braf* knockout, starting at adulthood, caused an increase in depression-like behaviour but showed no effect on the anxiety of mutant animals.

4.3   Local inactivation of *Braf* in the hippocampus

As the interplay between the different brain regions that affect emotional behaviour is not yet fully understood, I studied the role of the ERK/MAPK signalling pathway by the local inactivation of *Braf* in the hippocampus. It has been shown that the dorsal part of the hippocampus plays a major role in spatial memory whereas the ventral part is linked to emotions (Fanselow and Dong, 2010). In addition, the anxiety- and depression-related phenotypes of Braf[cko] and Braf[icko] mice, in which only forebrain regions are affected, restricted the putative area responsible for changes in mood and emotion. However, the structures that determine emotional behaviour are not exactly defined.

To disrupt locally the ERK/MAPK pathway in the ventral and the dorsal hippocampus, respectively, a recombinant adeno-associated virus (AAV, chimeric serotype 1/2) was injected bilaterally into the brains of Braf[flox/flox] mice (Fig. 26). The operative AAV vector (AAV-Cre) consists of the coding sequences of the Cre recombinase and of the enhanced green fluorescent protein (EGFP) under the control of the neuron-specific synapsin-1 promoter. The control AAV vector lacks the Cre recombinase and expresses only EGFP (AAV-GFP). The stereotactic coordinates for the injection into the dorsal and the ventral hippocampus are listed in the methods section (7.5).
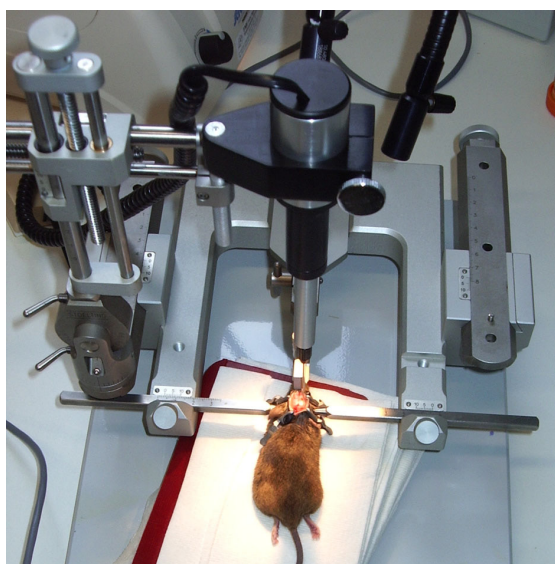
Fig. 26: Stereotactic injection of viral vectors
Representative picture of bilateral injection of AAV vectors into the mouse brain.
Detailed information about injection setup, instruments, and protocols can be found
in the materials and methods sections (6.7 and 7.5).

For the validation of the specific and restricted *Braf* knockout, brains of injected animals were analysed using immunohistochemistry with an antibody specific for the BRAF protein. In Fig. 27, representative IHC stainings of two brains are shown that were injected with AAV-GFP and AAV-Cre, respectively, into the dorsal part of the hippocampus. Animals injected with the effective AAV-Cre vector showed a clear reduction of BRAF protein in the DG of the anterior (Fig. 27 b), as well as in the DG of the posterior brain (Fig. 27 d). In all other brain regions, the levels of BRAF protein were unaffected. In control animals injected with the AAV-GFP virus, no BRAF depletion was observed (Fig. 27 a and c). Analysis of the AAV-Cre injected brains on the cellular level revealed that BRAF was completely depleted in all granular neurons of the DG and the CA3 region (Fig. 27 h and k), whereas in the CA2 and CA1 regions only some cells were negative for BRAF.
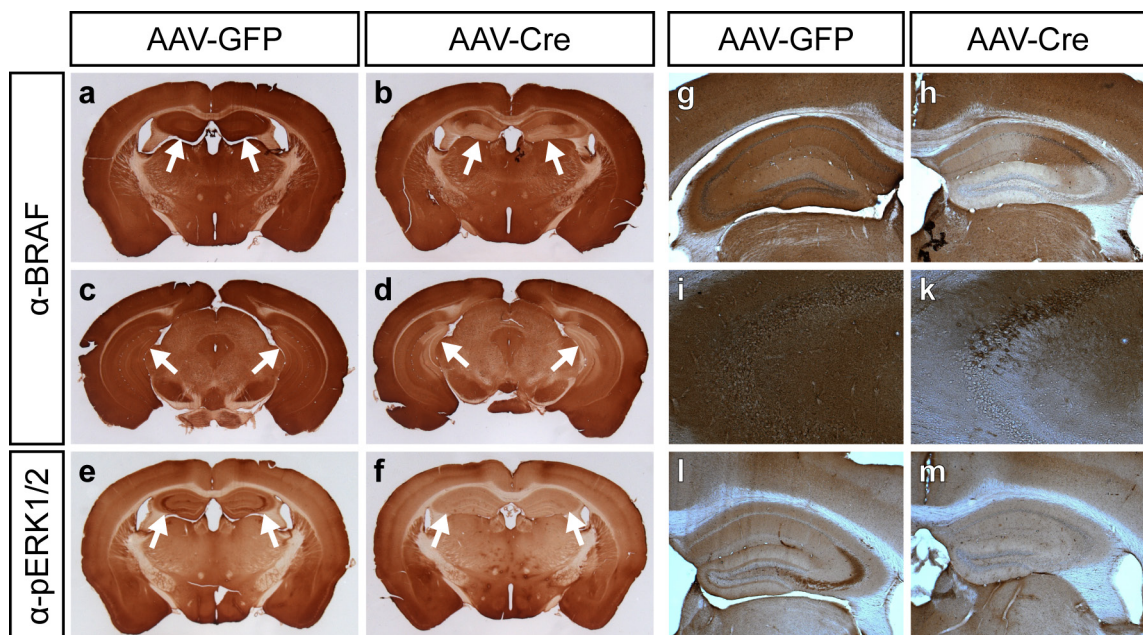
Fig. 27: IHC staining after injection of AAV in Braf^{flox/flox} mice
a-d) Coronal sections of IHC against BRAF protein. BRAF is depleted in the anterior (**b**) and posterior (**d**) DG after injection of AAV-Cre. No reduction was observed upon injection of AAV-GFP (**a,c**). **e,f**) Coronal sections of IHC against Phospho-ERK1/2. Depletion of BRAF inactivates the ERK/MAPK signalling. **g-k**) Higher magnification of the whole hippocampus (**g,h**) and of the CA2/3 region (**i,k**). **l,m**) Higher magnification of the loss of pERK1/2 in the hippocampus.

To test whether the viral vector-based *Braf* inactivation leads to the blockade of ERK/MAPK signalling, the phosphorylation of the downstream targets ERK1 and ERK2 were analysed by IHC. As shown in Fig. 27 e and f, the injection of

AAV-Cre led to a clear reduction of pERK1/2 in the CA1 region, compared to AAV-GFP injected controls. pERK1/2 was completely absent in all pyramidal cells of the CA3 region (Fig. 27 l and m).

4.3.1 *Braf* inactivation in dorsal hippocampal neurons

For the local inactivation of *Braf* in the dorsal hippocampus, I bilaterally injected 14 male Braf$^{flox/flox}$ mice with AAV-GFP and 15 male Braf$^{flox/flox}$ mice were injected with AAV-Cre. Animals were 10 weeks of age at the time of surgery and were afterwards single-housed for 4 weeks for recovery until behavioural analysis. Behavioural testing was performed in the German Mouse Clinic (GMC) under the supervision of Dr. S. Hölter-Koch.

After the testing battery, animals were sacrificed and analysed for correct placement of the injection site by immunofluorescence against GFP. Ten AAV-GFP animals and ten AAV-Cre animals were rated as correctly injected and were used for the analysis of the behaviour data. A summary of results of all measured parameters can be found in the appendix (9.3.4).

All mice recovered well from the surgery and displayed a good general condition during behavioural testing. To gain a general phenotypic overview, the animals were tested first in the modified hole board. All locomotion-related parameters (like total distance travelled (Fig. 28 a, left) and mean and maximum velocity) showed no significant changes. The number of board entries and the mean distance to the wall and to the board were also not altered, indicating a normal anxiety. Finally, all animals showed normal learning and memory skills and no changes in latency to their first action (Fig. 28 a, right). The depression-like behaviour in the forced swim test was unchanged in AAV-Cre animals, apparent from normal rising floating and declining struggling behaviour (Fig. 28 b). Furthermore, the anxiety behaviour was not altered in the elevated plus maze (Fig. 28 c) and in the light/dark box (Fig. 28 d). In both paradigms, the total time in the anxiogenic compartments and the total distance travelled were normal. Finally, the motor coordination measured in the rotarod test was comparable between AAV-GFP and AAV-Cre mice (Fig. 28 e).
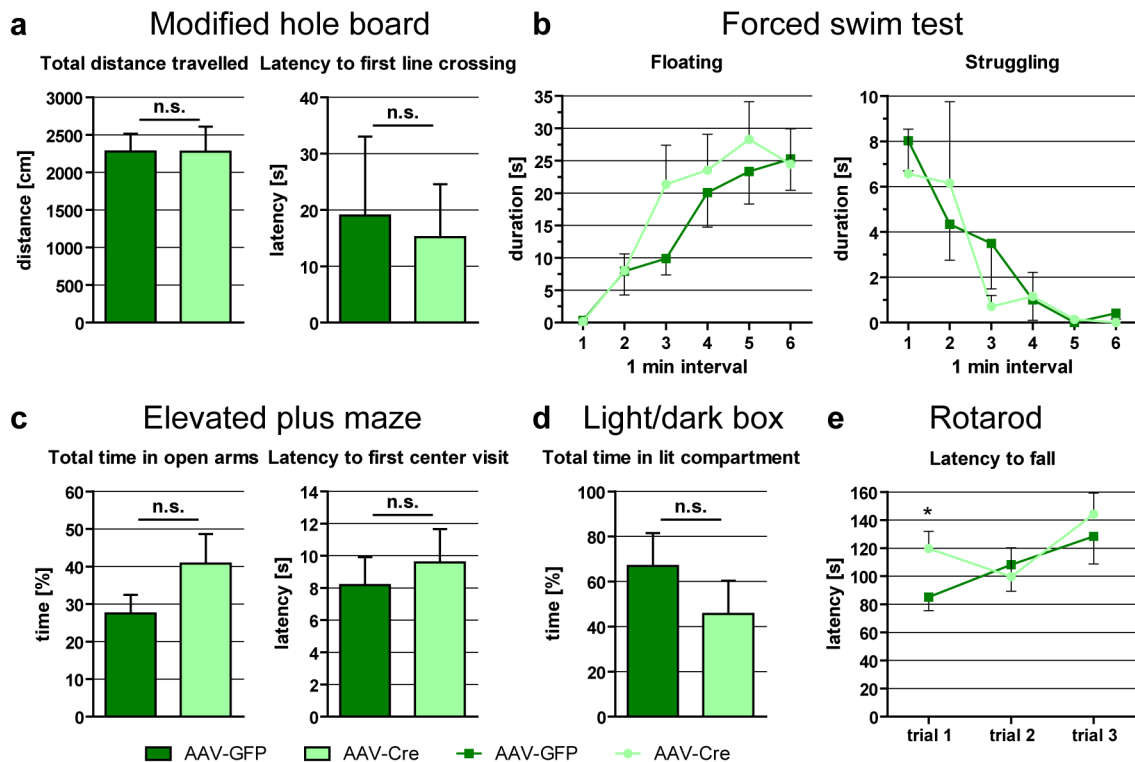
Fig. 28: Behavioural analysis of animals with local *Braf* knockout in dorsal hippocampal neurons
Local BRAF depletion in the dorsal hippocampus had no effect on general locomotion (**a**), depression-like behaviour (**b**), anxiety (**c,d**), and motor coordination (**e**). (n.s.: not significant, *: $p < 0.05$)

4.3.2 *Braf* inactivation in ventral hippocampal neurons

The local *Braf* inactivation in the ventral hippocampal neurons was achieved as described in the preceding section (see 4.3.1). I bilaterally injected 15 and 16 mice with AAV-GFP and AAV-Cre, respectively. Eleven mice of each group were assigned as correctly injected and used for analysis. Animals were ten weeks of age at surgery and were tested four weeks later. A summary of results of all measured parameters can be found in the appendix (9.3.4).

All mice recovered well from the surgery and displayed a good general condition during behavioural testing. All locomotion-related parameters of the modified hole board (total distance travelled and mean and maximum velocity) were unchanged (Fig. 29 a, left), as well as the parameters describing learning and memory, anxiety, and latency to first action (Fig. 29 a, left). The depression-like behaviour measured in the forced swim test showed no differences between AAV-GFP and AAV-Cre mice during the whole testing period (Fig. 29 b). In ad-

dition, the anxiety was not altered as shown in the elevated plus maze (Fig. 29 c) and the light/dark box (Fig. 29 d). Finally, no differences in motor coordination were revealed in the rotarod test (Fig. 29 e).
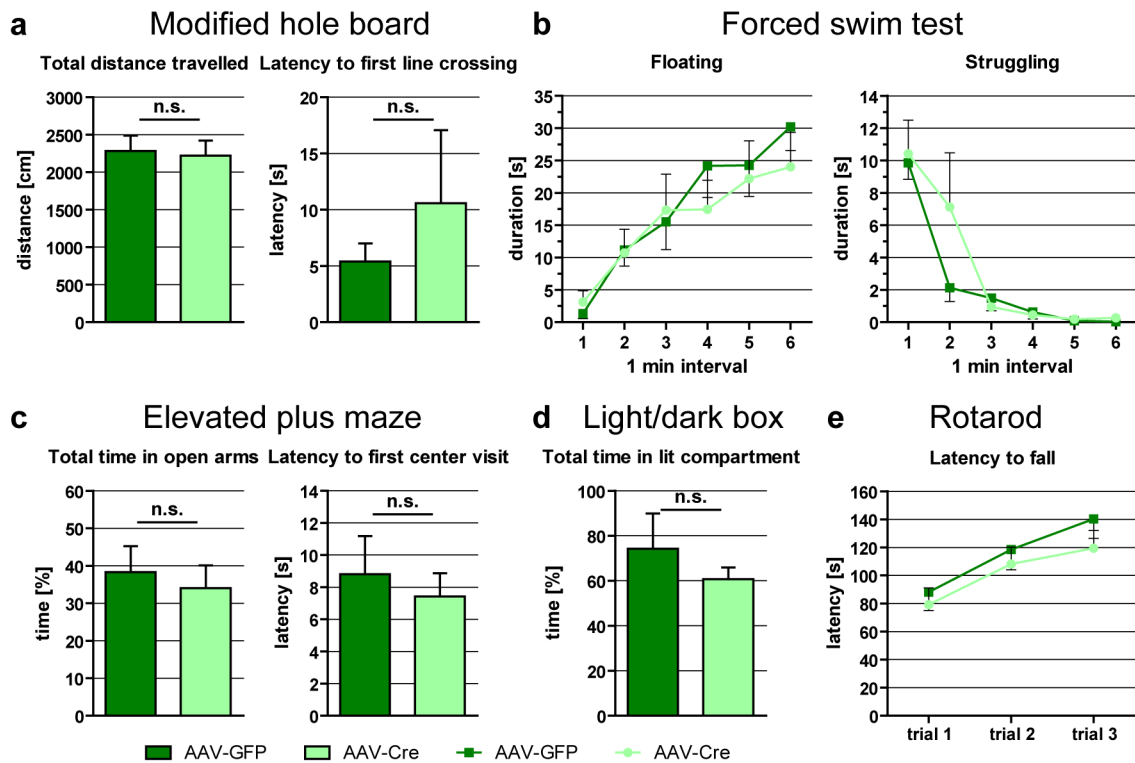
Fig. 29: Behavioural analysis of animals with local *Braf* knockout in ventral hippocampal neurons
Local BRAF depletion in the ventral hippocampus had no effect on general locomotion (**a**), depression-like behaviour (**b**), anxiety (**c,d**), and motor coordination (**e**). (n.s.: not significant)

4.3.3 Summary of results of local *Braf* inactivation

The experimental method of a local gene inactivation using a recombinant AAV vector expressing Cre recombinase worked flawlessly. Nevertheless, both the knockout of *Braf* in the dorsal and the ventral hippocampus did not reveal any significant differences in behaviour between AAV-GFP and AAV-Cre animals. All measured parameters, which included locomotion, learning, memory, anxiety, depression-like behaviour, and motor coordination showed no changes due to the loss of the BRAF protein in the respective part of the hippocampus.

4.4   BRAF overactivity in forebrain neurons

The ERK/MAPK signalling has recently been linked to a group of human diseases, named the RAS/MAPK or neuro-cardio-facial-cutaneous (NCFC) syndromes (Aoki et al., 2008; Bentires-Alj et al., 2006). In these syndromes, mutations in the members of the ERK/MAPK pathway were found that led not only to loss-of-function, but also to gain-of-function, by changing the activity of the kinase domains.

To study the effects of a forebrain-specific overactivation of the ERK/MAPK signalling on general physiology and emotional behaviour, I used the previously published Braf^{V600E} mouse line (Mercer et al., 2005). This line carries the human V600E substitution, which increases the kinase activity of the BRAF protein by ~700-fold (Wan et al., 2004). As shown in Fig. 30 a, the floxed Braf^{V600E} allele contains a cDNA expression cassette encoding the wild-type exons 18-22, which is located upstream of the mutant endogenous exon 18. Upon Cre-mediated recombination, the loxP-flanked cDNA cassette is excised, leading to the transcription of the mutant exon 18. The human V600E substitution corresponds to the murine homolog V637E, which is located in the kinase domain of the BRAF protein (Fig. 30 b). For the sake of simplicity, the term "V600E" is used here to describe both the human and the murine *Braf* mutation.
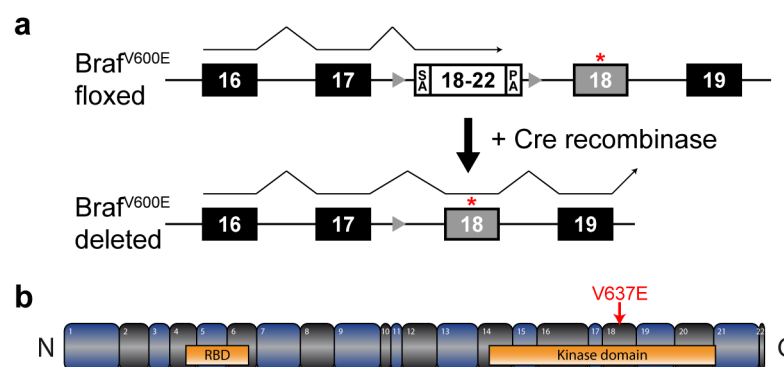
Fig. 30: Schematic illustration of the conditional mutant Braf^{V600E} allele
a) A cDNA expression cassette encoding wild-type exons 18-22 is placed upstream of the mutant exon 18. Upon Cre-mediated recombination, the cDNA cassette, which includes a polyA signal, is excised and the mutant exon 18 is transcribed. **b**) The human V600E substitution corresponds to murine V637E, which is located in the kinase domain of BRAF.

The constitutive expression of the V600E knockin during development was shown to cause early embryonic lethality (Mercer et al., 2005). Hence, in the first experiment, I crossed the Braf^{V600E} mouse line with the conditional CaM-KIIα-Cre line. However, I obtained no live Braf^{V600E,Cre} offspring, suggesting a similar embryonic lethal phenotype. Therefore, I next used the CaMKIIα-CreER^{T2} mouse line to obtain inducible Braf^{V600E,CreER} mice that were viable and did not show overt phenotypes. Littermates that lacked either the CreER^{T2} or the Braf^{V600E} allele were used as controls. Induction of controls and mutants was always performed in parallel.

4.4.1 General phenotype

To determine the efficiency of the BRAF overactivation, Braf^{V600E,CreER} mice were induced following the standard tamoxifen protocol with ten injections on five consecutive days (see methods section 7.3). Western blot analysis of cortical, hippocampal, and cerebellar protein samples, which were taken three days after the last injection, revealed an increased phosphorylation of ERK1 and ERK2 in mutant, but not in control animals (Fig. 31 a). Quantification of the Western blot showed that the levels of pERK1 were 4.6-fold increased in the cortex, 5.4-fold in the hippocampus, and 3.0-fold in the cerebellum (Fig. 31 b). Phosphorylation of ERK2 was increased 1.7-fold in the cortex, 2.6-fold in the hippocampus, and 2.5-fold in the cerebellum (Fig. 31 c).

An immunohistochemical staining with an antibody against pERK1/2 illustrated the activation of the ERK/MAPK signalling in the dentate gyrus and the CA3 region of the hippocampus (Fig. 31 d). No differences in pERK1/2 levels were found in the cerebellum (data not shown).

To assess the general physiology of Braf^{V600E} mice during and after the induction protocol, several physiological parameters were determined in parallel. The body weight of both sexes of Braf^{V600E} mutants did not significantly differ as compared to controls prior to the tamoxifen induction (Fig. 32 a). The body weight dramatically decreased in mutant animals starting 60 hours after the first tamoxifen injection (Fig. 32 b, n = 5), whereas controls continuously increased their body weight. Food intake in mutants was normal for 72 hours after the start of the induction, but was then stopped completely (Fig. 32 c, n = 5). In parallel,

the body temperature of two tested mutants strongly decreased after 80 hours of tamoxifen treatment to 34.1 °C and 30.2 °C, respectively (Fig. 32 d).
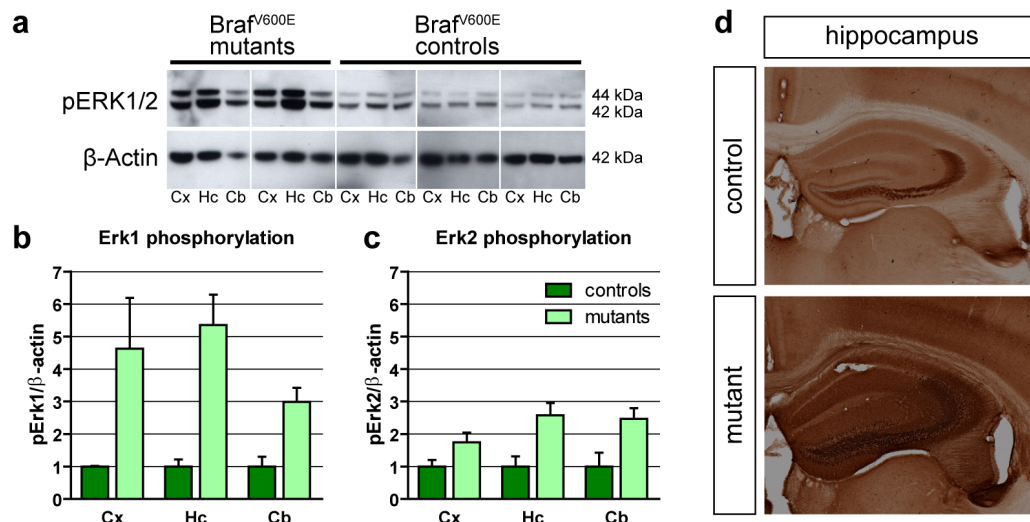
Fig. 31: Molecular analysis of *Braf* overactivation
a) Western blot analysis revealed increased levels of activated ERK1/2. **b,c**) Quantification of Western blot: 3.0 to 5.4-fold increase in pERK1 (**b**) and 1.7 to 2.6-fold increase in pERK2 levels in mutants (**c**). **d**) IHC against pERK1/2 in the hippocampus.

The complete induction of the Braf[V600E] mutation following the standard protocol with ten injections in five days is lethal as shown in Fig. 32 e. Among 27 Braf[V600E] mutants treated with tamoxifen for five days, none was alive by day 7. Severe seizures, shortness of breath, and a general lethargy were observed in many mutant animals from day 4 onwards. Not any of the 23 Braf[V600E] controls and the 24 CaMKIIα-CreER[T2] controls showed lethality (Fig. 32 e) or any overt phenotype at all.

In order to increase survival rate in the V600E mutants, the total tamoxifen dosage was reduced to achieve minor overactivation of the ERK/MAPK signalling. Test experiments revealed that four (instead of ten) injections were lethal as well, whereas a low dose (two injections) rendered survival for more than seven days (data not shown). Nevertheless, most induced mutant animals died 12 to 21 days after the low dose induction (Fig. 32 f), whereas controls survived the treatment without any phenotype.
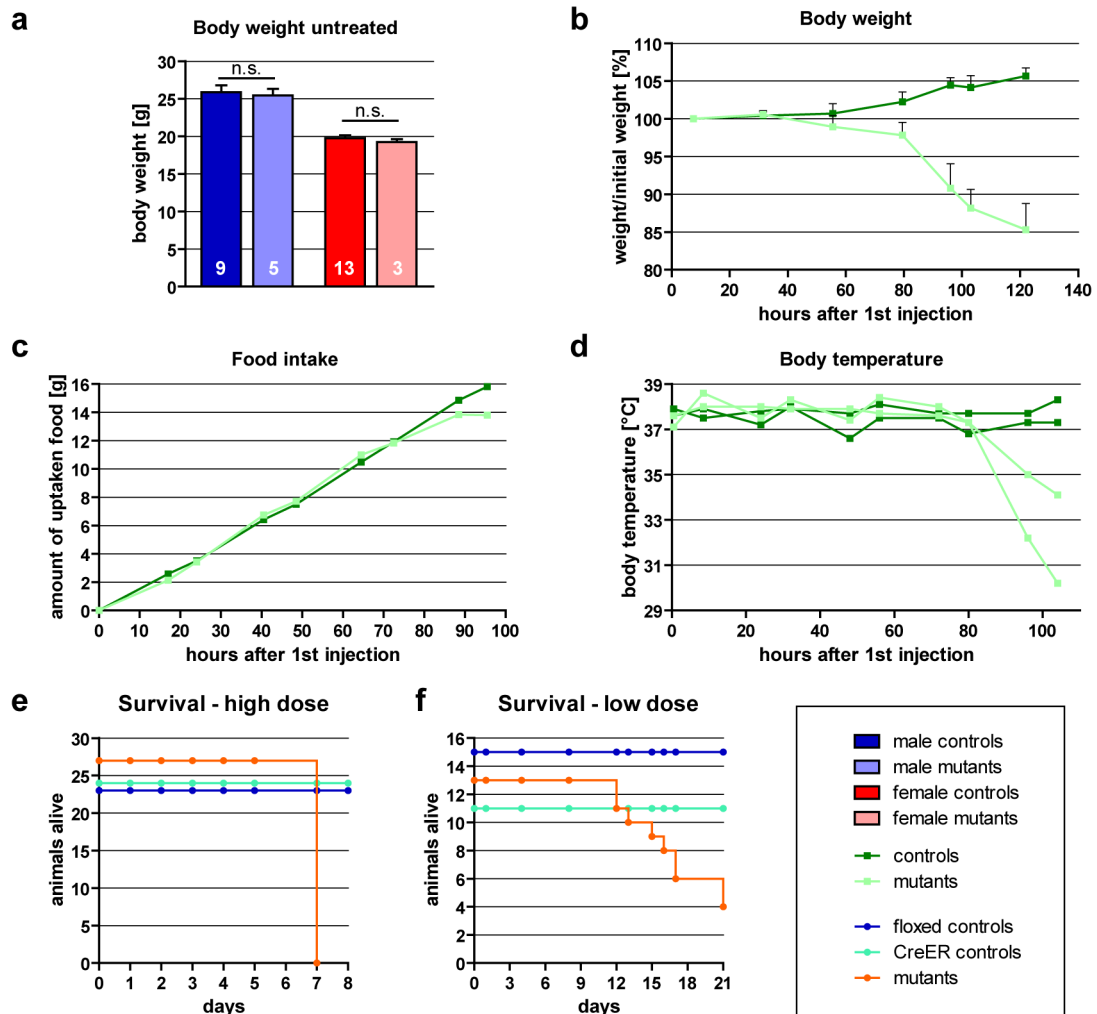
Fig. 32: Physiology of Braf^{V600E,CreER} mice upon tamoxifen treatment
a) Normal weight in non-induced knockin mice (white numbers in bars correspond to sample size). **b**) Body weight loss in treated animals. **c**) Food intake is stopped after 72 hours of treatment. **d**) Body temperature decreases dramatically after eight injections. **e,f**) Survival curves for high dose (10x) induction (**e**) and for low dose (2x) induction (**f**). (n.s.: not significant)

4.4.2 Behavioural analysis of Braf^{V600E,CreER} mutants

Due to the lethality of the standard induction protocol, the subjects for the behavioural analysis were induced with a modified protocol with two injections. 15 Braf^{V600E} controls, 11 CaMKIIα-CreER^{T2} controls, and 13 Braf^{V600E} mutants (only males used, 15-24 weeks of age) were induced and then tested two weeks later in the open field test and the elevated plus maze.

In general, mutant animals were in a poor condition at the testing date. Body weight varied between 28.0 and 18.5 g, and three mutants died before they could have been tested. Behavioural data from the two control groups were

analysed separately but were then pooled as no significant differences were found. In the open field test, mutants showed an overall decrease in locomotion (Fig. 33 a). The time spent in the centre of the field was also reduced (Fig. 33 b), whereas the latency for the first entry was increased (Fig. 33 c). In addition, the frequency of vertical exploration, measured by number of rearings, was significantly reduced in V600E mutants (data not shown). The diminished locomotion of the mutants was also observed in the elevated plus maze. The total distance travelled in the maze (Fig. 33 d), as well as the mean velocity of movement in the open and closed arms was significantly reduced (data not shown). Moreover, the latency for the first entry to the centre was increased (Fig. 33 f). Interestingly, the total time in the open arms (Fig. 33 e) and the number of visits to the ends of the open arms (data not shown), both anxiety-related parameters, were not significantly altered compared to the controls.
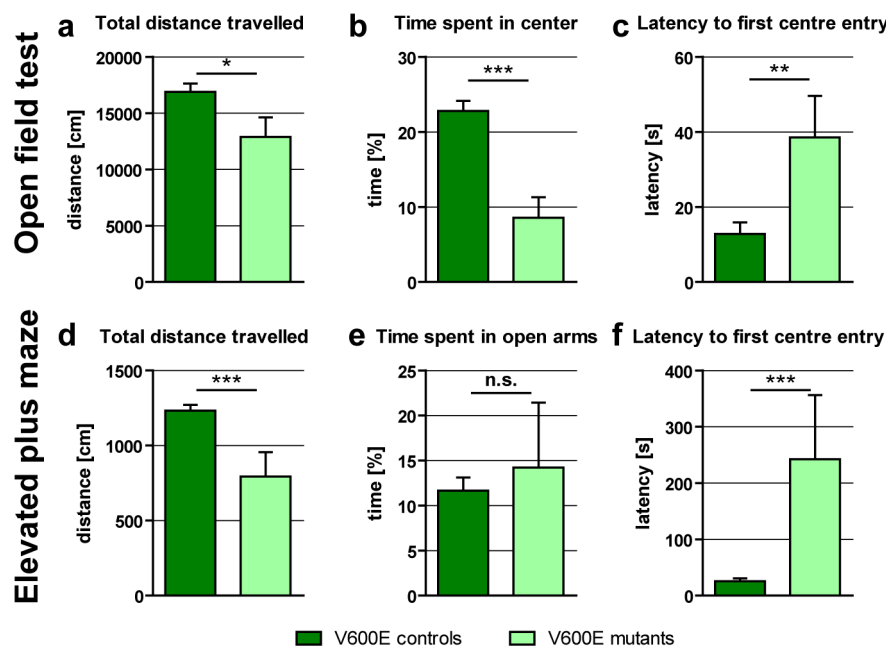
Fig. 33: Behavioural analysis of Braf^{V600E} mice
Mutant Braf^{V600E} animals showed decreased locomotor skills in the open field (**a-c**) and elevated plus maze (**d-f**). No changes in anxiety were observed (**e**).
($n_{controls}$ = 26, $n_{mutants(OF)}$ = 10, $n_{mutants(EPM)}$ = 6; n.s.: not significant, *: $p < 0.05$, **: $p < 0.01$, ***: $p < 0.001$)

In summary, the overactivation of the ERK/MAPK signalling in conditional forebrain knockin mice leads to a severe, embryonic lethal phenotype. Even a partial activation during adolescence causes a poor physiological condition result-

ing in a decrease in locomotion. Moreover, the anxiety-related behaviour seems not to be affected in Braf^{V600E} mutant mice.

4.4.3 Pathological analysis

In order to characterise further the pathophysiology of V600E mice, three Braf^{V600E} mutants and three Braf^{V600E} controls (all females, 11 weeks of age) were pathologically analysed by Dr. Irene Esposito and Dr. Julia Calzada-Wack from the Institute of Pathology at the Helmholtz Zentrum München. The animals were induced with five injections of tamoxifen on three consecutive days and were then immediately sacrificed for analysis.

The initial analysis of abdominal organs using haematoxylin and eosin (HE) staining did not show any macro- and microscopical abnormalities. As shown in Fig. 34, sections of the heart (a,f), liver (b,g), kidney (c,h), and spleen (d,i) of both samples did not reveal any differences. In the other organs tested, which were lung, thymus, pancreas, small and large intestine, fore/glandular stomach, muscle, skin, and urinary bladder, also no abnormalities were detected (data not shown). In the dentate gyrus of the hippocampus, a prominent vacuolisation was found in the mutant animals (Fig. 34 k), which was absent in the controls (Fig. 34 e).
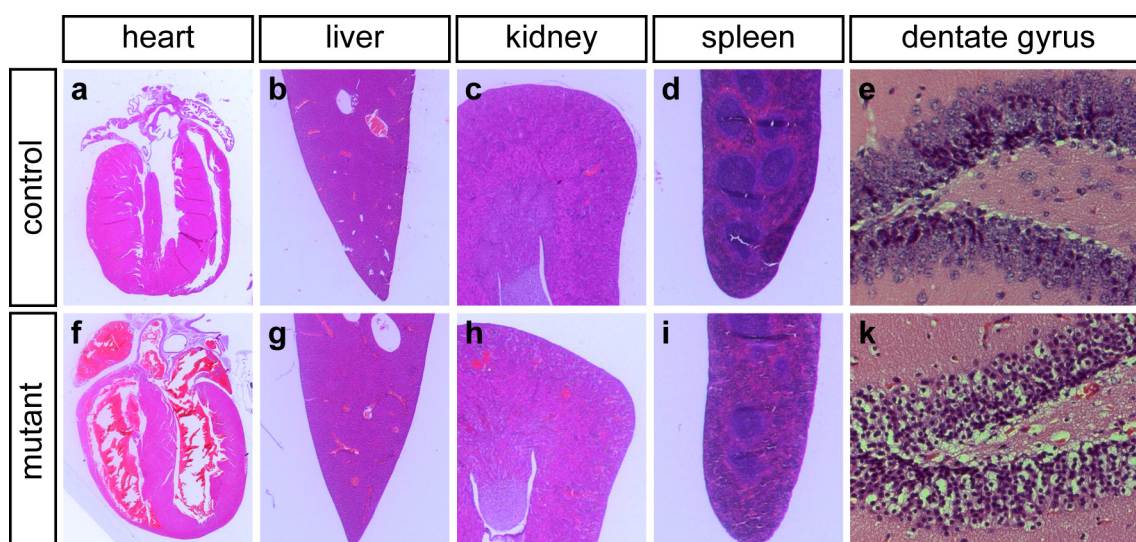
Fig. 34: Pathological analysis of representative Braf^{V600E} mice
Haematoxylin and eosin (HE) stainings of abdominal organs of Braf^{V600E} controls (**a-d**) and mutants (**f-i**) revealed no pathological abnormalities. In mutant animals, a vacuolisation was observed in the dentate gyrus of the hippocampus (**k**), which was absent in controls (**e**).

Subsequent analyses of histological stainings using Luxol fast blue (myelin marker) and antibodies detecting calbindin D28k (marker for cerebellar Purkinje cells), cleaved caspase 3 (apoptosis marker), glial fibrillary acidic protein, S100β (both astrocytic marker), and ionized calcium-binding adaptor molecule 1 (marker for inflammation) revealed no differences between mutants and controls (data not shown).

Taken together, the pathological analysis of the Braf^{V600E} mice did not disclose the reasons for the high mortality caused by the overactive ERK/MAPK signalling. All major organs were unaffected except from a vacuolisation in the granular cell layer of the dentate gyrus.

5 Discussion

The ERK/MAPK signalling pathway is one of the best studied and characterised signalling pathways in mammalian cells. It is activated by several different receptor kinases that recruit small GTPases, which in turn activate the ERK cascade. Numerous downstream targets of the ERKs are known and the function of the ERK/MAPK signalling has been implicated in many cellular processes like cell growth and proliferation. In addition, during the past two decades, increasing evidence linked the ERK/MAPK signalling pathway also to the modification of mood and emotional behaviour.

5.1 Generation of *Braf* knockout mice

In order to investigate the different roles of the ERK/MAPK signalling during the postnatal and adult life phase in the forebrain neurons of mice, I studied the phenotypes of conditional *Braf* knockout and knockin mouse lines in terms of circadian activity, neuronal transmission, gene expression, dendritogenesis, and emotional behaviour. The generation of the respective knockout and knockin mutants is described in the appropriate results section (4.1.2, 4.2.2, and 4.4).

5.1.1 Conditional *Braf* knockout mice

For the generation of a forebrain-specific knockout model, a CaMKIIα-Cre mouse line was used, which showed expression of the Cre recombinase in the cortex, hippocampus, and striatum (Minichiello et al., 1999). Anyhow, a *Rosa26* reporter assay of the mouse line that is maintained at the Helmholtz Zentrum München revealed a less specific expression pattern: Besides a strong expression in the expected forebrain regions, the Cre recombinase was also active in some regions of the mid- and hindbrain and of the spinal cord (Fig. 6). Nevertheless, prominent loss of the BRAF protein was only observed in the cortex, the hippocampus, the amygdala, and the striatum, but not in the mid- and hindbrain and the cerebellum (Fig. 8). Interestingly, the recombination of the *Braf* gene (Fig. 7) and the depletion of the BRAF protein (Fig. 8) were incomplete in the forebrain since the CaMKIIα promoter is inactive in interneurons (Fig. 9). The recombination of the *Braf* gene starts at two weeks of age and steadily in-

creases during the postnatal life phase until it reaches its maximum at eight weeks of age. In summary, although the CaMKIIα-Cre mouse line is not completely restricted to the forebrain, it is a useful tool for the conditional inactivation of target genes during the postnatal and adult life phase.

5.1.2 Inducible *Braf* knockout mice

In order to control the time point of recombination, the CaMKIIα-Cre mouse line was replaced by the inducible CaMKIIα-CreER^{T2} line, which was shown to be active only in the cortex, the hippocampus, the amygdala, and the hypothalamus (Erdmann et al., 2007). Using a *Rosa26* Cre reporter assay, this forebrain-specific pattern was confirmed (Fig. 20), demonstrating that the expression patterns of the CaMKIIα-Cre and CaMKIIα-CreER^{T2} lines are similar but not identical. However, an IHC analysis of Braf^{icko} mice showed BRAF depletion in the same regions compared to Braf^{cko} mutants (Fig. 21). For comparison of inducible and non-inducible conditional knockouts, these differences in Cre activity have to be considered as potential causes of phenotypes.

The earliest induction time point of the CreER^{T2} transgene is two weeks of age as i.p. treatment is harmful to younger animals and it is not possible to wean pups earlier for tamoxifen feeding. The progression of the recombination in Braf^{icko} mice is faster as compared to non-inducible Braf^{cko} mice: Two weeks after the first i.p. injection or three weeks after the first feeding with tamoxifen, respectively, the depletion of the BRAF protein is completed.

In summary, the CaMKIIα-CreER^{T2} mouse line represents a useful method for the time-specific knockout of *Braf* and the comparison of the loss of ERK/MAPK signalling during postnatal or adult life phases.

5.2 MAPK signalling and activity behaviour

5.2.1 Exploration and hyperactivity

In most of the behavioural tests, *Braf* deficient mice showed an overt phenotype in the latency to their first action. In Braf^cko mutants, this was observed in the modified hole board (mHB) and the elevated plus maze (EPM) (Fig. 5). Although the effect was weak in early induced Braf^icko mutants, the phenotype was observed in both paradigms (Fig. 22 and Fig. 23). In late Braf^icko mutants, which were not tested in the mHB, the latency was highly increased in the EPM (Fig. 23). Interestingly, in mutants with a *Braf* knockout restricted to the dorsal or the ventral hippocampus, the latencies to the first action were not altered (Fig. 28 and Fig. 29).

These results demonstrate an overall effect of the ERK/MAPK signalling pathway on the animal's response to a new environment. Whereas animals with normal ERK/MAPK signalling rapidly adapt to new situations and immediately start to explore, mutant animals take much longer for this adjustment. Given that the effect is present in adults after early and late *Braf* knockout induction, ERK/MAPK signalling is essential for this adaptation not only acutely during adulthood, but also chronically during the postnatal life phase. The fact that the phenotype does not appear in hippocampus-restricted *Braf* knockouts shows that the dorsal and ventral hippocampus are not exclusively involved in this phenotype but presumably in interaction with other forebrain regions.

In the accelerating rotarod test, a similar latency phenotype was observed in Braf^cko mice: Mutants were immobile at the beginning of the test, which subsequently led to an immediate dropping of the subject animal (Fig. 5). Early and late induced Braf^icko mice also showed a poor performance in the rotarod, however, given that this time the highly increased body weight caused the problems (Fig. 25), no conclusion could be drawn in regard to latency.

Even though an increased latency in the mHB and EPM and the poor performance in the rotarod can be correlated with hypoactivity, the observed phenotypes rather arise from a change in the exploration strategy. The delayed start of exploration is followed by a phase of hyperactivity characterised by

higher velocity in the behaviour tests and an easily startled and nervous behaviour in the home cage and the neurological test battery.

5.2.2 Circadian rhythm

The circadian rhythm in mammals is regulated by a transcription-translation feedback loop in the hypothalamic suprachiasmatic nucleus (SCN), which involves the main regulators *Clock*, *Bmal1*, *Per1/2*, and *Cry1/2* (Takahashi et al., 2008). Although this process acts cell-autonomously, it also receives extracellular signals that regulate the activation and the periodicity of the circadian rhythm via the ERK/MAPK pathway (Coogan and Piggins, 2004; Obrietan et al., 1998). ERK/MAPK signalling acts directly on the circadian transcription of *Bmal1* and *Per1/2*, as shown by pharmacological inhibition of the pathway (Akashi et al., 2008).

As shown in the gene expression study of CaMKIIα-Cre mice (Fig. 6), Cre recombinase is active in the SCN, resulting in a loss of ERK/MAPK signalling in this region of Braf^{cko} mutants. Nevertheless, the rhythmicity of the circadian clock in these animals was not altered (Fig. 12) as it is known from *Bmal1* knockout mice (Bunger et al., 2000). Animals were able to synchronise their activity to the endogenous rhythm and showed a clear separation of resting and activity phases. In addition, the period length, which was reduced in *Clock* knockout mice (Debruyne et al., 2006), was not altered in Braf^{cko} mutants (Fig. 12). Interestingly, mutants showed a reduced total running activity (Fig. 12), which was also present in *Bmal1* and *Clock* mutants (Bunger et al., 2000; Debruyne et al., 2006). Moreover, the activity patterns of Braf^{cko} mutants were clearly different from controls with a fragmentation during the active phase (Fig. 13) and an increase in total activity during the resting phase (Fig. 14).

These activity phenotypes are possibly caused by changes in the expression of specific target genes. In the hippocampus, the loss of ERK/MAPK signalling led to a decrease in *Per2* and *Bhlhe40* mRNA levels. As already mentioned, pharmacological MEK inhibition in the SCN resulted in a similar reduced expression of key regulators of the circadian network, including *Per2* (Akashi et al., 2008). *Bhlhe40* (also called *Dec1* or *Bhlhb2*) is another regulator of the cir-

cadian clock that interacts with *Bmal1* and represses the expression of other clock genes (Honma et al., 2002).

Taken together, the results from Braf[cko] mice suggest, that the ERK/MAPK signalling modulates the circadian clock by controlling the expression levels of several key regulators of the clock network. A loss of this control leads to alterations in the patterning of the diurnal activity but not to changes in period length and rhythmicity. The altered activity pattern could be the consequence of an abnormal sleeping behaviour with short sleep phases during the resting and active period. However, to understand the detailed mechanisms causing these phenotypes, further specialised investigations of the sleeping behaviour are necessary.

Abnormal regulation of circadian cycling and sleep disturbances are also common endophenotypes of psychiatric disorders like major depressive disorder, anxiety-related disorders, and bipolar disorder (Lenox et al., 2002; Wulff et al., 2010). Moreover, the already mentioned *Bhlhe40* controls the transcription of the *Bdnf* gene (Jiang et al., 2008), which is a common candidate for the predisposition for bipolar disorder. However, to gain a deeper insight into the interconnection of circadian clock genes and mood disorders, the basic principles of emotional behaviour have to be investigated beforehand in more detail.

5.3 MAPK signalling and emotional behaviour

As discussed in the introduction (3.1.3), the ERK/MAPK pathway was proposed to be important in the central nervous system for the establishment and control of emotional behaviour (Coyle and Duman, 2003). In already discussed human depressed patients treated with mood stabilizers or antidepressants, the activity of the ERK/MAPK signalling was found to be altered (Einat et al., 2003; Fumagalli et al., 2005; Hao et al., 2004; Kopnisky et al., 2003; Tiraboschi et al., 2004). The same conclusion was drawn from studies of post-mortem brains of untreated depressed patients (D'Sa and Duman, 2002), suggesting a role of ERK/MAPK signalling in mood disorders. However, little is known about the intracellular cascades and interactions involved in the regulation of emotional behaviours. Genetic mouse models have become useful tools for the investigation of the endophenotypes of mood disorders (Cryan and Holmes, 2005). In this work, I used the *Braf* knockout and knockin mouse models to study the involved brain regions, molecular mechanisms, and crucial phases of life that are involved in the modification of emotional behaviour by ERK/MAPK signalling.

5.3.1 Neuroanatomy of emotional behaviour

Previous studies using brain lesions, local pharmacological inhibition, and functional imaging were used to assign emotional behaviour to specific brain regions. As reviewed by Pratt et al. (1992), the most important brain areas for fear and anxiety are the limbic system with the amygdaloid complex and the hippocampus (for instinctive emotions), and the prefrontal cortex (for cognitive emotions). Depression shares similar brain regions, with the hippocampus, the frontal cortex, and the hypothalamic-pituitary-adrenal (HPA) axis as major components (Byrum et al., 1999).

The results of the behavioural analyses of the Braf[cko] and the early and late induced Braf[icko] mouse lines demonstrate the necessity of the ERK/MAPK pathway for the modification of emotions. Furthermore, given that the CaMKIIα-Cre and CaMKIIα-CreER[T2] mouse lines exhibit Cre recombinase activity only in forebrain regions (Fig. 6 and Fig. 20), the observed phenotypes in the EPM and

FST confirmed that these regions are involved into anxiety and depression-like behaviour.

Several recent publications suggest, that the hippocampus can be functionally separated into two structures (see review Fanselow and Dong, 2010). Accordingly, the dorsal hippocampus is mainly involved in certain forms of memory, whereas the ventral subregion, which is interconnected with the amygdala, was shown to play a role in anxiety-related behaviours (Bannerman et al., 2004).

To determine the effect of local hippocampal ERK/MAPK depletion on memory and emotional behaviour, *Braf* was knocked out exclusively in the two hippocampal subunits using a Cre recombinase-expressing viral vector. The memory-related parameters of the mHB revealed no differences in mutant animals of both experiments. However, in the mHB only object recognition memory is tested, whereas spatial memory, which is linked to the dorsal hippocampus, is not assessed. The behavioural tests related to emotional behaviour also showed no differences upon local hippocampal ERK/MAPK depletion. In the EPM, mutants demonstrated a normal aversion for open spaces and in the FST, depression-like behaviour was comparable between mutants and controls (Fig. 28 and Fig. 29). These results do not necessarily contradict the hypothesis of two spatially separated hippocampal subunits; however, they demonstrate that ERK/MAPK signalling in one single hippocampal subregion is not responsible for emotions. Rather the interplay of several regions, including the dorsal or ventral hippocampus, is required for the correct mediation of normal anxiety and depression.

5.3.2 Underlying molecular mechanisms

5.3.2.1 GABAergic signalling

It is well established that benzodiazepine anxiolytics, such as diazepam, facilitate GABAergic transmission in the mammalian CNS via positive allosteric modulation of the $GABA_A$ receptor complex (see review Rabow et al., 1995). Furthermore, it was shown that the GABAergic transmission is also modulated by intracellular phosphorylation mediated by the ERK/MAPK signalling (Bell-

Horner et al., 2006). This interaction was shown to act on the α1 subunit of the GABA$_A$ receptor, which is responsible for the sedative effect of diazepam (Rudolph et al., 1999). However, sequence analysis of the α2 subunit, which mediates the anxiolytic action of diazepam (Low et al., 2000), also revealed putative ERK1/2 binding and phosphorylation sites (P-site at position T393; own observations, data not shown). These facts suggest that the ERK/MAPK signalling possibly modulates the GABA$_A$ receptor by phosphorylation of the α2 subunit and thereby regulates anxiety behaviour.

To check whether an altered GABAergic neurotransmission might contribute to the low-anxiety phenotype of Braf^{cko} mice, slice electrophysiology of hippocampal neurons was performed. In the field potential measurements, the responses to GABA$_A$ receptor activation and inhibition were indifferent between the two Braf^{cko} genotypes. In addition, single cell measurements showed similar results in mutants and controls (Fig. 16). The results demonstrate that the GABAergic neurotransmission of Braf^{cko} mutants functions normal and that the loss of ERK/MAPK signalling has no effect on the activity and responsiveness of GABA$_A$ receptors in the hippocampus.

The results of the advanced analyses of the GABA$_A$ receptor inhibition disagree with the results of the preliminary experiment (Fig. 15), which can be explained by the replacement of bicuculline methiodide by the more specific receptor antagonist picrotoxin. Bicuculline methiodide was shown to inhibit not only the GABA$_A$ receptor, but also the small conductance calcium-activated potassium channels (SK channels) (Khawaled et al., 1999). Analysis of this SK channel signalling revealed changes in the response to SK channel modulators (Fig. 17), proving the idea of a GABA$_A$ receptor independent effect in the preliminary experiment. Although a recent publication suggests that the SK channels are implicated in anxiety behaviours (Mitra et al., 2009), the changes in channel activity are more likely related to the deficits in learning and memory that are prominent in the Braf^{cko} mutants (Chen et al., 2006a), as SK channels play an important role in hippocampal synaptic plasticity and long-term potentiation (Hammond et al., 2006). Nevertheless, the actual function of the SK chan-

nels in the Braf^{cko} animals is still unknown and further experiments are needed to clarify this mechanism.

5.3.2.2   Regulation of gene expression

As shown in the introduction, a major function of the ERK/MAPK signalling pathway is the modulation of gene expression. ERK1/2 predominantly activate two transcription factors, CREB1 and ELK-1, which subsequently regulate the promoter activity of a multitude of genes (see review Treisman, 1996). The aim of the gene expression study was to find direct downstream targets of the ERK/MAPK signalling, whose altered expression in the Braf^{cko} mutants might contribute to the behavioural phenotypes. To validate the functional relevance of these targets, the evolutionary conservation of the transcription factor binding sites was assessed (Cohen et al., 2006) as higher conservation implies higher relevance.

Twelve genes were determined that were differentially expressed in Braf^{cko} mutants and that exhibit conserved binding sites for CREB1 or ELK-1 (Table 4 and Table 7). Seven of them were highly conserved in at least six species, suggesting that these genes play fundamental physiological roles. Interestingly, all of these seven genes were conserved between mice and humans, which suggests similar functions in both species. This in turn suggests that associations between these genes and phenotypes found in mice are likely valid also in humans.

The two dual specificity phosphatases, *Dusp4* and *Dusp5*, are members of the ERK/MAPK pathway that negatively regulate its activity. *Gria3*, *D15Wsu169e*, *Spata13*, *Zfp326*, *Egr4*, and *Cacna1g* are not yet studied extensively und have not been linked to any behavioural phenotypes yet. In contrast, *Sst*, *Nos1*, *Bdnf*, and *Egr1* have already been implicated in emotional behaviours and will be hence discussed in more detail.

Intracerebroventricular administration of the neuropeptide somatostatin (SST) in adult rats led to weak anxiolytic and prominent antidepressant-like effects (Engin et al., 2008). An opposite phenotype with increased depression-like behaviour was observed in late induced Braf^{icko} animals. Given that the loss of

ERK/MAPK signalling in Braf^{cko} mice resulted in a reduction of SST, the antidepressant effect of SST could be confirmed by my results.

Neuronal NO synthase (*Nos1*), together with its product nitric oxide, was also implicated in the regulation of behavioural processes. The selective inhibition of NOS1 was shown to cause anxiolytic and antidepression-like effects (Volke et al., 2003). In addition, homozygous *Nos1* knockout mice displayed reduced anxiety in the EPM (Zhang et al., 2010). However, these results are contradictory to the anxiolytic phenotype of Braf^{cko} mutants that exhibited increased levels of *Nos1* mRNA.

The next interesting keyplayer, which was differentially expressed in Braf^{cko} mice and which harbours a conserved CREB binding site, is the *Bdnf* gene. The promoter of the *Bdnf* transcript variant 3, in which the conserved CREB binding site was found, was shown to be an initial target in the therapeutic action of the two mood stabilizers lithium and valproic acid (Yasuda et al., 2009). Moreover, the genetic variant BDNF^{Val66Met}, which was found in human patients, was shown to lead to an increase in anxiety-related behaviour (Chen et al., 2006b) and the same is true for the conditional deletion of the *Bdnf* receptor TrkB in adult hippocampal progenitor cells (Bergami et al., 2008). In contrary, in Braf^{cko} mutants, a decrease in *Bdnf* mRNA level followed by an anxiolytic effect was observed.

Finally, *Egr1*, a transcription factor downstream of the ERK/MAPK pathway, was implicated in anxiety, as *Egr1* knockout mice showed an anxiolytic phenotype in the EPM (Ko et al., 2005). This observation fits to the reduced *Egr1* mRNA level and the anxiolytic phenotype of Braf^{cko} mice.

Some of the emotional phenotypes found in literature are contradictory to the findings in the *Braf* knockout mutants. However, one has to keep in mind, that the experiments are not directly comparable in respect to spatial and temporal modification and that loss-of-function and gain-of-function mutations not necessarily lead to opposite effects. Likely, the interplay of different brain regions, as well as of levels and time points of the expression of effector genes, is important for the modulation of emotional behaviour. As shown for *C. elegans*, biological phenotypes that are controlled by the MAPK signalling are mediated by func-

tional groups of 2-10 interacting proteins (Arur et al., 2009). Therefore, further studies are required to decipher the functional roles of specific regulated genes in the emergence of the behavioural and morphological phenotype of Braf[cko] mice.

Interestingly, besides their roles in emotional behaviour, *Sst*, *Nos1*, *Egr1*, and *Bdnf* have also been linked to long-term potentiation and learning and memory. In addition, phenotypes in emotional behaviours and in memory exhibit a coincidence in several mouse models, e.g. in forebrain conditional *Braf* knockout mice (results at hand and Chen et al., 2006a). This indicates an interconnection of these two cellular processes that leads to a reciprocal dependency.

5.3.2.3   Effects on dendritogenesis

The loss of ERK/MAPK signalling in Braf[cko] mice also resulted in reduced levels of four genes related to neuronal development (Table 3). The adjacent analysis of granular neurons of the dentate gyrus showed a strong reduction in dendritic complexity apparent from reduced branching and a decrease in the total length of the dendrites (Fig. 18). In contrast, synaptogenesis and dendritic routing were not affected (Fig. 19).

Similar effects on dendritogenesis were found in a mouse model with a conditional knockout of the BDNF receptor TrkB, which exhibited reduced dendritic complexity in neurons of the CA3 region (Bergami et al., 2008). Moreover, the heterozygous knockout as well as the Val66Met mutation of the *Bdnf* gene diminishes the dendritic branching of hippocampal neurons (Chen et al., 2006b). As already discussed in the previous section (5.3.2.2), in these three models also phenotypes concerning anxiety behaviour were found, which suggests that emotional behaviours are dependent on a normal dendritogenesis. Hence, the anxiolytic phenotype in Braf[cko] possibly emerges due to the defective dendritic growth.

In this study, it was only possible to analyse granular neurons of the dentate gyrus. Since several other brain regions are linked with emotions, further investigations are required to gain deeper insights into the effects of dendritogenesis on emotional behaviours.

Nevertheless, the results of Braf^{cko} mice clearly demonstrate a time-specific effect of diminished ERK/MAPK signalling on neuronal growth. Dendritogenesis occurs only during embryonic and postnatal development and given that re-combination in Braf^{cko} mutants takes place shortly after birth, this emphasises postnatal brain development as crucial for the determination of anxiety in adults.

5.3.3 Developmental effects on emotional behaviours

As discussed in the preceding section, the ERK/MAPK signalling plays a role in the growth of hippocampal neurons during the postnatal development of the mouse brain. During this period of life, a rapid development of neuronal circuits occurs and the mature pattern of hippocampal connectivity is established. Moreover, Gross et al. (2002) demonstrated a critical role of the postnatal phase in the establishment of anxiety. Using a regulatable serotonin 1A receptor knockin mouse line, they showed the time-specific function of the receptor during postnatal development.

In order to distinguish whether the behavioural phenotypes of *Braf* conditional knockout mutants arise during the juvenile phase or during adulthood, I compared two groups of Braf^{icko} animals, which only differed in their point in time of induction.

Mutant mice that lost forebrain ERK/MAPK signalling shortly after birth showed a prominent anxiolytic phenotype, which was not found in adult induced mutants (Fig. 23). This demonstrates that the ERK/MAPK signalling influences anxiety only during the juvenile phase, but not in the adult brain. In contrast, early induced Braf^{icko} mutants displayed a normal depression-like phenotype, whereas the late induced mutants showed highly increased depression-like behaviour (Fig. 24). Although these results again demonstrate a time-specific role of the ERK/MAPK signalling in emotional behaviours, the question arises why the observed depression-like phenotype did not appear in early induced Braf^{icko} mice, which also exhibit a depleted ERK/MAPK signalling during the adult life phase. One possibility is that the early postnatal loss of ERK/MAPK signalling and the subsequently reduced anxiety modify the neuronal circuits that mediate depression-like behaviour. Another possibility is that early induced Braf^{icko} mice

indeed exhibit a depression-like phenotype, which is balanced to a normal level by the overlaying anxiolysis.

Another interesting fact is that the increase in depression-like phenotype, was accompanied by a reduction of swimming, but not of struggling (Fig. 24). The reason for this is unclear, but since struggling comprises only a minor fraction of active FST behaviour, further reduction is hard to detect.

In summary, the ERK/MAPK signalling is an important modifier of emotional behaviour that fulfils different roles during early postnatal development and adulthood. The anxiolytic phenotype of *Braf* mutants that loose BRAF activity shortly after birth emphasises the activity of ERK/MAPK instructed effectors that shape juvenile forebrain development to establish normal anxiety levels in adults.

Besides their emotional behaviour, further phenotypes were found in early and late induced Braf^{icko} mice. The body weight of induced mutants was highly increased in both groups (Fig. 25), indicating an acute effect of the loss of ERK/MAPK signalling independently of the life phase. Interestingly, in non-inducible Braf^{cko} mutants, who are comparable to early induced Braf^{icko}, a reduction in body weight was observed. It was described that administration of tamoxifen leads to a weight gain (Vogt et al., 2008), however, as only mutants but no controls showed this increase, this possibility could be ruled out. More likely, either the slightly different expression patterns of CaMKIIα-Cre and CaMKIIα-CreER^{T2} mice or the coincidence of deleted ERK/MAPK signalling and tamoxifen treatment is responsible for the opposite phenotypes.

Another parameter analysed was the latency to the first action, which was also found to be acutely altered by the loss of ERK/MAPK signalling. Independent from the point in time of induction, this phenotype was observed in Braf^{icko} as well as in Braf^{cko} mice (Fig. 5 and Fig. 23).

Finally, the learning deficit that was found in the rotarod experiment of Braf^{cko} mice (Fig. 5) was reproducible in early, but not in late induced Braf^{icko} mice (Fig. 25). This supposes a juvenile role of the ERK/MAPK signalling in learning. However, as all mutants showed an overall poor performance on the rotarod, the learning deficit could also be a secondary effect. To exclude this, further

behavioural analyses in paradigms specific for the different forms of learning and memory are necessary.

5.4 BRAF overactivity in forebrain neurons

In human patients suffering from neuro-cardio-facial-cutaneous syndromes, both loss-of-function and gain-of-function mutations in the members of the ERK/MAPK pathway were found. My analyses of the conditional *Braf* knockout mouse models revealed that the loss of ERK/MAPK signalling in forebrain neurons causes alterations in emotional behaviour. To investigate whether an increase in ERK/MAPK signalling activity also affects emotions, I studied the forebrain-specific Braf^{V600E} knockin mutation (Mercer et al., 2005). The V600E mutation results in a constitutively overactive BRAF kinase function (Wan et al., 2004).

5.4.1 Effects on physiology

The temporal analysis of the recombination activity of the CaMKIIα-Cre transgene in Braf^{cko} mice revealed that the Cre recombinase becomes active shortly after birth (Fig. 7). However, the forebrain-specific V600E knockin in Braf^{V600E,Cre} mutants leads to embryonic lethality so that no double-heterozygous offspring could be obtained. This fact suggests a low Cre activity already during embryonic development that is sufficient for a partial recombination of the floxed allele during this phase.

To circumvent this effect, inducible Braf^{V600E,CreER} mice were used to activate the mutation not until adulthood. Despite the high *in vitro* kinase activity of ^{V600E}BRAF (up to 700 times) (Wan et al., 2004), the phosphorylation of ERK1/2 was increased *in vivo* only 2-5 times (Fig. 31). Surprisingly, even in the cerebellum, where no CreER activity was detected in the reporter mouse assay, the ERK/MAPK signalling was overactivated. Either this result is misleading due to the low signal-to-noise ratio of the Western blotting, or the V600E knockin was weakly activated indeed in the cerebellum by a low, undetectable level of CreER.

High dose induction of adult Braf^{V600E,CreER} mutants led to their rapid death and even a low dose induction killed most mutants within three weeks (Fig. 32). One possible reason for the delayed phenotype in low dose animals could be a slower progress of recombination. However, it is unlikely that unmetabolised

tamoxifen is still present in the body three weeks after the i.p. injections. Rather a partial recombination in some, but not all cells of the forebrain could cause a less severe, but still lethal phenotype. *Braf* is a known oncogene, leading to carcinogenesis upon overactivation. However, as progression of the pathology was very fast, a metabolic effect for the lethality is more likely than a cancer-related cause. As shown in Fig. 32, the body weight of mutants declined already 60 hours after the first injection, whereas food intake and body temperature were normal until ~90 hours after the first injection. Moreover, leftovers of food were found in the stomach and intestines of affected animals, indicating that the refusal of food intake in the last hours was a secondary effect and did not initially cause the mortality.

The pathological analysis of the Braf^{V600E,CreER} mutants revealed a prominent vacuolisation of hippocampal granular neurons (Fig. 34). However, no alterations in glial and neuronal cell death, inflammation, and demyelination were found in mutants suggesting a normal histopathology. In addition, the search for secondary effects in all other major organs did not reveal any changes. Therefore, no explanation for the physiological phenotype of the Braf^{V600E,CreER} mutants was found and it remains unclear whether the hippocampal vacuolisation is the cause or the consequence of the phenotype.

In summary, the analysis of the physiology and pathology of Braf^{V600E,CreER} mice did not reveal any explanation for the lethality of the mutant animals. However, carcinogenesis, alterations in neuronal morphology (e.g. by neuronal degeneration), and starvation due to refusal of food intake could be excluded as causes of death.

5.4.2 Effects on behaviour

Mutant Braf^{V600E,CreER} animals displayed a strong locomotory phenotype in the open field test and the elevated plus maze. The overall distance travelled, the velocity, and the latency to the first action were strongly reduced (Fig. 33). This deficit in motility was caused by a form of lethargy that was present in all severely affected mutants. As defects in locomotion can mimic anxiety-like and depression-like phenotypes due to diminished exploration, no reliable statements on emotional behaviours can be made.

Therefore, the behavioural analysis of Braf^{V600E,CreER} mice did not allow any conclusion on the impact of an overactivation of ERK/MAPK signalling on emotional behaviour.

5.5   Conclusions and outlook

With the use of conditional *Braf* knockout mice, I was able to unravel new roles of the ERK/MAPK signalling pathway in emotional behaviour. Moreover, I demonstrated that the ERK/MAPK signalling in forebrain neurons is not only an important regulator of anxiety and depression-like behaviour, but also of gene expression, circadian rhythms, and dendritogenesis. Furthermore, my studies revealed for the first time, that the different roles of the ERK/MAPK signalling mediating emotional behaviours are dependent on the period of life. The juvenile life phase was found to be the critical period during which the ERK/MAPK signalling mediates the development of normal anxiety behaviour. In contrast, depression-like behaviour is modified by this pathway exclusively during the adulthood.
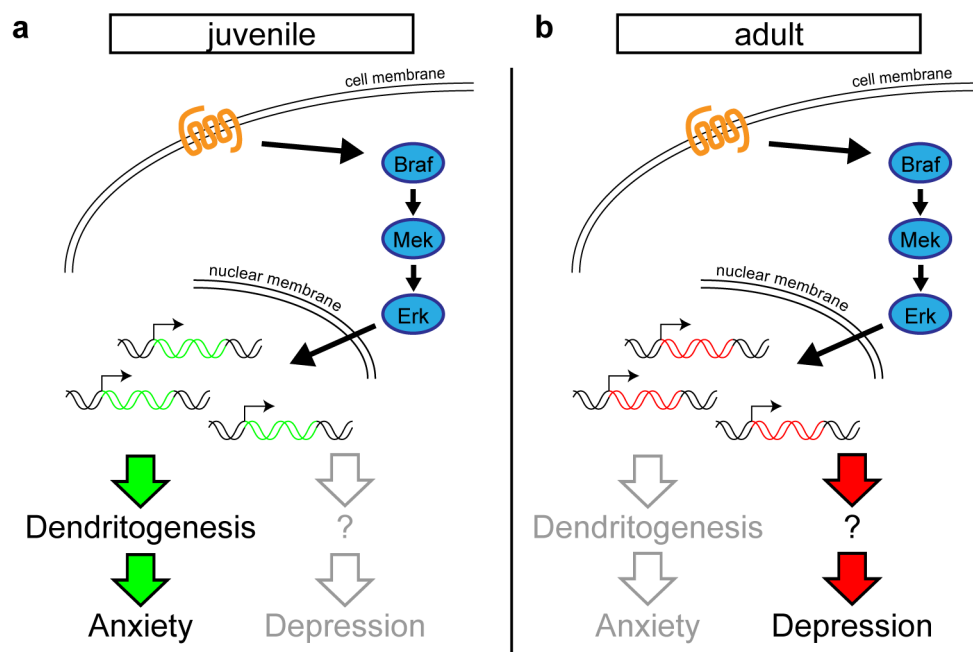
Fig. 35: Putative ERK/MAPK dependent regulation of emotional behaviours
a) During the juvenile phase of life, ERK/MAPK signalling regulates the expression of genes related to dendritogenesis, which in turn mediate normal anxiety. **b**) During adulthood, a different subset of genes is regulated by the ERK/MAPK pathway, thereby regulating depression-like behaviour.

The results of this study imply that, during juvenile brain development, ERK/MAPK signalling directly regulates the expression of important mediators of anxiety behaviour. These mediators then control at least partly the formation and maturation of neural circuits in the hippocampus, which are essential for the

establishment of normal anxiety behaviour (Fig. 35 a). In the adult brain, the ERK/MAPK signalling also regulates gene expression, but during this life phase either a different subset of genes is activated or the physiological effects differ, which results in altered depression-like behaviour (Fig. 35 b).

Although the present study gave new interesting insights into the role of the ERK/MAPK signalling in emotional behaviours and the associated molecular mechanisms, new questions and tasks arose that should be investigated in future experiments.

Especially the molecular processes in the adult brain should be studied in detail as most experiments in this study were done in Braf^{cko} mice, in which the knockout starts already postnatally. The analysis of gene expression of Braf^{cko} mice revealed interesting candidate genes for emotional behaviour, but it is unclear whether these genes are also differentially regulated if the ERK/MAPK pathway is inactivated only during adulthood. Furthermore, the analysis of the neuronal differentiation should be performed also in late induced Braf^{icko} mice. It is unlikely that the dendritic growth and arborisation is altered in these mice as the maturation of the circuits is completed during adolescent development. Anyhow, as neuronal networks in the brain exhibit a high plasticity, spine formation and synaptic activity should be investigated.

Another interesting field for future studies is the upstream activation of the ERK/MAPK signalling as initial mechanism in regulating emotional behaviour. Known activators of the ERK/MAPK signal in the adult brain are the corticotropin-releasing hormone receptor 1 (CRHR1) and the glucocorticoid receptor (GR) (Refojo et al., 2005; Revest et al., 2005) that act as receptors for the stress hormones CRH and corticosteroids, respectively. Various constitutive and conditional knockout mouse models, like mutants for *Crhr1* or the glucocorticoid receptor *Nr3c1* gene, exhibit reduced anxiety behaviour in adults (Muller et al., 2003; Tronche et al., 1999). Therefore, these two receptors are suitable candidates for further investigations of the upstream regulation of emotional behaviour in relation to stress.

Finally, the strong overactivation of the ERK/MAPK signalling did not allow a conclusion on behavioural modification due to the lethality of the hyperactive

knockin allele. The use of a different mouse model with a less active *Braf* knockin mutation could avoid this complication and answer the question whether an increase of ERK/MAPK signalling also affects anxiety and depression-like behaviour. This knowledge could contribute to the further understanding of the pathophysiology of mood disorders.

6 Materials

6.1 Instruments

autoclave	*Aigner*, type 667-1ST
balances	*Sartorius*, LC6201S, LC220-S
bottles for hybridization	*ThermoHybaid*
cassettes for autoradiography	*Amersham*, Hypercassette
centrifuges	*Sorvall*, Evolution RC; *Eppendorf*, 5415D, 5417R; *Heraeus*, Varifuge 3.0R, Multifuge 3L-R
chambers for electrophoresis (DNA)	*MWG Biotech*; *Peqlab*
cryostat	*Mikrom*, HM560
developing machine	*Agfa*, Curix 60
digital camera	*Zeiss*, AxioCam MRc
DNA/RNA electrophoresis chip analyzer	*Agilent*, 2100 Bioanalyzer
DNA sequencer	*Applied Biotech*, DNA Analyzer 3730
electric homogenizer	*IKA*, Ultra-Turrax T25 basic
electroporation system	*BioRad*, Gene Pulser XCell
freezer (−20 °C)	*Liebherr*
freezer (−80 °C)	*Heraeus* HFU 686 Basic
fridges (4 °C)	*Liebherr*
gel documentation system	*Herolab*, E.A.S.Y.
gel-/blottingsystem "Criterion"	*BioRad*
gel-/blottingsystem "Xcell SureLock™ Mini-Cell"	*Invitrogen*
glass homogenizer (tissue grinder, 2 mL)	*KIMBLE / KONTES*
glass pipettes	*Hirschmann*
glassware	*Schott*
ice machine	*Scotsman*, AF 30
imaging analyzer	*Fuji*, FLA-3000
incubators (for bacteria)	*New Brunswick Scientific*, innova 4230
incubators (for cell culture)	*Heraeus*
laminar flow	*Nunc* Microflow 2
light source for microscopy	*Leica* KL 1500
liquid scintillation counter	*Hidex*, Triathler
luminometer	*Berthold*, Orion I
magnetic stirrer / heater	*Heidolph*, MR3001
microscope	*Zeiss* Axioplan 2
microwave oven	*Sharp* R-937 IN
Neubauer counting chamber	*Brand*
oven for hybridisation	*Memmert*, UM 400; *MWG-Biotech*, Mini 10; *ThermoElectron*, Shake'n'Stack

PCR machine	*Eppendorf*, MasterCycler Gradient
perfusion pump	*Watson-Marlow Bredel*, 401U/D1
pH-meter	*InoLab*, pH Level 1
photometer	*Eppendorf*, Biophotometer 6131; *PeqLab*, NanoDrop ND-1000
pipette filler, electronic	*Eppendorf*, Easypet; *Hirschmann*, Pipettus akku
pipettes	*Gilson*, Pipetman P10, P20, P200, P1000
power supplies for electrophoresis	*Consort*, E443; *Pharmacia Biotech*, EPS200; *Thermo*, EC250-90, EC3000-90
radiation monitor	*Berthold*, LB122
Real-Time PCR system	*Applied Biosystems*, 7900HT
rotating rod apparatus	*Bioseb*, Letica LE 8200
running wheels (for mice)	*Med Associates*, low-profile wireless running wheel
shaker	*Heidolph*, Promax 2020
slide warmer	*Adamas instrument*, BV SW 85
sliding microtom	*Leica*, SM2000R
sonifier	*Branson* sonifier, cell disrupter B15
stereomicroscope	*Zeiss*, Stemi SV6
thermomixer	*Eppendorf*, comfort
ultramicrotom	*Microm*, HM 355S
UV-DNA/RNA-crosslinker	*Scotlab*, Crosslinker SL-8042; *Stratagene*, UV-Stratalinker 1800
UV-lamp	*Benda*, N-36
vortex	*Scientific Industries*, Vortex Genie 2
water bath	*Lauda*, ecoline RE 112; *Leica*, HI1210; *Memmert*, WB7
water conditioning system	*Millipore*, Milli-Q biocel

6.2   Chemicals

3,3'-diaminobenzidine (DAB)	*Sigma*
4-NBT (Nitro blue tetrazolium)	*Roche*
α-^{32}P-dCTP	*Amersham*
α-^{35}S-UTP	*Amersham*
β-mercaptoethanol	*Sigma, Gibco*
γ-^{32}P-dATP	*Amersham*
acetic acid	*Merck*
acetic anhydride	*Sigma*
agarose (for gel electrophoresis)	*Biozym*

albumin fraction V	*Roth*
aluminum potassium sulfate dodecahydrate	*Sigma*
ammonium acetate	*Merck*
ampicillin	*Sigma*
Ampuwa	*Fresenius*
Aquapolymount	*Polysciences*
bacto agar	*Difco*
bacto peptone	*BD Biosciences*
BCIP (5-bromo-4-chloro-3-indolyl phosphate)	*Roche*
bicine	*Fluka*
bis-tris	*Sigma*
Blocking reagent	*Roche, Perkin Elmer*
boric acid	*Merck*
bovine serum albumin (BSA, 20 mg/mL)	*NEB, Sigma*
bromphenol blue	*Sigma*
caesium chloride (CsCl)	*Sigma*
calcium chloride (CaCl$_2$)	*Sigma*
carrier DNA	*Sigma*
chicken serum	*Perbio*
chloral hydrate	*Sigma*
chlorobutanol	*Sigma*
chloroform	*Sigma*
citric acid	*Sigma*
Complete® Mini (protease inhibitors)	*Roche*
cresyl violet acetate	*Sigma*
dextran sulphate	*Sigma*
dimethylformamide	*Sigma*
dithiotreitol (DTT)	*Roche*
DMEM	*Gibco*
DMSO	*Sigma*
dNTP (100 mM dATP, dTTP, dCTP, dGTP)	*Fermentas*
EDTA	*Sigma*
EGTA	*Sigma*
Eosin Y	*Sigma*
ethanol absolute	*Merck*
ethidiumbromide	*Fluka*
ethylene glycol	*Sigma*
fetal calf serum (FCS)	*PAN, Hybond*
Ficoll 400	*Sigma*
formaldehyde	*Sigma*
formamide	*Sigma*
freezing medium	*Tissue Tek, OCT compound*
gelatin	*Sigma*

(D-)glucose	*Sigma*
glycerol	*Sigma*
hematoxylin	*Fluka*
Hepes	*Gibco, Sigma*
Hyb-mix	*Ambion*
hydrochloric acid (HCl)	*Merck*
hydrogen peroxide (30 %)	*Sigma*
iodoacetamide	*Sigma*
isopropanol	*Merck*
kanamycin	*Sigma*
kynurenic acid	*Sigma*
lidocaine N-ethyl bromide (QX-314)	*Sigma*
luxol fast blue MBS	*CHROMA*
magnesium chloride ($MgCl_2 \cdot 4H_2O$)	*Merck*
maleic acid	*Sigma*
MEM nonessential aminoacids	*Gibco*
MES hydrate	*Sigma*
methanol	*Merck*
mineral oil	*Sigma*
MOPS	*Sigma*
Nonidet P40 (NP-40)	*Fluka*
orange G	*Sigma*
paraformaldehyde	*Sigma*
PBS (for cell culture)	*Gibco*
Pertex mounting medium	*HDScientific*
phenol:chloroform:isoamyl alcohol	*Fluka*
PIPES	*Sigma*
potassium chloride (KCl)	*Merck*
potassium ferricyanide ($K_3Fe(CN)_6$)	*Sigma*
potassium ferrocyanide ($K_4Fe(CN)_6 \cdot 3H_2O$)	*Sigma*
potassium hydroxid (KOH)	*Sigma*
potassium phosphate ($KH_2PO_4 \cdot H_2O$, K_2HPO_4)	*Roth*
RapidHyb buffer	*Amersham*
RNaseZAP®	*Sigma*
Roti-HistoKit® II	*Roth*
Roti-Histol®	*Roth*
salmon sperm DNA	*Fluka*
S.O.C. medium	*Invitrogen*
sheep serum	*Gibco*
skim milk powder	*BD Biosciences*
sodium acetate (NaOAc)	*Merck, Sigma*
sodium chloride (NaCl)	*Merck*
sodium citrate	*Sigma*

sodium desoxycholate	*Sigma*
sodium dodecylsulfate (SDS)	*Merck*
sodium fluoride	*Sigma*
sodium hydrogen carbonate ($NaHCO_3$)	*Sigma*
sodium hydroxide (NaOH)	*Roth*
sodium iodate	*Sigma*
sodium phosphate ($NaH_2PO_4 \cdot H_2O$, Na_2HPO_4)	*Sigma*
spermidin	*Sigma*
sucrose	*Sigma*
sunflower seed oil	*Sigma*
tamoxifen free base	*Sigma*
triethanolamine	*Merck*
TriReagent	*Sigma*
Tris (Trizma-Base)	*Sigma*
Triton-X 100	*Biorad*
Trizol	*Invitrogen*
tRNA	*Roche*
trypsin	*Gibco*
tryptone	*BD Biosciences*
Tween 20	*Sigma*
X-Gal	*Fermentas*
xylol	*Fluka*
yeast extract	*Difco*

6.3   Consumables and others

1kb+ DNA Ladder	*Invitrogen*
cell culture dishes (Ø 30, 60, 100, 150 mm)	*Nunc*
cell strainer (100 µm)	*BD Biosciences*
centrifuge tubes (15 mL, 50 mL)	*Corning*
coverslips (24 x 50 mm, 24 x 60 mm)	*Menzel Gläser*
Criterion™ XT Bis-Tris-gels, 10 % (protein)	*BioRad*
cuvettes for electroporation (0.1 cm, 0.2 cm, 0.4 cm)	*Biorad*
embedding pots	*Polysciences, Peel-A-Way*
films for autoradiography	*Kodak: Biomax MS, Biomax MR*
filter paper	*Whatman 3MM*
filter tips 10 µL, 20 µL, 200 µL, 1 mL	*Art, Starlab*
FuGENE 6 transfection reagent	*Roche*
gloves	*Kimberley-Clark, Safeskin PFE Safeskin, Nitrile*
HiMark™ Pre-Stained protein standard	*Invitrogen*
Hybond N Plus (nylon membrane)	*Amersham*

Hyperfilm (chemiluminescence detection)	*Amersham*
HyperLadder I	*Bioline*
LASCRdiet® CreActive TAM400	*LASvendi*
MicroSpin S-300	*Amersham*
multiwell plates (6, 12, 48, 96 wells)	*Nunc*
Novex® Sharp pre-stained protein standard	*Invitrogen*
NuPAGE® Novex Bis-Tris gels, 10 % (protein)	*Invitrogen*
one-way needles (20G, 27G)	*Terumo, Neolus*
one-way syringes (1 mL, 10 mL, 20 mL)	*Terumo*
Pasteur pipettes	*Brand*
PCR reaction tubes (0.2 mL), lids	*Biozym*
Phase Lock Gel™, heavy	*Eppendorf*
pipette tips	*Gilson*
plastic pipettes (1 mL, 5 mL, 10 mL, 25 mL)	*Greiner*
PVDF membrane (protein)	*Pall Biosciences*
reaction tubes (0.5 mL, 1.5 mL, 2 mL)	*Eppendorf*
SeeBlue® Plus2 pre-stained protein standard	*Invitrogen*
slide mailers (end-opening)	*Heathrow Scientific*
SmartLadder DNA marker	*Eurogentec*
Superfrost Plus slides	*Menzel Gläser*
tissue cassettes	*Merck*
tissue embedding molds	*Polysciences*

6.4   Commonly used stock solutions

loading buffer for agarose gels	15 %	Ficoll 400
	200 mM	EDTA
	1-2 %	Orange G
paraformaldehyde solution (PFA, 4 %)	4 %	PFA w/v in PBS
PBS (1x)	171 mM	NaCl
	3.4 mM	KCl
	10 mM	Na_2HPO_4
	1.8 mM	KH_2PO_4
		pH 7.4
SSC (saline sodium citrate, 20x)	3 M	NaCl
	0.3 M	sodium citrate
		pH 7.0
sucrose solution (25 %)	25 %	sucrose w/v in PBS
TAE (10x)	0.4 M	Tris base
	0.1 M	acetate
	0.01 M	EDTA
TBE (10x)	0.89 M	Tris base
	0.89 M	boric acid
	0.02 M	EDTA

TBS (10x)	0.25 M	Tris-HCl pH 7.6
	1.37 M	NaCl
TBS-T (1x)	1x	TBS
	0.05 %	Tween 20
TE (Tris-EDTA)	10 mM	Tris-HCl pH 7.4
	1 mM	EDTA
Tris-HCl	1 M	Tris base
		pH 7.5

6.5   Kits

ECL Detection Kit	*Amersham*
ECL Plus Detection Kit	*Amersham*
FD Rapid GolgiStain™ Kit	*FD NeuroTechnologies*
High Prime DNA Labeling Kit	*Roche*
HiSpeed Plasmid Maxi Kit	*QIAGEN*
Illumina® TotalPrep RNA Amplification Kit	*Ambion*
MEF Nucleofector Kit 1	*Amaxa*
Pierce® BCA Protein Assay Kit	*Thermo Scientific*
Power SYBR® Green PCR Master Mix	*Applied Biosystems*
QIAGEN Plasmid Maxi Kit	*QIAGEN*
QIAprep Spin Miniprep Kit	*QIAGEN*
QIAquick Gel Extraction Kit	*QIAGEN*
QIAquick PCR Purification Kit	*QIAGEN*
RNA 6000 Nano Kit	*Agilent*
High-Capacity cDNA Reverse Transcription Kit	*Applied Biosystems*
Vectastain Elite ABC Kit	*Vector Labs*
Wizard Genomic DNA Purification Kit	*Promega*
Zero Blunt® TOPO® PCR Cloning Kit	*Invitrogen*

6.6   Molecular biology reagents

6.6.1   *E. coli* strains

DH5α	*Invitrogen*
Stbl2™	*Invitrogen*
SURE®	*Stratagene*

6.6.2   Solutions

LB medium (Luria-Bertani)	10 g	Bacto peptone
	5 g	yeast extract
	5 g	NaCl
	ad 1 L	H_2O
LB agar	98.5 %	LB-Medium
	1.5 %	Bacto agar
Ampicillin selection medium		LB medium with 50 µg/mL ampicillin
Kanamycin selection medium		LB medium with 25 µg/mL kanamycin
Ampicillin selection agar		LB agar with 100 µg/mL ampicillin
Kanamycin selection agar		LB agar with 50 µg/mL kanamycin

6.6.3   Southern blot analysis

Lysis buffer for genomic DNA extraction	50 mM	Tris-HCl pH 8.0
	100 mM	EDTA
	1 %	SDS
	100 mM	NaCl
	0.1 mg/mL	Proteinase K
Church buffer	0.5 M	Na_2HPO_4
	0.5 M	NaH_2PO_4
	1 %	BSA
	7 %	SDS
	1 mM	EDTA pH 8,0
	0.1 mg/mL	salmon sperm DNA
Denaturing solution	0.5 M	NaOH
	1.5 M	NaCl
Neutralising solution	0.1 M	Tris-HCl pH 7.5
	0.5 M	NaCl
Wash solution I	2x	SSC
	0.5 %	SDS
Wash solution II	1x	SSC
	0.5 %	SDS
Stripping solution	0.1x	SSC
	1 %	SDS
		boil in solution for 10 min

6.6.4 Western blot analysis

6.6.4.1 Solutions

Blocking solution	4 %	skim milk powder in TBS-T
Laemmli buffer (5x)	313 mM	Tris-HCl pH 6.8
	50 %	glycerol
	10 %	SDS
	0.05 %	bromphenolblue
	25 %	β-mercaptoethanol
MES running buffer (10x, for NuPAGE gels)	500 mM	MES
	500 mM	Tris
	1 %	SDS
	10 mM	EDTA
		pH 7.2
MOPS running buffer (10x, for Criterion gels)	500 mM	MOPS
	500 mM	Tris
	1 %	SDS
	10 mM	EDTA
		pH 7.7
NuPAGE transfer buffer (10x, for NuPAGE gels)	250 mM	bicine
	250 mM	Bis-Tris
	10 mM	EDTA
	0.05 mM	chlorobutanol
NuPAGE transfer buffer (1x, for NuPAGE gels)	10 %	10x NuPAGE transfer buffer
	10 %	methanol
RIPA buffer	50 mM	Tris-HCl pH 7.4
	1 %	NP-40
	0.25 %	sodium desoxycholate
	150 mM	NaCl
	1 mM	EDTA

6.6.4.2 Antibodies for Western blotting

Antibodies	Organism	Dilution	Company
α-βActin, monoclonal	mouse	1:100,000	Abcam
α-HPRT, polyclonal	rabbit	1:10,000	Santa Cruz Biotechnology
α-total-ERK1/2, polyclonal	rabbit	1:1,000	Cell Signaling Technology
α-phospho-ERK1/2, polyclonal	rabbit	1:1,000	Cell Signaling Technology
α-mouse, polyclonal, peroxidase-conjugated	goat	1:1,000	Jackson ImmunoResearch
α-rabbit, polyclonal, peroxidase-conjugated	goat	1:5,000	Dianova

6.6.5 Enzymes

Alkaline Phosphatase, Calf Intestinal (CIP)	*NEB*
Antarctic Phosphatase	*NEB*
Cre recombinase	*NEB*
DNA Polymerase (Phusion)	*NEB*
DNA Polymerase (Taq)	*Qiagen*
DNase I (RNase-free)	*Roche*
Klenow fragment of DNA Polymerase I	*NEB*
PCR-Mastermix 5x	*5 PRIME*
Polynucleotide kinase (PNK)	*NEB*
Proteinase K	*Roche*
Restriction enzymes	*NEB, Fermentas, Roche*
RNase A	*Serva*
T4 DNA ligase	*NEB*

6.6.6 Oligonucleotides

6.6.6.1 Oligonucleotides for genotyping

Name	Sequence	Conditions	Size of product
Braf_9 Braf_11 Braf_17	5'-GCA TAG CGC ATA TGC TCA CA-3' 5'-CCA TGC TCT AAC TAG TGC TG-3' 5'-GTT GAC CTT GAA CTT TCT CC-3'	94 °C 45 sec 60 °C 60 sec 30x 72 °C 60 sec	wt: 357 bp flox: 413 bp del: 282 bp
Cre1 Cre2	5'-ATG CCC AAG AAG AAG AGG AAG GT-3' 5'-GAA ATC AGT GCG TTC GAA CGC T-3'	94 °C 30 sec 55 °C 40 sec 30x 72 °C 60 sec	mut: 447 bp
CreER1 CreER2 CreER3	5'-GGT TCT CCG TTT GCA CTC AGG-3' 5'-CTG CAT GCA CGG GAC AGC TCT-3' 5'-GCT TGC AGG TAC AGG AGG TAG T-3'	95 °C 30 sec 63 °C 60 sec 35x 72 °C 60 sec	wt: 290 bp mut: 375 bp
R26R-D1 R26R-R1 R26R-Mut	5'-CCA AAG TCG CTC TGA GTT GTT AT-3' 5'-CAC ACC AGG TTA GCC TTT AAG CC-3' 5'-GCG AAG AGT TTG TCC TCA ACC-3'	94 °C 60 sec 57 °C 60 sec 30x 72 °C 60 sec	wt: 254 bp mut: 320 bp
V600E-A V600E-B V600E-C	5'-GCC CAG GCT CTT TAT GAG AA-3' 5'-GCT TGG CTG GAC GTA AAC TC-3' 5'-AGT CAA TCA TCC ACA GAG ACC T-3'	94 °C 30 sec 60 °C 30 sec 35x 72 °C 30 sec	wt: 466 bp mut: 518 bp

6.6.6.2   Oligonucleotides for PCR amplification

Name	Sequence	Conditions	Size of product
Brafprobefor Brafproberev	5'-AGG CAC AGG AAC TTG GGA GT-3' 5'-TCC GAG GAT GAG GAA GAA GA-3'	98 °C 10 sec 64 °C 30 sec 35x 72 °C 90 sec	440 bp (Southern blot probe)

6.7   Stereotactic injections

6.7.1   Equipment

Lab Standard Stereotaxic Instrument	*Stoelting*
Nanoliter 2000 injector	*World Precision Instruments*
Glass capillary puller (PC-10)	*Narishige*
Glass capillaries	*World Precision Instruments*
Suture (Marlin violett HR 17)	*Catgut*

6.7.2   Virus preparations

Name	Virus type	Transgene	Produced by
AAV-1/2 SEWB "V"	Adeno-associated virus	*EGFP*	S. Kügler, University of Göttingen
AAV-1/2 6P CRE EWB "I"	Adeno-associated virus	*Cre, EGFP*	S. Kügler, University of Göttingen

6.8   Gene expression analysis

6.8.1   Microarray chips

MouseWG-6 v1.1 Expression BeadChip	*Illumina*

6.8.2   TaqMan PCR assays

Gene name	Assay ID	Supplier
Bhlhe40	Mm00478593_m1	*Applied Biosystems*
Npy	Mm00445771_m1	*Applied Biosystems*
Oxr1	Mm00504603_m1	*Applied Biosystems*
Per2	Mm00478113_m1	*Applied Biosystems*

6.8.3   Primer pairs for SYBR Green PCR assays

Gene name	Primer pairs (forward & reverse)	Size of product
Bach2	5'-GAA GTG AGG GTT CTG AAA CA-3' 5'-TGA GTG TCC ACC TTG TTC AT-3'	104 bp
Bcl6	5'-AGA CTC TGA AGA GCC ATC TG-3' 5'-GGT TAC ACT TCT CAC AAT GGT AAG-3'	65 bp
Bdnf	5'-CTG CCT TGA TGT TTA CTT TGA C-3' 5'-GCA ACC GAA GTA TGA AAT AAC C-3'	105 bp
Camk1g	5'-GAG AAG ATC AAA GAG GGT TAC TAC-3' 5'-AAA TCC TTG GCT GAC TCA GA-3'	73 bp
Cck	5'-CCA TCC AAA GCC ATG AAG AG-3' 5'-GTA GCT TCT GCA GGG ACT AC-3'	97 bp
Cdca7l	5'-CTC CCA GTG ACG ATG AAG AG-3' 5'-CAC ATT CTG CTG TTT CTC CAA-3'	112 bp
Chd4	5'-CCT ACA CAA AGT CCT GAA ACA-3' 5'-TTC CGC TCT GAC ATC TGT AA-3'	125 bp
Crhbp	5'-GGG ATT TCC TGA AGG TAT TTG A-3' 5'-GTA AGA CCA CTC TCA CAG AAA TC-3'	117 bp
Dusp4	5'-TCT CTT CAG ACT GTC CCA AT-3' 5'-CTT TAC TGC GTC GAT GTA CT-3'	127 bp
Dusp5	5'-CAC CTA CAC TAC AAG TGG AT-3' 5'-TCC CTG ACA CAG TCA ATA AA-3'	97 bp
Dusp6	5'-CCC AAT TTG CCC AAT CTG TT-3' 5'-CCT CGG GCT TCA TCT ATG AAA-3'	130 bp
Egr1	5'-GAA CAA CCC TAT GAG CAC CT-3' 5'-CCA TCG CCT TCT CAT TAT TCA G-3'	69 bp
Egr4	5'-TAT CCT GGA GGC GAC TTC TT-3' 5'-CAG GAA GCA GGA GTC TGT TAA-3'	77 bp
Etv1	5'-GCC TTC AGG TTG ATA GAA GTC-3' 5'-TCT GCT CCT CTT CGC AAA TA-3'	94 bp
Etv5	5'-CTC ACT CAC TTC CAG AAC CT-3' 5'-CTG TCG CTG AAA TCT CTG TT-3'	130 bp
Gria3	5'-GCC TAT GAA ATA GCC AAA CAC-3' 5'-ATC AGC TCT TCC ATA GAC AAG-3'	134 bp
Homer1	5'-ACT GTT TAT GGA CTG GGA TTC T-3' 5'-TCC TGC TGA TTC CTG TGA AG-3'	149 bp
Klk8	5'-CCC TCA AGA GAA CTT TCC AA-3' 5'-CAC ACT TGT TCT GGG AAT AGA T-3'	67 bp
Lmo2	5'-CCT CTA CTA CAA GCT GGG AC-3' 5'-CCA GGT GAT ACA CTT TGT CTT T-3'	142 bp

Mycl1	5'-CAG CGA TTC TGA AGG TGA AG-3' 5'-CTG TTG GTG GAT AGA GAT ATG GA-3'	144 bp
Neurod2	5'-GGG AAC AAT GAA ATA AGC GAG A-3' 5'-GCA TGG TGC CTC AGA GA-3'	105 bp
Pgk1 (control)	5'-GAG CCC ATA GCT CCA TGG T-3' 5'-ACT TTA GCG CCT CCC AAG A-3'	139 bp
Prss12	5'-TGA GCA ATG TCC AAA GAG TT-3' 5'-TGA CAC CAT CTG TTA GAG GAA-3'	91 bp
Rasd1	5'-TAT CCT CAC AGG AGA CGT TT-3' 5'-TTT GTT CTT GAG ACA GGA CTT G-3'	117 bp
Spred1	5'-GTC AGC CAG ATA CCA TTC AG-3' 5'-GCT CCC ACA TTC CTT AGA TAT T-3'	92 bp
Zbtb7	5'-GAT TCA CCA GAC AGG ACA AG-3' 5'-GGT TCT TCA GGT CGT AGT TG-3'	113 bp
Zfpm1	5'-CTG TGC AGG AAC CAG TAG AA-3' 5'-AAG ACG TCC TTG TTG ATG ACT-3'	120 bp
Zfpm2	5'-TAA CAA AGG TGA TGA CGA AGG A-3' 5'-TGT CCT GGT TTG TCT GAA TG-3'	74 bp

6.9   Histological methods

6.9.1   Solutions

cryo protection solution	30 %	ethylene glycol
	30 %	glycerol
	in	PBS
PBS-T	0.2 %	Triton-X-100
	in	PBS
TBS	0.05 M	Tris-HCl pH 7.5
	0.15 M	NaCl
	0.1 mM	NaF
TB	0.05 M	Tris-HCl pH 7.5
TBS-T	0.2 %	Triton-X-100
	in	TBS

6.9.2   Antibodies for histology

Antibodies	Organism	Dilution	Company
α-GFP, polyclonal	chicken	1:1,000	Aves Labs
α-BRAF, polyclonal	rabbit	1:100	Santa Cruz Biotechnology
α-phospho-ERK1/2, polyclonal	rabbit	1:100	Cell Signaling Technology

α-NeuN, monoclonal	mouse	1:200	Chemicon
α-Parvalbumin, polyclonal	mouse	1:2,000	Swant
α-chicken, polyclonal, FITC-conjugated	donkey	1:400	Jackson ImmunoResearch
α-rabbit, polyclonal, biotinylated	goat	1:300	Dianova
α-mouse, polyclonal, Cy2-conjugated	goat	1:300	Jackson ImmunoResearch
α-mouse, polyclonal, Cy3-conjugated	goat	1:300	Jackson ImmunoResearch

6.9.3 LacZ staining solutions

LacZ fix	4 %	PFA
	5 mM	EGTA
	10 mM	$MgCl_2$
	in	PBS
LacZ staining solution *prepare fresh, protect from light*	1 mg/mL	X-Gal
	5 mM	potassium ferricyanide
	5 mM	potassium ferrocyanide
	in	PBS

6.9.4 Staining solutions

cresyl violet staining solution	0.5 %	cresyl violet acetate
	2.5 mM	sodium acetate
	0.31 %	acetic acid
	ad 500 mL	H_2O
		filter before use
eosin-red staining solution	0.1 %	Eosin-Y solution
	in	H_2O
luxol fast blue staining solution	0.1 %	luxol fast blue
	solve in	96% ethanol
	0.05 %	acetic acid
Mayer's hematoxylin	0.1 %	hematoxylin
	0.02 %	sodium iodate
	5 %	aluminum potassium sulfate dodecahydrate
	5 %	chloral hydrate
	0.1 %	citric acid
	in	H_2O
		filter before use

6.10 Slice electrophysiology

6.10.1 Equipment

CCD camera (contrast-enhanced)	*Hamamatsu Photonics*
Multiclamp 700B microelectrode amplifier	*Molecular Devices*
Digidata 1440A data acquisition interface	*Molecular Devices*
pCLAMP 10 software	*Molecular Devices*
Clampfit 10 software	*Molecular Devices*

6.10.2 Solutions

high-sucrose solution	75 mM	sucrose
	87 mM	NaCl
	3 mM	KCl
	0.5 mM	$CaCl_2$
	7 mM	$MgCl_2$
	1.25 mM	NaH_2PO_4
	25 mM	$NaHCO_3$
	10 mM	D-glucose
artificial cerebrospinal fluid (ACSF)	125 mM	NaCl
	3 mM	KCl
	2 mM	$CaCl_2$
	2 mM	$MgCl_2$
	1.25 mM	NaH_2PO_4
	25 mM	$NaHCO_3$
	10 mM	D-glucose
		pH 7.4
modified artificial cerebrospinal fluid	125 mM	NaCl
	3 mM	KCl
	1 mM	$CaCl_2$
	3 mM	$MgCl_2$
	1.25 mM	NaH_2PO_4
	25 mM	$NaHCO_3$
	10 mM	D-glucose
		pH 7.4
patch pipette solution	130 mM	CsCl
	3 mM	$MgCl_2$
	5 mM	EGTA
	5 mM	Hepes
	2 mM	Na_2-ATP
	0.3 mM	Na-GTP
	5 mM	QX-314
		pH 7.25

6.11 Mouse strains

6.11.1 Wild-type and other used mouse strains

C57BL/6J	Wild-type inbred mouse line
Braf^{flox} (Chen et al., 2006a)	Conditional *Braf* knockout mouse line, carrying a floxed exon 14 of the endogenous *Braf* gene
Rosa26 Cre reporter (Soriano, 1999)	Reporter mouse line, carrying a floxed *lacZ* gene in the *Rosa26* locus.
CaMKIIα-Cre (Minichiello et al., 1999)	Mouse line expressing the Cre recombinase under the control of the CaMKIIα promoter; active in forebrain excitatory neurons and partially in further CNS areas starting P14.
CaMKIIα-CreER^{T2} (Erdmann et al., 2007)	Mouse line expressing the inducible CreER^{T2} recombinase under the control of the CaMKIIα promoter; active in forebrain excitatory neurons and partially in further CNS areas starting P14.
Braf^{V600E} (Mercer et al., 2005)	Conditional *Braf* knockin mouse line, carrying a gain-of-function mutation (V600E) and a floxed knockin cDNA for wild-type exons 18-22

6.11.2 Generated mouse lines

Name, short	Description
Braf^{cko}	Braf^{flox} x CaMKIIα-Cre
Braf^{icko}	Braf^{flox} x CaMKIIα-CreER^{T2}
R26R^{Cre}	*Rosa26* Cre reporter x CaMKIIα-Cre
R26R^{CreER}	*Rosa26* Cre reporter x CaMKIIα-CreER^{T2}
Braf^{V600E,Cre}	Braf^{V600E} x CaMKIIα-Cre
Braf^{V600E,CreER}	Braf^{V600E} x CaMKIIα-CreER^{T2}

7 Methods

7.1 Molecular biology

7.1.1 Cloning and work with plasmid DNA

7.1.1.1 Production and transformation of competent bacteria

For cloning of plasmid DNA, electro competent *E. coli* bacteria were used. For normal plasmids, the conventional DH5α strain was used; for more complicated plasmids (i.e. containing hairpins or inverted terminal repeats), the recombination deficient strains SURE® and Stabl2™ were applied. Electro competent bacteria were prepared as follows: From an after-overnight culture at 37 °C on a LB agar plate without antibiotic selection, a single colony was picked and inoculated in 5 mL of LB medium. After incubation over night at 37 °C, 2.5 mL of the preparatory culture were transferred to 250 mL LB medium and incubated on an orbital shaker at 37 °C. The extinction of the bacteria solution was checked regularly with a photometer at 600 nm until it reached 0.5. The absorption should not exceed 0.65. The bacteria suspension was split in four 50 mL tubes and cooled down on ice for 10 minutes. Then, the tubes were centrifuged at 4000x g for 15 min at 4 °C. The supernatants were discarded and the pellets were carefully resolved in 25 mL of ice-cold 10 % glycerol and pooled in two 50 mL tubes. Centrifugation procedure was repeated twice and finally the bacteria were resuspended in 800 µL of 10 % glycerol, split in aliquots of 50 µL, and stored at −80 °C. The transformation efficiency was checked for each batch by transformation with 10 pg pUC18 control plasmid.

For one transformation, one aliquot of electro competent *E. coli* was thawed on ice and 1 µL of ligation batch or 10 pg of pure plasmid were added. The suspension was mixed carefully and then transferred into an electroporation cuvette. Electroporation was performed with a Biorad electroporation system following the manufacturer's instructions and then the cell suspension was transferred immediately to 1 mL SOC medium and incubated at 37 °C for 30-60 min. Afterwards, the bacteria were plated on LB agar plates containing an appropri-

ate antibiotic and incubated over night at 37 °C. Typically, 100 μg ampicillin or 50 μg kanamycin were used for selection of transformed clones.

7.1.1.2 Preparation of plasmid DNA

Plasmid DNA was isolated from transformed bacteria using the following kits: The Qiagen MiniPrep Kit for screening for correctly transformed clones and the Qiagen Plasmid Maxi Kit or Qiagen HiSpeed Plasmid Maxi Kit for higher yield plasmid preparation.

For MiniPrep production, a single colony was inoculated in 5 mL LB medium with antibiotic overnight at 37 °C. For MaxiPrep production, 150 μL of MiniPrep culture were added to 150 mL LB medium with antibiotic and incubated overnight at 37 °C.

After isolation of the DNA, the concentration was determined with a spectrophotometer. The optical density (OD) was measured at a wavelength of 260 nm and the concentration was calculated (OD_{260} = 1.0 corresponds to 50 μg/mL double stranded and 33 μg/mL single stranded DNA).

7.1.1.3 Restriction digest of plasmid DNA

For the digestion of plasmid DNA, 2 units (U) of restriction enzyme were used per μg of DNA. The reaction conditions and the type of buffer were chosen following the manufacturer's instructions. The restriction digest was incubated for 1-2 hours at 37 °C (unless a different temperature was recommended for the used enzyme). For the generation of blunt ends, the digested DNA was incubated with Klenow fragment of DNA polymerase I. Therefore, 5 U Klenow fragment and 25 nM dNTPs were added and incubated at RT for 20 min. Afterwards, Klenow fragment was inactivated by incubation at 75 °C for 20 min.

In order to prevent unwanted religation of the opened plasmid, the terminal phosphates of the vector fragment were removed. Therefore, 10 U alkaline phosphatase (CIP) or 5 U antarctic phosphatase were added and incubated at 37 °C for 45 min.

7.1.1.4 Isolation of DNA fragments

After restriction digest, the DNA fragments were separated by gel electrophoresis. DNA samples were supplemented with DNA loading buffer and loaded on

agarose gels containing ethidium bromide for visualisation of the DNA. For general purpose, 0.9 % agarose gels and for larger fragments 2-4 % agarose gels were used. The gel run was performed in 1x TAE buffer at a voltage of 100 V for 30-60 min dependent on the size of the fragments. After the separation of the bands, the DNA was visualised using long wave UV light (366 nm) and the appropriated bands were cut out using a scalpel.

The DNA was extracted from the gel slice using the Qiagen Gel Extraction Kit following the manufacturer's instructions. After elution, the DNA concentration was determined by spectrophotometry.

7.1.1.5   Ligation of DNA fragments

For the ligation of the linearised vector and the insert, 100 ng of vector DNA and 1/3 (molar ratio) of insert were mixed. For very short inserts (<500 bp) a molar ratio of 1:6 was used. T4 DNA ligase buffer and 600 U T4 DNA ligase were added in a total volume of 15 µL. The reaction was incubated for 1 hour at RT for sticky end ligation or overnight at 16 °C for blunt end ligation. Afterwards, 1 µL of the reaction batch was used for transformation (7.1.1.1).

7.1.2 Analysis of genomic DNA

7.1.2.1   Isolation of genomic DNA

Genomic DNA from mouse tails for genotyping was isolated using the Promega Wizard genomic DNA purification kit following manufacturer's instructions. Genomic DNA from brain samples for large-scale DNA extraction was isolated using the phenol/chloroform method. Therefore, the tissue was homogenised in lysis buffer using a glass homogeniser and then extracted with phenol/chloroform/isoamyl alcohol (ratio 25:24:1).

7.1.2.2   Polymerase Chain Reaction (PCR)

For the amplification of DNA fragments from either genomic or plasmid DNA, a polymerase chain reaction (PCR) was performed. For common 2-primer genotyping reactions, a 5x PCR MasterMix was used – for 3-primer genotyping or difficult templates, the following reaction batch was used:

0.5 µL template DNA (1-10 µg)

2.5 µL 10x PCR buffer

0.5 µL Primer 1 (10 µM)

0.5 µL Primer 2 (10 µM)

0.5 µL Primer 3 (10 µM)

0.5 µL dNTP mix (10 mM each)

0.2 µL DNA polymerase (Taq or Phusion)

ad 25 µL H_2O

The specific conditions (i.e. primer sequences, initiation/annealing/elongation temperatures, cycle duration, and number of repetitions) were adjusted individually for each PCR and can be found in the materials section (6.6.6).

7.1.2.3 Southern Blot analysis

For Southern blot analysis, approximately 6 µg of genomic DNA were digested overnight with 30 U of the appropriate restriction enzyme in a total volume of 30 µL. Then, additional 10 U of enzyme were added and again incubated for 4 hours. Digested DNA was separated on a 0.8 % agarose gel with TBE as running buffer for 15 to 18 hours at 30-55 V, dependent on the size of the expected bands. After the run, the DNA in the gel was denatured by shaking for 1 hour in denaturing solution. Then, neutralisation was performed by shaking the gel for 1 hour in neutralising solution and subsequent rinsing with 2x SSC. Blotting was performed overnight via capillary transfer using 20x SSC and a nylon membrane. After the transfer, the membrane was rinsed briefly with 2x SSC and crosslinked by UV radiation before proceeding with the hybridisation.

50 to 100 ng of DNA probe were radioactively labelled with α-^{32}P-dCTP using the Roche HighPrime Kit following manufacturer's instructions. To remove unincorporated radioactive nucleotides, Microspin S-300 columns were used. The labelling efficiency was determined by measuring 1 µL probe in a liquid scintillation counter.

Before hybridisation, the membrane was preincubated with Church buffer for 1 hour at 65 °C in a hybridisation bottle. Meanwhile, the labelled probe was denatured for 5 min at 95 °C, chilled on ice, and then added to the Church buffer to a final activity of 100,000 to 900,000 cpm/mL. The membrane was hybridised

at 65 °C for 5 hours to overnight. Afterwards, in order to remove unbound and unspecifically hybridised probe, the membrane was washed two times with pre-warmed wash solution I at 65 °C for 30 min. If necessary, a third washing step with wash solution II at 65 °C for 30 min was added.

For detection of the signal, the hybridised membrane was wrapped in saran wrap and exposed to an autoradiography film for 1-2 days at −80 °C. To increase the intensity of the signal, Biomax MS films together with Biomax screens were used. After exposure, the films were developed using a developing machine.

If the membrane should be used for hybridisation with a second probe after the first detection, the first probe could be washed away with stripping solution. Therefore, the membrane was boiled 5-10 min in stripping solution and briefly rinsed with 2x SSC before the prehybridisation could be started.

7.1.3 Analysis of RNA

7.1.3.1   Sample preparation and isolation of RNA

For all RNA work, RNAse free solutions, tubes, and pipette tips were used. The working place and all glass and plastic equipments were cleaned with RNa-seZAP® or 70 % ethanol and rinsed with Milli-Q water before use. Samples were handled with fresh gloves and kept on ice to reduce RNA degradation.

For the preparation of the brains, mice were asphyxiated with CO_2, decapitated, and the brains were dissected removing bones and meninges. Either the whole brain or dissected parts of it were immediately frozen on dry ice and stored at −80 °C until further processing.

Total RNA from tissue samples was isolated by guanidinium thiocyanate-phenol-chloroform extraction (Chomczynski and Sacchi, 1987) using Trizol or TriReagent. RNA concentration was measured by spectrophotometry with an OD_{260} of 1.0 corresponding to a concentration of 40 µg/mL. RNA was stored at −80 °C until further processing.

To determine the integrity and quality of the RNA, the samples were analysed on an RNA electrophoresis chip using the Agilent 2100 Bioanalyzer. RNA 6000 Nano Chips were prepared and used following manufacturer's instructions

and an RIN (RNA integrity number) of 6.0 was used as minimum threshold for following experiments.

7.1.3.2   Microarray analysis

For the microarray analysis, labelled cRNA was prepared using the Illumina To-talPrep RNA Amplification Kit following the manufacturer's instructions with 500 ng of total RNA as starting material. Quality and concentration of the cRNA products were determined using an RNA electrophoresis chip (see previous section). cRNA was stored at −80 °C until further processing.

The gene expression analysis was performed in collaboration with P. Weber and C. Kühne at the Max Planck Institute of Psychiatry in Munich. Whole ge-nome arrays (Illumina MouseWG-6 v1.1 Expression BeadChips), yielding 46657 gene probes, were used following the "Whole-Genome Gene Expression Direct Hybridization Assay Guide". Statistical analysis of the results was done by P. Weber and Dr. B. Pütz.

7.1.3.3   Quantitative Real-Time PCR

For the quantitative real-time PCR (qPCR) we either used pre-designed TaqMan® Gene Expression Assays (Applied Biosystems) or self-designed SYBR® Green PCR assays. β-Actin and Pgk served as positive controls and for the normalisation of the results. Primer pairs for SYBR® Green PCR assays were designed using the PerlPrimer software, version 1.1.17 (Marshall, 2004).

The cDNA synthesis by reverse transcription (RT) was performed using the High-Capacity cDNA Reverse Transcription Kit (Applied Biosystems). The fol-lowing reaction batch was used:

10 µL	RNA template
2.0 µL	10x RT buffer
0.8 µL	25x dNTP Mix (100mM)
2.0 µL	10x RT random primers
1.0 µL	RNase inhibitor
1.0 µL	MultiScribe™ Reverse Transcriptase
ad 20 µL	nuclease-free H_2O

The reaction batch was incubated at 25 °C for 10 min and then at 37 °C for 120 min. The reaction was stopped at 85 °C for 5 sec and the cDNA was stored at 4 °C or −20 °C until further progression.

For the quantitative analysis of the cDNA by TaqMan® Gene Expression Assays, 50 ng of cDNA were applied to the following real-time PCR batch:

4 µL	cDNA template
10 µL	2x TaqMan® Universal Master Mix
1 µL	20x TaqMan® Assay
ad 20 µL	nuclease-free H_2O

For the analysis of the cDNA using the SYBR® Green system, 1-3 ng cDNA per sample were used according to the following protocol:

4.5 µL	cDNA template
5 µL	2x SYBR® Green PCR Master Mix
0.25 µL	forward primer (100 nM final conc.)
0.25 µL	reverse primer (100 nM final conc.)

Both assays, the TaqMan® Gene Expression and the SYBR® Green assay, were analysed on a 7900HT Fast Real-Time PCR System with the SDS software v2.3 (Applied Biosystems). The calculation of the measured signals and the statistical analysis were done with Microsoft Office Excel.

7.1.3.4 *In silico* promoter region analysis

The *in silico* search for transcription factor binding sites and the analysis of evolutionary conservation was done in collaboration with Dr. D. Trümbach.

All gene symbols, promoter, and transcript identifier were derived from the promoter sequence retrieval database ElDorado (Genomatix). Selection of putative target genes was based on significantly regulated genes from microarray datasets of Braf[cko] and control mice. Promoter sequences from up to ten different mammalian species were aligned with the DiAlign TF program (Cartharius et al., 2005) in the Genomatix software suite GEMS Launcher to evaluate overall promoter similarity and to identify conserved CREB1 and ETS/SRF binding sites (BSs). The promoter regions were defined as ~900 bp upstream and 100 bp downstream of the transcriptional start site. Position weight matrices were used according to Matrix Family Library Version 8.1 (June 2009) for pro-

moter analyses. BS or combination of BSs (i.e. Module) were considered as "conserved BS/Module" only if the promoter sequences for all given orthologs could be aligned in the region of CREB1 BS or ETS/SRF Module with the help of the DiAlign TF program (using default settings). The ETS/SRF module was defined by the ModelInspector (Genomatix / GEMS Launcher) with a distance of 9 to 19 bp between the ETS and the SRF BS and was tested for its presence in the c-fos promoter of different species (Wasylk et al., 1998). The genes were ranked by the degree of conservation of predicted CREB1 BS or ETS/SRF module across ten mammalian species.

7.1.4 Analysis of protein samples

7.1.4.1 Preparation of protein samples

Tissue and protein samples were kept on ice during all steps of preparation to prevent proteolysis, dephosphorylation, and denaturation of the proteins. For mouse brains, tissue (whole brain or parts of it) was homogenised in RIPA buffer with a glass homogeniser. For one hemisphere of a brain, approximately 1 µL of ice-cold buffer was used. To shear the DNA, the samples were sonificated and then incubated on an orbital shaker for 15 min at 4 °C. The cell debris was pelleted by centrifugation at 13,000 rpm for 15 min at 4 °C, and afterwards the supernatant containing the proteins was collected and stored at −20 °C.

The protein concentration was determined by bicinchoninic acid (BCA) assay. Therefore, 1 µL of protein sample was mixed with 49 µL RIPA buffer and 1 mL of BCA working reagent was added. Samples were incubated at 37 °C in a water bath for 30 min, cooled down to RT and the absorption was measured at 562 nm in a photometer. For each measurement, a BSA standard curve was included to calculate the protein concentration dependent on the adsorption.

7.1.4.2 Western blot analysis

Proteins were separated according to their size using SDS polyacrylamide gel electrophoresis (SDS-PAGE) (Laemmli, 1970). Precasted gel systems from Invitrogen (NuPAGE® Novex) and Biorad (Criterion™ XT) were used. 5-50 µg of total protein samples, dependent on the specificity of the used antibody, were mixed with 5x Laemmli buffer, denatured at 95 °C for 5 min, chilled on ice and

then loaded onto the gel. As molecular weight marker, 5 µL of the SeeBlue® Plus2 or Novex® Sharp pre-stained protein standard were loaded. Electrophoresis was performed at 200 V for 1-1.5 hours, depending on the expected protein size and the concentration of the used gel. Afterwards, the gel was blotted on a PVDF membrane which has been activated by soaking in 100 % methanol for 1 min. Blotting was performed at 30 V for 1 hour at RT with the Invitrogen system and at 50 V for 4 hours at 4 °C with the Biorad system.

After blotting, the membrane was transferred immediately in blocking solution to prevent unspecific binding. For normal proteins, 4 % skim milk and for phospho-proteins 4 % BSA in TBS-T was used for 1 hour at RT. Afterwards, the membrane was incubated with the primary antibody in blocking solution for 1 hour at RT or overnight at 4 °C. Then, the membrane was washed three times with TBS-T for 10 min each, incubated with the secondary, horseradish-peroxidase-conjugated antibody in TBS-T for 45 min at RT, and washed again three times. The detection reaction was initiated with ECL detection reagent following the manufacturer's instructions and the membrane was exposed to a chemiluminescent film for 30 sec to several minutes, depending on the intensity of the signal. Exposed films were developed using a developing machine and, if necessary, quantified using ImageJ (Abramoff et al., 2004).

7.2 Mouse husbandry

All mice were kept and bred at the Helmholtz Zentrum München in accordance to national and institutional guidelines. Mice were group-housed in individually ventilated cages (IVC) with five animals per cage at maximum. Animals were separated by sex, but not by genotype. Food and water were given *ad libitum* and a 12 hours light/dark cycle was maintained. The temperature in the animal facility was kept at 22 ± 2 °C with a relative humidity of 55 ± 5 %. For behavioural analysis, the animals were transferred to the German Mouse Clinic (GMC) with same housing conditions, except of smaller IVCs with four animals per cage.

For breeding, one male was paired with one or two females and pups were weaned at an age of three weeks. At weaning, mice were separated according

to their gender, earmarks were made for identification, and tail clips were taken for genotyping.

7.3 Tamoxifen treatment

The activation of the inducible CreER^{T2} was achieved by treating the animals with tamoxifen or tamoxifen citrate by i.p. injection or oral application, respectively.

For i.p. injection, a tamoxifen stock solution was prepared as followed: 1 g tamoxifen free base was dissolved in 10 mL 100 % ethanol. 90 mL sunflower seed oil were added and the solution was stirred at RT for several hours until the tamoxifen was completely solved. Aliquots were prepared and stored at −20 °C for up to four weeks. Mutant animals as well as control animals lacking either the CreER^{T2} or the floxed allele were treated twice a day for five consecutive days at a dosage of 40 mg/kg body weight.

For oral application, animals were fed with special chow (LASCRdiet® Cre-Active TAM400) containing 400 mg/kg tamoxifen citrate for at least 2 weeks.

7.4 Slice electrophysiology

Using standard procedures, transverse hippocampal slices (350 µm thick) were prepared from the brain of adult mice, which were deeply anesthetized with halothane prior to decapitation. The slices were initially maintained in a high-sucrose solution, which was ice-cold for cutting and warmed to 35 °C for 20 minutes immediately after that. The slices were then incubated in modified artificial cerebrospinal fluid (ACSF) at room temperature (21-24 °C) for at least 2 hours before being transferred into the recording chamber individually. Recordings were performed at room temperature in normal ACSF, which was exchanged by means of a gravity-driven perfusion system (flow rate 2-3 mL/min). All solutions were constantly gassed with 95 % O_2/5 % CO_2. CA1 pyramidal cells were visualised with a contrast-enhanced CCD camera. Electrophysiological signals were filtered at 1 kHz (for field potentials) or 2 kHz (for whole-cell currents) and sampled at 10 kHz using a Multiclamp 700B amplifier in conjunction with Digidata 1440A interface and pCLAMP 10 software.

CA1 pyramidal cell population spike (PS) was induced by constant current pulses (pulse width 0.1 ms, every 10 s) delivered to a bipolar tungsten electrode located in CA1 stratum radiatum. The extracellular recording pipette in pyramidal cell layer was filled with modified ACSF, in which bicarbonate was replaced with Hepes to avoid pH change. For whole-cell recording of the evoked inhibitory postsynaptic currents (IPSC) in CA1 pyramidal cells, patch pipettes were filled with patch pipette solution. The electrode resistance ranged from 2.5 to 4 MΩ when filled with internal solution. Series resistance in whole-cell configuration was about 10-25 MΩ, which was compensated by 60-80 %. Constant current pulses (pulse width 0.1 ms) of 50-200 µA were delivered every 30 s to the concentric bipolar electrode located close to the pyramidal cell layer. IPSCs were recorded at −70 mV, after correcting for liquid junction potentials. $GABA_A$ receptor-mediated IPSCs were pharmacologically isolated by perfusing the slices with ionotropic glutamate receptor antagonist kynurenic acid (2 mM).

Data were analysed off-line with the Clampfit 10 software. The PS amplitude was calculated as the averaged value from negative peak to two positive peaks. For evoked IPSCs, we determined peak amplitude, time width at half peak amplitude ($T_{1/2}$) and area above the curve. Spontaneous IPSCs were analysed using an automated event detection algorithm with an amplitude threshold set as $4 \times \sigma_{noise}$. The frequency was measured for spontaneous IPSCs. Data are expressed as means ± s.e.m. Statistical comparisons of data were performed using Student's t-test. Significance was assumed for $p < 0.05$.

7.5   Stereotactic surgery

For the site-specific gene delivery into restricted brain areas of mice, we used stereotactic injections of viral vectors. In order to locally knockout floxed genes in mutant mice, recombinant adeno-associated virus (AAV) vectors expressing Cre recombinase were injected. Appropriate coordinates for the different brain regions were taken from the stereotactic atlas "The mouse brain in stereotaxic coordinates" (Paxinos and Franklin, 2001) and the surgery procedure was adapted from Cetin et al. (2006).

Mice were anesthetized with Ketamin/Xylazin/NaCl. 140 mg/kg b.wt. Ketamin and 7 mg/kg b.wt. Xylazin were used for i.p. injection and animals were placed

into their home cage until completely sedated. Then the animal was fixed in the stereotactic apparatus (Stoelting) using ear bars and a mouse nose clamp. Eye ointment was applied to prevent corneal drying during the surgery. The fur on the skull was cleaned with 70 % ethanol and the scalp was opened with a sterile scalpel along the midline. Small surgical clamps were used to keep the area open and the skull was moistened regularly with PBS. The coordinates of Bregma and Lambda were measured and the target injection coordinates were calculated. The following coordinates based on Bregma were used:

	dorsal hippocampus	ventral hippocampus
anterior/posterior	−2.0 mm	−3.1 mm
medial/lateral	±1.8 mm	±3.3 mm
dorsal/ventral	−1.8 mm	−3.5 mm

Small holes were drilled at the injection sites with a hand-held drill and then the micropipette was positioned at the correct coordinates. With a motorised Nanoliter injector (World Precision Instruments), 1 µL of the viral vector solution was injected within 4 min. Afterwards the micropipette remained for additional 4 min in the brain to allow spreading of the virus and was then pulled out slowly and carefully. The injection procedure was repeated at the second hemisphere to obtain symmetrical gene delivery. Finally, the surgery area was cleaned and was subsequently sutured using an absorbable thread. The animal was placed on a heat plate at 37 °C for recovery from anesthesia. All animals were kept single-housed after surgery.

7.6   Histology

7.6.1   Perfusion and dissection of adult mice

For perfusion, mice were asphyxiated with CO_2, fixed with their paws onto a polystyrene board, and the thoracic cavity was dissected to gain access to the heart. The left ventricle was cut and a blunt needle was inserted carefully into the ascending aorta and fixed with a clamp. To decrease pressure in the blood vessel system, the left atrium was opened. Using a perfusion pump, blood vessels were rinsed with ice-cold PBS for 1 min or until the liver became pale. Then perfusion was performed with ice-cold 4 % paraformaldehyde (PFA) in PBS for approximately 5 min until the body became stiff. After perfusion, the mouse was

decapitated and the brain was dissected by carefully removing skull bone and meninges. For post-fixation, brains were kept in 4 % PFA/PBS for 1 hour to overnight at 4 °C, dependent on the following procedure.

7.6.2 Preparation of frozen sections

After post-fixation, brains were equilibrated in 25 % sucrose solution overnight at 4 °C. For longer storage, 0.01 % sodium azide was added to the sucrose solution. Depending on the purpose, either free-floating or mounted sections were prepared.

For free-floating sections, a sliding cryomicrotom was used. Brains were mounted on the sample table with freezing medium and completely frozen using dry ice. Slices of 40 µm were cut, collected in 4-8 series in cryoprotection solution, and stored at −20 °C.

For mounted sections, a cryostat was used. Brains were mounted on the sample holder with freezing medium and cooled to −20 °C. Slices of 16-30 µm were cut, directly mounted on glass slides, and dried. Slides were kept either at −20 °C or at −80 °C for longer storage.

7.6.3 Nissl staining (cresyl violet)

Nissl staining of dried, mounted sections was performed according to the following protocol:

step	time	solution	remarks
staining	1-5 min	cresyl violet staining solution	
rinse		H_2O	
differentiate	1 min	70 % ethanol	until slide is clear
differentiate	10-60 sec	96 % ethanol + 0.5 % acetic acid	
dehydration	2 x 1 min	96 % ethanol	
dehydration	2 x 2 min	100 % ethanol	
embedding	2 x 10 min	Roti-Histol	

Sections were lidded immediately with Roti-Histokitt II and dried overnight under the hood.

7.6.4 Immunohistochemistry

7.6.4.1 DAB staining

All steps were performed at RT with gentle shaking in 6 well plates with cell strainers, unless otherwise stated.

step	time	solution	remarks
wash	6 x 10 min	1x PBS	remove of cryoprotection solution
quenching	15 min	0.3 % H_2O_2 in PBS/MeOH (1:1)	quenching of endogenous peroxidases
wash	3 x 10 min	1x PBS-T	
blocking	30 min	5 % FCS in 1x PBS-T	
1st antibody	overnight	1st antibody in 5 % FCS/PBS-T	in 96 well plate, 4 °C
wash	3 x 10 min	1x PBS	
2nd antibody	2 h	2nd antibody in 5 % FCS/PBS-T	in 96 well plate
wash	3 x 10 min	1x PBS	
ABC incubation	90 min	1:300 in 1x PBS	keep dark
wash	10 min	1x PBS	
wash	2 x 10 min	1x TB	
DAB staining	3-30 min	0.05 % DAB, 0.02 % H_2O_2 in TB	
wash	3 x 10 min	1x TB	

Sections were mounted on slides, air-dried, and dehydrated in a standard alcohol series as follows:

step	time	solution	remarks
wash	2 x 2 min	H_2O	
dehydration	2 x 2 min	70 % ethanol	
dehydration	2 x 2 min	96 % ethanol	
dehydration	2 x 2 min	100 % ethanol	
embedding	2 x 5 min	Roti-Histol	

Slides were lidded immediately with Roti-Histokitt II and dried overnight under the hood.

For the detection of phosphorylated proteins, TBS and TBS-T were used instead of PBS and PBS-T, respectively.

7.6.4.2 Immunofluorescence

All steps were performed at RT with gentle shaking in 6 well plates with cell strainers, unless otherwise stated.

step	time	solution	remarks
wash	6 x 10 min	1x PBS	remove of cryoprotection solution
quenching	15 min	0.3 % H_2O_2 in PBS/MeOH (1:1)	quenching of endogenous peroxidases
wash	3 x 10 min	1x PBS-T	
blocking	30 min	5 % FCS in 1x PBS-T	
1st antibody	overnight	1st antibody in 5 % FCS/PBS-T	in 96 well plate, 4 °C
wash	3 x 10 min	1x PBS-T	
2nd antibody	2 h	2nd antibody in 5 % FCS/PBS-T	in 96 well plate
wash	3 x 10 min	1x PBS-T	add DAPI in 2nd step
wash	2 x 10 min	1x PBS	

Sections were mounted on slides, air-dried, and lidded immediately with Aquapolymount to prevent fading of the fluorescent signal.

For the detection of phosphorylated proteins, TBS and TBS-T were used instead of PBS and PBS-T, respectively.

7.6.5 LacZ staining

The *lacZ* gene is a common reporter in various applications. Its product, the enzyme β-galactosidase, converts X-Gal into galactosidase and 5,5'-dibromo-4,4'-dichloro-indigo, an insoluble blue product. For the detection of *lacZ* expression in mice, the following protocol was used. To maintain the activity of β-galactosidase in the tissue, all solutions used for LacZ staining were supplemented with $MgCl_2$ and EGTA, and the staining was performed as soon as possible after preparation for optimal results.

The mice were perfused with LacZ fix, which contained 4 % PFS/PBS, following the standard perfusion protocol (see 7.6.1). For post-fixation, brains were kept in LacZ fix for 1-1.5 hours at 4 °C and were then washed in PBS for 1 hour with gentle shaking. Brains were stored in PBS at 4 °C until sectioning, but no longer than overnight.

For sectioning, the fixed brains were embedded in 4 % agarose/PBS and then 100 µm thick sections were made using a vibratom and directly mounted on glass slides. Slides were air-dried for 1 hour and then incubated in LacZ staining solution overnight, protected from light at 37 °C. Then, slides were washed twice in PBS, post-fixed with 4 % PFA for 5 min, washed again twice in PBS, and then further processed according to the following protocol:

step	time	solution	remarks
counterstaining	10 min	0.1 % Eosin-red staining solution	optional step
differentiate	5-10 min	PBS	optional step
dehydration	3 min	25 % ethanol	
dehydration	3 min	50 % ethanol	
dehydration	3 min	75 % ethanol	
dehydration	3 min	100 % ethanol	
embedding	2 x 5 min	Roti-Histol	

Slides were lidded immediately with Roti-Histokitt II and dried overnight under the hood.

7.6.6   Golgi staining

The Golgi staining, also called Golgi's method or Golgi-Cox impregnation (Ramon-Moliner, 1970), is a unspecific staining method for nervous tissue that dyes the soma of neurons as well as axons, dendrites and spines. For the staining of mouse brain, the FD Rapid GolgiStain™ Kit was used following the manufacturer's instructions. All procedures were performed at RT with clean glass containers protected from light whenever possible. No metal implements, except of the metal blades for sectioning, were used.

Mice were asphyxiated with CO_2 and the brain was dissected without perfusion. Impregnation was performed in Solution A+B (which was prepared 24 hours in advance) for 14 days. Solution A+B was renewed at day 2. Afterwards, the tissue was immersed in Solution C for 3-4 days for clearing and then the brain was cut into 140 µm thick sections with a cryostat and mounted on glass slides. After complete drying overnight, the slides were stained with Solution D+E for 10-15 sec, washed with Milli-Q water and subsequently dehydrated in a standard alcohol series (see 7.6.4.1). Slides were lidded immediately with Roti-Histokitt II and dried overnight under the hood.

7.7   Behavioural testing

All behavioural tests except of the neurological test battery were done in the German Mouse Clinic (GMC) in the laboratory of Dr. S. Hölter-Koch. The neurological test battery was performed in the mouse breeding facility.

7.7.1 Voluntary wheel running

For the determination of the daily voluntary wheel running activity, mice were housed individually in a separate sound and light insulated room. A Low Profile Wireless Running Wheel (Med Associates) in each cage recorded the activity in bins of 5 min and transmitted it to a personal computer equipped with the data acquisition software (Wheel manager, Med Associates). Cages were handled only once a week during the light phase for cleaning and otherwise left unattended. All data were analysed with Microsoft Office Excel and CHRONO v2 (Roenneberg and Taylor, 2000).

To determine the endogenous circadian rhythm, mice were kept in a 1/23h light/dark cycle in order to circumvent the influences of the light phase on circadian activity.

7.7.2 Modified hole board test

The modified hole board (mHB) test was carried out as previously described (Vauti et al., 2007). The test apparatus consisted of a box (150 x 50 x 50 cm) which was divided into a test arena (100 x 50 cm) and a group compartment (50 x 50 cm) by a transparent PVC partition (50 x 50 x 0.5 cm) with 111 holes (1 cm diameter) staggered in 12 lines to allow group contact. A board (60 x 20 x 2 cm) with 23 holes (1.5 x 0.5 cm) staggered in 3 lines with all holes covered by movable lids was placed in the middle of the test arena, thus representing the central area of the test arena as an open field. The area around the board was divided into 12 similarly sized quadrants by lines taped onto the floor of the box (see Ohl et al., 2001). Both box and board were made of dark grey PVC. All lids were closed before the start of a trial. For each trial, an unfamiliar object (a blue plastic tube lid, similar in size to the metal cube) and the familiar object (metal cube) were placed into the test arena with a distance of 2 cm between them. The illumination levels were set at approximately 150 lux in the corners and 200 lux in the middle of the test arena. At the beginning of the experiment, all animals of a cage were allowed to habituate to the test environment together in the group compartment for 20 min. Then each animal was placed individually into the test arena and allowed to explore it freely for 5 min, during which the

cage mates stayed present in the group compartment. The animals were always placed into the test arena in the same corner next to the partition, facing the board diagonally. The two objects were placed in the corner quadrant diametrical to the starting point. During the 5 min trial, the animal's behaviour was recorded by a trained observer with a hand-held computer. Data were analysed by using the Observer 4.1 Software (Noldus). Additionally, a camera was mounted 1.20 m above the centre of the test arena, and the animal's track was videotaped and its locomotor path analysed with a video-tracking system (Ethovision 2.3, Noldus). After each trial, the test arena was cleaned carefully with a disinfectant. All measured parameter are listed in the appendix (9.3.1.1).

7.7.3 Open field test

The open field (OF) test was carried out according to the standardised phenotyping screens, developed by the EUMORPHIA partners and available at www.empress.har.mrc.ac.uk.

The test apparatus from TSE Systems (ActiMot) consisted of a transparent and infrared light permeable acrylic test arena (internal measurements: 45.5 x 45.5 x 39.5 cm) with a smooth floor. For data analysis, the arena was divided by the computer in two areas, the periphery defined as a corridor of 8 cm width along the walls and the remaining area representing the centre of the arena.

The illumination levels were set at approximately 150 lux in the corners and 200 lux in the middle of the test arena. At the beginning of the experiment, all animals were transported to the test room and left undisturbed for at least 30 min before the testing started. Then each animal was placed individually into the middle of one side of the arena facing the wall and allowed to explore it freely for 20 min. After each trial, the test arena was cleaned carefully with a disinfectant. All measured parameter are listed in the appendix (9.3.1.2).

7.7.4 Elevated plus maze

The test arena was made of light grey PVC and consisted of two open arms (30 x 5 x 0.3 cm) and two closed arms of the same size with 15 cm walls. The open arms and accordingly the closed arms were facing each other connected via a central square (5 x 5 cm). The apparatus was elevated 75 cm above the floor by

a pole fixed underneath the central square. The illumination level was set at approximately 100 lux in the centre of the maze. For testing, each mouse was placed at the end of a closed arm (distal to the centre) facing the wall and was allowed to explore the maze for 5 min. A camera was mounted above the centre of the maze to video monitor each trial by a trained observer in an adjacent room. The number of entries into each type of arm (placement of all four paws into an arm defining an entry), latency to enter the open arms as well as the time spent in the open and closed arms were recorded by the observer with a hand-held computer. Data were analysed by using the Observer 4.1 Software (Noldus). After each trial, the test arena was cleaned carefully with a disinfectant. All measured parameter are listed in the appendix (9.3.1.3).

7.7.5 Light/dark box

The test box was made of PVC and divided into two compartments, connected by a small tunnel (4 x 6 x 9 cm high). The lit compartment (29 x 19 x 24 cm high) was made of white PVC and was illuminated by cold light with an intensity of 650 lux in the middle; the dark compartment (14 x 19 x 24 cm high) was made of black PVC and not directly illuminated (approx. 20 lux in the centre). The mouse was placed in the centre of the black compartment and allowed to freely explore the apparatus for 5 min. Behaviours were observed by a trained observer sitting next to the box using a hand-held computer. Data were analysed with respect to (1) the number of entries, latency to first entry, and time spent in both compartments and the tunnel; (2) the number of rearings in both compartments and the tunnel. Additionally, grooming behaviour was recorded. An entry into a compartment was defined as placement of all four paws into the compartment. Additionally, a camera was mounted above the centre of the test arena to videotape the trial, and the animal's locomotor path in the lit compartment was analysed with a video-tracking system (Ethovision 2.3, Noldus). The box was cleaned with a disinfectant before each trial. All measured parameter are listed in the appendix (9.3.1.4).

7.7.6 Forced swim test

The forced swimming procedure was adapted from Ebner et al. (2002). The forced swimming apparatus consisted of a cylindrical 10 L glass tank (24.5 cm in diameter) filled to a depth of 20 cm with water (25 ± 1 °C). A trained observer recorded the animal's behaviour in moderate lighting conditions (approx. 30 lux) for 6 min with a hand-held computer scoring the following behaviours: (1) struggling, defined as movements during which the forelimbs brake the water surface; (2) swimming, defined as movement of the animal induced by movements of the forelimbs and hindlimbs without breaking the water surface, and (3) floating, defined as the behaviour during which the animal uses limb movement just to keep its balance without any movement of the trunk. Data were analysed by using the Observer 4.1 Software (Noldus). After each trial, the mouse tested was dried with a tissue and put in a new cage, and the water was renewed before testing the next animal. All measured parameter are listed in the appendix (9.3.1.5).

7.7.7 Accelerating rotarod

Motor coordination and balance were assessed using the rotating rod apparatus from Bioseb (Letica LE 8200). The rod diameter was approximately 4.5 cm made of hard plastic material covered by soft black rubber foam with a lane width of approximately 5 cm. The test phase consisted of three trials separated by 15 min intertrial intervals. On each trial, three mice were placed on the rod leaving an empty lane between two mice. The rod was initially rotating at 4 rpm constant speed to allow positioning of all mice in their respective lanes. Once all mice were positioned, the trial was started and the rod accelerated from 4 rpm to 40 rpm in 300 sec. Latency and rpm at which each mouse fell off the rod were measured. Passive rotations were counted as a fall and the mouse was immediately carefully removed from the rod. After each trial, the apparatus was disinfected and let dry. This protocol is based on the EUMODIC EMPReSS Slim standard operating procedure (see www.eumodic.org). All measured parameter are listed in the appendix (9.3.1.6).

7.7.8 Neurological test battery

The neurological test battery was adapted from Irwin (1968) and Crawley and Paylor (1997). It consists of a series of behaviour tests and was used for a general phenotypic screen of conditional knockout mice. During this test battery, the general health of the animals, the home cage behaviour, and the reflexes on standard neurological tests were analysed. Furthermore, simple locomotor functions were tested using the wire test, the hindlimb extension reflex (adapted from Barneoud et al., 1997), and the beam walk. The physiological strength was determined with the grip strength test and the sensory processes and the cognition were analysed using the hotplate and the elevated platform test, respectively. All measured parameter are listed in the appendix (9.3.1.7).

7.7.9 Statistical analysis

All data are reported as the means ± standard error (s.e.m.) unless otherwise stated. Statistical comparisons were assessed by analysis of variance (ANOVA) with the SPSS software (SPSS Inc.). The accepted level of significance was $p < 0.05$. If separate data analysis for males and females did not reveal significant sex differences in the parameters of interest, data of both sexes were pooled.

8 References

Abramoff, M.D., Magelhaes, P.J., and Ram, S.J. (2004). Image Processing with ImageJ. Biophotonics International *11*, 36-42.

Akashi, M., Hayasaka, N., Yamazaki, S., and Node, K. (2008). Mitogen-activated protein kinase is a functional component of the autonomous circadian system in the suprachiasmatic nucleus. J Neurosci *28*, 4619-4623.

Altschul, S.F., Gish, W., Miller, W., Myers, E.W., and Lipman, D.J. (1990). Basic local alignment search tool. J Mol Biol *215*, 403-410.

American Psychiatric Association (1994). Diagnostic and Statistical Manual of Mental Disorders - DSM-IV, 4th edn (Washington, DC: American Psychiatric Association).

Aoki, Y., Niihori, T., Narumi, Y., Kure, S., and Matsubara, Y. (2008). The RAS/MAPK syndromes: novel roles of the RAS pathway in human genetic disorders. Hum Mutat *29*, 992-1006.

Arur, S., Ohmachi, M., Nayak, S., Hayes, M., Miranda, A., Hay, A., Golden, A., and Schedl, T. (2009). Multiple ERK substrates execute single biological processes in Caenorhabditis elegans germ-line development. Proc Natl Acad Sci U S A *106*, 4776-4781.

Bannerman, D.M., Rawlins, J.N., McHugh, S.B., Deacon, R.M., Yee, B.K., Bast, T., Zhang, W.N., Pothuizen, H.H., and Feldon, J. (2004). Regional dissociations within the hippocampus--memory and anxiety. Neurosci Biobehav Rev *28*, 273-283.

Barneoud, P., Lolivier, J., Sanger, D.J., Scatton, B., and Moser, P. (1997). Quantitative motor assessment in FALS mice: a longitudinal study. Neuroreport *8*, 2861-2865.

Barnier, J.V., Papin, C., Eychene, A., Lecoq, O., and Calothy, G. (1995). The mouse B-raf gene encodes multiple protein isoforms with tissue-specific expression. J Biol Chem *270*, 23381-23389.

Bell-Horner, C.L., Dohi, A., Nguyen, Q., Dillon, G.H., and Singh, M. (2006). ERK/MAPK pathway regulates GABAA receptors. J Neurobiol *66*, 1467-1474.

Bentires-Alj, M., Kontaridis, M.I., and Neel, B.G. (2006). Stops along the RAS pathway in human genetic disease. Nat Med *12*, 283-285.

Bergami, M., Rimondini, R., Santi, S., Blum, R., Gotz, M., and Canossa, M. (2008). Deletion of TrkB in adult progenitors alters newborn neuron

integration into hippocampal circuits and increases anxiety-like behavior. Proc Natl Acad Sci U S A *105*, 15570-15575.

Bunger, M.K., Wilsbacher, L.D., Moran, S.M., Clendenin, C., Radcliffe, L.A., Hogenesch, J.B., Simon, M.C., Takahashi, J.S., and Bradfield, C.A. (2000). Mop3 is an essential component of the master circadian pacemaker in mammals. Cell *103*, 1009-1017.

Byrum, C.E., Ahearn, E.P., and Krishnan, K.R. (1999). A neuroanatomic model for depression. Prog Neuropsychopharmacol Biol Psychiatry *23*, 175-193.

Cartharius, K., Frech, K., Grote, K., Klocke, B., Haltmeier, M., Klingenhoff, A., Frisch, M., Bayerlein, M., and Werner, T. (2005). MatInspector and beyond: promoter analysis based on transcription factor binding sites. Bioinformatics *21*, 2933-2942.

Cetin, A., Komai, S., Eliava, M., Seeburg, P.H., and Osten, P. (2006). Stereotaxic gene delivery in the rodent brain. Nat Protoc *1*, 3166-3173.

Chen, A.P., Ohno, M., Giese, K.P., Kuhn, R., Chen, R.L., and Silva, A.J. (2006a). Forebrain-specific knockout of B-raf kinase leads to deficits in hippocampal long-term potentiation, learning, and memory. J Neurosci Res *83*, 28-38.

**Chen, Z.Y., Jing, D., Bath, K.G., Ieraci, A., Khan, T., Siao, C.J., Herrera, D.G., Toth, M., Yang, C., McEwen, B.S.*, et al.* (2006b). Genetic variant BDNF (Val66Met) polymorphism alters anxiety-related behavior. Science *314*, 140-143.

Chomczynski, P., and Sacchi, N. (1987). Single-step method of RNA isolation by acid guanidinium thiocyanate-phenol-chloroform extraction. Anal Biochem *162*, 156-159.

Citri, A., and Malenka, R.C. (2008). Synaptic plasticity: multiple forms, functions, and mechanisms. Neuropsychopharmacology *33*, 18-41.

**Cohen, C.D., Klingenhoff, A., Boucherot, A., Nitsche, A., Henger, A., Brunner, B., Schmid, H., Merkle, M., Saleem, M.A., Koller, K.P.*, et al.* (2006). Comparative promoter analysis allows de novo identification of specialized cell junction-associated proteins. Proc Natl Acad Sci U S A *103*, 5682-5687.

Coogan, A.N., and Piggins, H.D. (2004). MAP kinases in the mammalian circadian system--key regulators of clock function. J Neurochem *90*, 769-775.

Coyle, J.T., and Duman, R.S. (2003). Finding the intracellular signaling pathways affected by mood disorder treatments. Neuron *38*, 157-160.

Crawley, J.N., and Paylor, R. (1997). A proposed test battery and constellations of specific behavioral paradigms to investigate the behavioral phenotypes of transgenic and knockout mice. Horm Behav *31*, 197-211.

Cryan, J.F., and Holmes, A. (2005). The ascent of mouse: advances in modelling human depression and anxiety. Nat Rev Drug Discov *4*, 775-790.

D'Sa, C., and Duman, R.S. (2002). Antidepressants and neuroplasticity. Bipolar Disord *4*, 183-194.

**Davies, H., Bignell, G.R., Cox, C., Stephens, P., Edkins, S., Clegg, S., Teague, J., Woffendin, H., Garnett, M.J., Bottomley, W.*, et al.* (2002). Mutations of the BRAF gene in human cancer. Nature *417*, 949-954.

Debruyne, J.P., Noton, E., Lambert, C.M., Maywood, E.S., Weaver, D.R., and Reppert, S.M. (2006). A clock shock: mouse CLOCK is not required for circadian oscillator function. Neuron *50*, 465-477.

Ebner, K., Wotjak, C.T., Landgraf, R., and Engelmann, M. (2002). Forced swimming triggers vasopressin release within the amygdala to modulate stress-coping strategies in rats. Eur J Neurosci *15*, 384-388.

Einat, H., Yuan, P., Gould, T.D., Li, J., Du, J., Zhang, L., Manji, H.K., and Chen, G. (2003). The role of the extracellular signal-regulated kinase signaling pathway in mood modulation. J Neurosci *23*, 7311-7316.

Engel, S.R., Creson, T.K., Hao, Y., Shen, Y., Maeng, S., Nekrasova, T., Landreth, G.E., Manji, H.K., and Chen, G. (2009). The extracellular signal-regulated kinase pathway contributes to the control of behavioral excitement. Mol Psychiatry *14*, 448-461.

Engin, E., Stellbrink, J., Treit, D., and Dickson, C.T. (2008). Anxiolytic and antidepressant effects of intracerebroventricularly administered somatostatin: behavioral and neurophysiological evidence. Neuroscience *157*, 666-676.

Erdmann, G., Schutz, G., and Berger, S. (2007). Inducible gene inactivation in neurons of the adult mouse forebrain. BMC Neurosci *8*, 63.

Fanselow, M.S., and Dong, H.W. (2010). Are the dorsal and ventral hippocampus functionally distinct structures? Neuron *65*, 7-19.

Fumagalli, F., Molteni, R., Calabrese, F., Frasca, A., Racagni, G., and Riva, M.A. (2005). Chronic fluoxetine administration inhibits extracellular signal-regulated kinase 1/2 phosphorylation in rat brain. J Neurochem *93*, 1551-1560.

Galabova-Kovacs, G., Catalanotti, F., Matzen, D., Reyes, G.X., Zezula, J., Herbst, R., Silva, A., Walter, I., and Baccarini, M. (2008). Essential role of B-Raf in oligodendrocyte maturation and myelination during postnatal central nervous system development. J Cell Biol *180*, 947-955.

Giroux, S., Tremblay, M., Bernard, D., Cardin-Girard, J.F., Aubry, S., Larouche, L., Rousseau, S., Huot, J., Landry, J., Jeannotte, L., and Charron, J. (1999). Embryonic death of Mek1-deficient mice reveals a role for this kinase in angiogenesis in the labyrinthine region of the placenta. Curr Biol *9*, 369-372.

Gorman, J.M. (2006). Gender differences in depression and response to psychotropic medication. Gend Med *3*, 93-109.

Gross, C., Zhuang, X., Stark, K., Ramboz, S., Oosting, R., Kirby, L., Santarelli, L., Beck, S., and Hen, R. (2002). Serotonin1A receptor acts during development to establish normal anxiety-like behaviour in the adult. Nature *416*, 396-400.

Hammond, R.S., Bond, C.T., Strassmaier, T., Ngo-Anh, T.J., Adelman, J.P., Maylie, J., and Stackman, R.W. (2006). Small-conductance Ca2+-activated K+ channel type 2 (SK2) modulates hippocampal learning, memory, and synaptic plasticity. J Neurosci *26*, 1844-1853.

Hao, Y., Creson, T., Zhang, L., Li, P., Du, F., Yuan, P., Gould, T.D., Manji, H.K., and Chen, G. (2004). Mood stabilizer valproate promotes ERK pathway-dependent cortical neuronal growth and neurogenesis. J Neurosci *24*, 6590-6599.

Hasler, G., Drevets, W.C., Manji, H.K., and Charney, D.S. (2004). Discovering endophenotypes for major depression. Neuropsychopharmacology *29*, 1765-1781.

Hatano, N., Mori, Y., Oh-hora, M., Kosugi, A., Fujikawa, T., Nakai, N., Niwa, H., Miyazaki, J., Hamaoka, T., and Ogata, M. (2003). Essential role for ERK2 mitogen-activated protein kinase in placental development. Genes Cells *8*, 847-856.

Hettema, J.M., Neale, M.C., and Kendler, K.S. (2001). A review and meta-analysis of the genetic epidemiology of anxiety disorders. Am J Psychiatry *158*, 1568-1578.

Hitz, C. (2007). The role of MAP-Kinases in anxiety disorders and depression - studies with knockout and knockdown mouse models. PhD dissertation. Technical University Munich

Honma, S., Kawamoto, T., Takagi, Y., Fujimoto, K., Sato, F., Noshiro, M., Kato, Y., and Honma, K. (2002). Dec1 and Dec2 are regulators of the mammalian molecular clock. Nature *419*, 841-844.

Irwin, S. (1968). Comprehensive observational assessment: Ia. A systematic, quantitative procedure for assessing the behavioral and physiologic state of the mouse. Psychopharmacologia *13*, 222-257.

Jacobi, F., Wittchen, H.U., Holting, C., Hofler, M., Pfister, H., Muller, N., and Lieb, R. (2004). Prevalence, co-morbidity and correlates of mental disorders in the general population: results from the German Health Interview and Examination Survey (GHS). Psychol Med *34*, 597-611.

**Jiang, X., Tian, F., Du, Y., Copeland, N.G., Jenkins, N.A., Tessarollo, L., Wu, X., Pan, H., Hu, X.Z., Xu, K.*, et al.* (2008). BHLHB2 controls Bdnf promoter 4 activity and neuronal excitability. J Neurosci *28*, 1118-1130.

Khawaled, R., Bruening-Wright, A., Adelman, J.P., and Maylie, J. (1999). Bicuculline block of small-conductance calcium-activated potassium channels. Pflugers Arch *438*, 314-321.

Ko, S.W., Ao, H.S., Mendel, A.G., Qiu, C.S., Wei, F., Milbrandt, J., and Zhuo, M. (2005). Transcription factor Egr-1 is required for long-term fear memory and anxiety. Sheng Li Xue Bao *57*, 421-432.

Kopnisky, K.L., Chalecka-Franaszek, E., Gonzalez-Zulueta, M., and Chuang, D.M. (2003). Chronic lithium treatment antagonizes glutamate-induced decrease of phosphorylated CREB in neurons via reducing protein phosphatase 1 and increasing MEK activities. Neuroscience *116*, 425-435.

Laemmli, U.K. (1970). Cleavage of structural proteins during the assembly of the head of bacteriophage T4. Nature *227*, 680-685.

Lenox, R.H., Gould, T.D., and Manji, H.K. (2002). Endophenotypes in bipolar disorder. Am J Med Genet *114*, 391-406.

Low, K., Crestani, F., Keist, R., Benke, D., Brunig, I., Benson, J.A., Fritschy, J.M., Rulicke, T., Bluethmann, H., Mohler, H., and Rudolph, U. (2000). Molecular and neuronal substrate for the selective attenuation of anxiety. Science *290*, 131-134.

Ma, X.M., Wang, Y., Ferraro, F., Mains, R.E., and Eipper, B.A. (2008). Kalirin-7 is an essential component of both shaft and spine excitatory synapses in hippocampal interneurons. J Neurosci *28*, 711-724.

Malumbres, M., and Barbacid, M. (2003). RAS oncogenes: the first 30 years. Nat Rev Cancer *3*, 459-465.

Marais, R., Light, Y., Paterson, H.F., Mason, C.S., and Marshall, C.J. (1997). Differential regulation of Raf-1, A-Raf, and B-Raf by oncogenic ras and tyrosine kinases. J Biol Chem *272*, 4378-4383.

Marshall, O.J. (2004). PerlPrimer: cross-platform, graphical primer design for standard, bisulphite and real-time PCR. Bioinformatics *20*, 2471-2472.

Mazzucchelli, C., Vantaggiato, C., Ciamei, A., Fasano, S., Pakhotin, P., Krezel, W., Welzl, H., Wolfer, D.P., Pages, G., Valverde, O.*, et al.* (2002). Knockout of ERK1 MAP kinase enhances synaptic plasticity in the striatum and facilitates striatal-mediated learning and memory. Neuron *34*, 807-820.

Mercer, K., Giblett, S., Green, S., Lloyd, D., DaRocha Dias, S., Plumb, M., Marais, R., and Pritchard, C. (2005). Expression of endogenous oncogenic V600EB-raf induces proliferation and developmental defects in mice and transformation of primary fibroblasts. Cancer Res *65*, 11493-11500.

Mikula, M., Schreiber, M., Husak, Z., Kucerova, L., Ruth, J., Wieser, R., Zatloukal, K., Beug, H., Wagner, E.F., and Baccarini, M. (2001). Embryonic lethality and fetal liver apoptosis in mice lacking the c-raf-1 gene. EMBO J *20*, 1952-1962.

Minichiello, L., Korte, M., Wolfer, D., Kuhn, R., Unsicker, K., Cestari, V., Rossi-Arnaud, C., Lipp, H.P., Bonhoeffer, T., and Klein, R. (1999). Essential role for TrkB receptors in hippocampus-mediated learning. Neuron *24*, 401-414.

Mitra, R., Ferguson, D., and Sapolsky, R.M. (2009). SK2 potassium channel overexpression in basolateral amygdala reduces anxiety, stress-induced corticosterone secretion and dendritic arborization. Mol Psychiatry *14*, 847-855, 827.

Morice, C., Nothias, F., Konig, S., Vernier, P., Baccarini, M., Vincent, J.D., and Barnier, J.V. (1999). Raf-1 and B-Raf proteins have similar regional distributions but differential subcellular localization in adult rat brain. Eur J Neurosci *11*, 1995-2006.

Muller, M.B., Zimmermann, S., Sillaber, I., Hagemeyer, T.P., Deussing, J.M., Timpl, P., Kormann, M.S., Droste, S.K., Kuhn, R., Reul, J.M.*, et al.*

(2003). Limbic corticotropin-releasing hormone receptor 1 mediates anxiety-related behavior and hormonal adaptation to stress. Nat Neurosci *6*, 1100-1107.

Obrietan, K., Impey, S., and Storm, D.R. (1998). Light and circadian rhythmicity regulate MAP kinase activation in the suprachiasmatic nuclei. Nat Neurosci *1*, 693-700.

Ohl, F., Sillaber, I., Binder, E., Keck, M.E., and Holsboer, F. (2001). Differential analysis of behavior and diazepam-induced alterations in C57BL/6N and BALB/c mice using the modified hole board test. J Psychiatr Res *35*, 147-154.

Paxinos, G., and Franklin, K.B.J. (2001). The mouse brain in stereotaxic coordinates, 2nd edn (San Diego: Academic Press).

Pratt, J.A. (1992). The neuroanatomical basis of anxiety. Pharmacol Ther *55*, 149-181.

Pritchard, C.A., Bolin, L., Slattery, R., Murray, R., and McMahon, M. (1996). Post-natal lethality and neurological and gastrointestinal defects in mice with targeted disruption of the A-Raf protein kinase gene. Curr Biol *6*, 614-617.

Pritchard, C.A., Samuels, M.L., Bosch, E., and McMahon, M. (1995). Conditionally oncogenic forms of the A-Raf and B-Raf protein kinases display different biological and biochemical properties in NIH 3T3 cells. Mol Cell Biol *15*, 6430-6442.

Rabow, L.E., Russek, S.J., and Farb, D.H. (1995). From ion currents to genomic analysis: recent advances in GABAA receptor research. Synapse *21*, 189-274.

Ramon-Moliner, E. (1970). The Golgi-Cox technique. Contemporary Research Methods in Neuroanatomy.

Refojo, D., Echenique, C., Muller, M.B., Reul, J.M., Deussing, J.M., Wurst, W., Sillaber, I., Paez-Pereda, M., Holsboer, F., and Arzt, E. (2005). Corticotropin-releasing hormone activates ERK1/2 MAPK in specific brain areas. Proc Natl Acad Sci U S A *102*, 6183-6188.

Revest, J.M., Di Blasi, F., Kitchener, P., Rouge-Pont, F., Desmedt, A., Turiault, M., Tronche, F., and Piazza, P.V. (2005). The MAPK pathway and Egr-1 mediate stress-related behavioral effects of glucocorticoids. Nat Neurosci *8*, 664-672.

Roenneberg, T., and Taylor, W. (2000). Automated recordings of bioluminescence with special reference to the analysis of circadian rhythms. Methods Enzymol *305*, 104-119.

Rubinfeld, H., and Seger, R. (2005). The ERK cascade: a prototype of MAPK signaling. Mol Biotechnol *31*, 151-174.

Rudolph, U., Crestani, F., Benke, D., Brunig, I., Benson, J.A., Fritschy, J.M., Martin, J.R., Bluethmann, H., and Mohler, H. (1999). Benzodiazepine actions mediated by specific gamma-aminobutyric acid(A) receptor subtypes. Nature *401*, 796-800.

Saba-El-Leil, M.K., Vella, F.D., Vernay, B., Voisin, L., Chen, L., Labrecque, N., Ang, S.L., and Meloche, S. (2003). An essential function of the mitogen-activated protein kinase Erk2 in mouse trophoblast development. EMBO Rep *4*, 964-968.

Samuels, I.S., Karlo, J.C., Faruzzi, A.N., Pickering, K., Herrup, K., Sweatt, J.D., Saitta, S.C., and Landreth, G.E. (2008). Deletion of ERK2 mitogen-activated protein kinase identifies its key roles in cortical neurogenesis and cognitive function. J Neurosci *28*, 6983-6995.

Scobie, K.N., Hall, B.J., Wilke, S.A., Klemenhagen, K.C., Fujii-Kuriyama, Y., Ghosh, A., Hen, R., and Sahay, A. (2009). Kruppel-like factor 9 is necessary for late-phase neuronal maturation in the developing dentate gyrus and during adult hippocampal neurogenesis. J Neurosci *29*, 9875-9887.

Sklar, P. (2002). Linkage analysis in psychiatric disorders: the emerging picture. Annu Rev Genomics Hum Genet *3*, 371-413.

Soriano, P. (1999). Generalized lacZ expression with the ROSA26 Cre reporter strain. Nat Genet *21*, 70-71.

Storm, S.M., Cleveland, J.L., and Rapp, U.R. (1990). Expression of raf family proto-oncogenes in normal mouse tissues. Oncogene *5*, 345-351.

Takahashi, J.S., Hong, H.K., Ko, C.H., and McDearmon, E.L. (2008). The genetics of mammalian circadian order and disorder: implications for physiology and disease. Nat Rev Genet *9*, 764-775.

Tiraboschi, E., Tardito, D., Kasahara, J., Moraschi, S., Pruneri, P., Gennarelli, M., Racagni, G., and Popoli, M. (2004). Selective phosphorylation of nuclear CREB by fluoxetine is linked to activation of CaM kinase IV and MAP kinase cascades. Neuropsychopharmacology *29*, 1831-1840.

Treisman, R. (1996). Regulation of transcription by MAP kinase cascades. Curr Opin Cell Biol *8*, 205-215.

Tronche, F., Kellendonk, C., Kretz, O., Gass, P., Anlag, K., Orban, P.C., Bock, R., Klein, R., and Schutz, G. (1999). Disruption of the glucocorticoid receptor gene in the nervous system results in reduced anxiety. Nat Genet *23*, 99-103.

Vauti, F., Goller, T., Beine, R., Becker, L., Klopstock, T., Holter, S.M., Wurst, W., Fuchs, H., Gailus-Durner, V., de Angelis, M.H., and Arnold, H.H. (2007). The mouse Trm1-like gene is expressed in neural tissues and plays a role in motor coordination and exploratory behaviour. Gene *389*, 174-185.

Vogt, M.A., Chourbaji, S., Brandwein, C., Dormann, C., Sprengel, R., and Gass, P. (2008). Suitability of tamoxifen-induced mutagenesis for behavioral phenotyping. Exp Neurol *211*, 25-33.

Volke, V., Wegener, G., Bourin, M., and Vasar, E. (2003). Antidepressant- and anxiolytic-like effects of selective neuronal NOS inhibitor 1-(2-trifluoromethylphenyl)-imidazole in mice. Behav Brain Res *140*, 141-147.

Wan, P.T., Garnett, M.J., Roe, S.M., Lee, S., Niculescu-Duvaz, D., Good, V.M., Jones, C.M., Marshall, C.J., Springer, C.J., Barford, D., and Marais, R. (2004). Mechanism of activation of the RAF-ERK signaling pathway by oncogenic mutations of B-RAF. Cell *116*, 855-867.

Wasylyk, B., Hagman, J., and Gutierrez-Hartmann, A. (1998). Ets transcription factors: nuclear effectors of the Ras-MAP-kinase signaling pathway. Trends Biochem Sci *23*, 213-216.

Wellbrock, C., Karasarides, M., and Marais, R. (2004). The RAF proteins take centre stage. Nat Rev Mol Cell Biol *5*, 875-885.

Williamson, D.E., Forbes, E.E., Dahl, R.E., and Ryan, N.D. (2005). A genetic epidemiologic perspective on comorbidity of depression and anxiety. Child Adolesc Psychiatr Clin N Am *14*, 707-726, viii.

Wittchen, H.U., and Jacobi, F. (2001). Die Versorgungssituation psychischer Störungen in Deutschland. Bundesgesundheitsblatt - Gesundheitsforschung - Gesundheitsschutz *44*, 993-1000.

Wojnowski, L., Stancato, L.F., Larner, A.C., Rapp, U.R., and Zimmer, A. (2000). Overlapping and specific functions of Braf and Craf-1 proto-oncogenes during mouse embryogenesis. Mech Dev *91*, 97-104.

Wojnowski, L., Zimmer, A.M., Beck, T.W., Hahn, H., Bernal, R., Rapp, U.R., and Zimmer, A. (1997). Endothelial apoptosis in Braf-deficient mice. Nat Genet *16*, 293-297.

Wu, G.Y., Deisseroth, K., and Tsien, R.W. (2001). Spaced stimuli stabilize MAPK pathway activation and its effects on dendritic morphology. Nat Neurosci *4*, 151-158.

Wulff, K., Gatti, S., Wettstein, J.G., and Foster, R.G. (2010). Sleep and circadian rhythm disruption in psychiatric and neurodegenerative disease. Nat Rev Neurosci.

Yao, Y., Li, W., Wu, J., Germann, U.A., Su, M.S., Kuida, K., and Boucher, D.M. (2003). Extracellular signal-regulated kinase 2 is necessary for mesoderm differentiation. Proc Natl Acad Sci U S A *100*, 12759-12764.

Yasuda, S., Liang, M.H., Marinova, Z., Yahyavi, A., and Chuang, D.M. (2009). The mood stabilizers lithium and valproate selectively activate the promoter IV of brain-derived neurotrophic factor in neurons. Mol Psychiatry *14*, 51-59.

Zhang, J., Huang, X.Y., Ye, M.L., Luo, C.X., Wu, H.Y., Hu, Y., Zhou, Q.G., Wu, D.L., Zhu, L.J., and Zhu, D.Y. (2010). Neuronal nitric oxide synthase alteration accounts for the role of 5-HT1A receptor in modulating anxiety-related behaviors. J Neurosci *30*, 2433-2441.

Zhong, J., Li, X., McNamee, C., Chen, A.P., Baccarini, M., and Snider, W.D. (2007). Raf kinase signaling functions in sensory neuron differentiation and axon growth in vivo. Nat Neurosci *10*, 598-607.

9 Appendix

9.1 Abbreviations

A	purine base adenine
AAV	adeno-associated virus
Ac	acetate
ATP	adenosine triphosphate
b.wt.	body weight
BCA	bicinchoninic acid
BIM	bicuculline (methiodide)
bp	basepair
Braf	*Braf* transforming gene
BS	binding site
Bs	brainstem
BSA	bovine serum albumin
°C	degree Celsius
c	centi (10^{-2})
C	pyrimidine base cytosine
CA	enclosed arms (of the elevated plus maze)
CA1/2/3	cornu ammonis area 1/2/3 of the hippocampus
$CaCl_2$	calcium chloride
Cb	cerebellum
cDNA	complementary DNA
cko	conditional knockout
CIP	calf intestinal phosphatase
CNS	central nervous system
CO_2	carbon dioxide
cpm	counts per minute
CREB	cAMP-responsive element binding-protein 1
cRNA	complementary RNA
CTP	cytosine triphosphate
Cx	cortex
Da	Dalton
DAB	3,3'-diaminobenzidine
DB	dark box (of the light/dark box test)
Dh	dorsal horn (of the spinal cord)
DH5α	*E.coli* strain DH5α
DMSO	dimethylsulfoxide
DNA	desoxyribonucleic acid
dNTP	desoxyribonucleotide triphosphate
DTT	1,4-dithiothreitol
E	embryonic day

E.coli	*Escherichia coli*
e.g.	exempli gratia, for example
EDTA	ethylendiamintetraacetate
EGTA	ethylenglycol-bis-(b-aminoethylether)-N,N,N´,N´-tetraacetate
ELK1	ETS domain-containing protein Elk-1
EPM	elevated plus maze
ERK	extracellular signal-regulated kinase
EtOH	ethanol
F	Farad
f	female
FC	fold change
FCS	fetal calf serum
FGF	fibroblast growth factor
Fig.	figure
FST	forced swim test
g	acceleration of gravity ($9.81 m/s^2$)
g	gramme
G	purinbase guanine
GABA	γ-aminobutyric acid
Gc	gray commissure
GMC	German Mouse Clinic
h	hour(s)
Hb	hindbrain
Hc	hippocampus
HCl	hydrochloric acid
HPRT	hypoxanthine phosphoribosyltransferase
Ht	hypothalamus
i.p.	intraperitoneal (injection)
Ic	inferior colliculus
icko	inducible conditional knockout
IF	immunofluorescence
IHC	immunohistochemistry
IPSC	inhibitory postsynaptic current
IVC	indivudally ventilated cages
kb	kilobasepairs
kD	kilodalton
kg	kilogram
Klenow	Large fragment of *E.coli* DNA polymerase I
L	litre
LacZ	β-Galactosidase gene
LB	light box (of the light/dark box test)
LB	Luria Broth
LD	light/dark box test

m	male
m	metre
m	milli (10^{-3})
M	molar (mol/L)
µ	micro (10^{-6})
MEK	mitogen-activated protein kinase kinase
MeSH	Medical Subject Headings
$MgCl_2$	magnesium chloride
mHB	modified hole board test
min	minute(s)
mRNA	messenger ribonucleic acid
MSK1/2	mitogen- and stress-activated protein kinase-1 and -2
mut	mutant
n.t.	not tested
n	nano (10^{-9})
n	sample size
NaCl	sodium chloride
NaOAc	sodium acetate
NH_4OAc	ammonium acetate
nm	nanometre
no.	number
NP-40	Nonidet P-40
nt	nucleotides
OA	open arms (of the elevated plus maze)
oB	olfactory bulb
OD	optical density
OF	open field test
ORF	open reading frame
p	pico (10^{-12})
p	p-value (for statistical analysis)
PBS	phosphate buffered saline
PCR	polymerase chain reaction
PFA	paraformaldehyde
Pir	piriform cortex
PNK	polynucleotide kinase
PNS	peripheral nervous system
PS	population spike
qPCR	quantitative real-time polymerase chain reaction
RIPA	radioimmunoprecipitation assay (buffer)
RNA	ribonucleic acid
rpm	rounds per minute
RT	room temperature
RT	reverse transcription

SCN	suprachiasmatic nucleus
SDS	sodium dodecyl sulfate
sec or s	second(s)
SEM	standard error of the mean
SK (channel)	small conductance calcium-activated potassium (channel)
SSC	sodium saline citrate
St	striatum
T	pyrimidine base thymine
Tab.	table
TAE	tris acetate with EDTA
TBE	tris borate with EDTA
TBS(-T)	tris buffered saline (with Tween)
TE	tris-EDTA
temp.	temperature
Th	thalamus
Tris	trishydroxymethyl-aminoethane
U	unit(s)
UTP	uracil triphosphate
UTR	untranslated region (of an mRNA)
UV	ultraviolet
V	volt
Vh	ventral horn (of the spinal cord)
Vol.	volume or volumetric content
wt	wild-type
x	Symbol for crosses between mouse lines

9.2 Index of figures and tables

Figures:

Tables:

9.3   Supplementary data

9.3.1   Measured parameters in the behavioural analysis

9.3.1.1   Modified hole board test

Behaviour	Parameters
forward locomotion	distance moved, line crossings (latency, frequency)
speed of movement	velocity (mean, maximum, angular)
exploration	vertical: rearings (box, board; latency, frequency) horizontal: holes (latency, frequency), objects (novel, familiar; latency, frequency, duration)
risk assessment	stretched attends (latency, frequency)
anxiety-related	board entries (latency, frequency, duration); distance to the wall
grooming	grooming (latency, frequency, duration)
defecation	boli (latency, frequency)
social affinity	exploration of the partition (latency, frequency, duration)
object memory	object recognition index

9.3.1.2   Open field test

Behaviour	Parameters
forward locomotion	distance moved (arena, periphery, centre)
speed of movement	velocity (arena, periphery, centre)
exploration	vertical: rearings (frequency) horizontal: resting time (arena, periphery, centre), permanence (arena, periphery, centre)
anxiety-related	centre entries (distance, latency, frequency, duration)

9.3.1.3   Elevated plus maze

Behaviour	Parameters
forward locomotion	distance moved (total, open arms, closed arms)
speed of movement	velocity (mean, maximum)
anxiety-related	compartment entries (latency, frequency, duration)

9.3.1.4   Light/dark box

Behaviour	Parameters
forward locomotion	distance moved (total), turn angle (number, mean), meander
speed of movement	velocity (mean, maximum, angular)
exploration	rearings in compartments (latency, frequency)
grooming	grooming in compartments (frequency, duration)
anxiety-related	compartment entries (latency, frequency, duration)

9.3.1.5   Forced swim test

Behaviour	Parameters
forward locomotion/ depression-like	swimming, floating (total duration, per min)
anxiety-related	struggling (total duration, per min)

9.3.1.6   Accelerating rotarod

Behaviour	Parameters
forward locomotion	latency to fall from rod (per trials, mean), passive rotations
speed of movement	speed of rotating rod
general	body weight

9.3.1.7   Neurological test battery

Test	Parameters
general health	weight, whiskers, bald hair patches, palpebral closure, ex-ophthalmia, piloerection
empty cage behaviour	wild running, freezing, sniffing, licking, rearing at wall, jumping, defecation, number of boli, urination
rapid cage movement	splayed limbs, strobe tail, fall over
righting reflex	time to right
whisker response	whiskers stop moving, turn toward touch
touch reflex	reflex (eye, ear)
elevated platform	latency to edge, number of head pokes
wire test	latency to climb up, latency to reach edge, fall down
hindlimb extension reflex	score
grip strength	strength (forelimbs, hindlimbs)
beam walk	time, number of falls
hot plate	latency (lifting, licking, jumping)

9.3.2 Suppl. results – Neurological test battery

Table 5: Results of the neurological test battery

Genotype	Ear clip	Gender	Age	General Health							Behaviour in empty cage (3 min)									
				Weight [g]	Whiskers	Bald Hair Patches	Palpebral Closure	Exophtalmas	Piloerection	Other	Wild-running	Freezing	Sniffing	Licking	Rearing	Jumping	Defecation	Number of boli	Urinate	Other
wt	832	m	115	25	short	-	-	-	-	-	-	-	-	-	-	-	-	-	-	-
mut	834	m	115	21	-	-	-	-	-	-	x	-	-	-	-	-	-	-	-	aroused
mut	856	m	101	19	-	-	-	-	-	-	-	-	-	-	low	-	x	1	-	-
wt	867	m	97	24	-	-	-	-	-	-	-	-	-	-	-	-	-	-	-	-
wt	875	m	89	27	-	-	-	-	-	-	-	-	-	-	-	-	-	-	-	-
wt	881	m	89	26	-	-	-	-	-	-	-	-	-	-	-	-	-	-	-	-
wt	883	f	89	25	-	-	-	-	-	-	-	-	-	-	-	-	-	-	-	calm
mut	884	m	89	22	-	-	-	-	-	-	-	-	-	-	low	-	x	1	-	-
mut	886	m	83	22	-	-	-	-	-	-	-	-	-	-	low	-	-	-	-	calm
wt	887	m	83	25	-	-	-	-	-	-	-	-	-	-	-	-	x	2	-	calm
wt	889	f	83	24	-	-	-	-	-	-	-	-	-	-	-	low	x	1	-	-
mut	890	f	83	18	-	-	-	-	-	-	x	-	-	-	-	x	-	-	-	aroused
mut	892	m	82	22	-	-	-	-	-	-	x	-	-	-	-	x	x	1	-	aroused
mut	894	f	82	16	-	-	-	-	-	-	-	-	-	-	low	-	-	-	-	-
mut	895	f	82	20	-	-	-	-	-	-	-	-	-	-	-	-	-	-	-	-
wt	896	f	82	20	-	-	-	-	-	-	-	-	-	-	-	-	-	-	-	-
mut	901	f	63	19	-	-	-	-	-	-	-	-	-	-	low	-	-	-	-	-
wt	905	f	63	20	-	-	-	-	-	-	-	-	-	-	-	-	x	3	-	-
wt	924	f	61	18	-	-	-	-	-	-	-	-	-	-	-	-	-	-	-	-
mut	926	f	61	17	-	-	-	-	-	-	-	-	-	-	-	-	-	-	-	-

Genotype	Ear clip	Gender	Age	Cage side to side			Cage up and down			Righting reflex		Whisker response			Touch reflex	
				splayed limbs	strobe tail	fall over	splayed limbs	strobe tail	fall over	remains on back	time to right	whiskers stop moving	turn towards touch	other	eye	ear
wt	832	m	115	-	-	-	-	-	-	-	-	-	-	-	-	-
mut	834	m	115	-	-	-	-	-	-	-	-	-	-	-	-	-
mut	856	m	101	-	-	-	-	-	-	-	-	-	-	-	-	-
wt	867	m	97	-	-	-	-	-	-	-	-	-	-	-	-	-
wt	875	m	89	-	-	-	-	-	-	-	-	-	-	-	-	-
wt	881	m	89	-	-	-	-	-	-	-	-	-	-	-	-	-
wt	883	f	89	-	-	-	-	-	-	-	-	-	-	-	-	-
mut	884	m	89	-	#	-	-	#	-	-	-	-	#	-	#	-
mut	886	m	83	-	-	-	-	-	-	-	-	-	-	-	-	-
wt	887	m	83	-	-	-	-	-	-	-	-	-	-	-	-	-
wt	889	f	83	-	-	-	-	-	-	-	-	-	-	-	-	-
mut	890	f	83	-	#	-	-	#	-	#	-	-	#	-	#	-
mut	892	m	82	-	-	-	-	#	-	-	-	-	-	-	-	-
mut	894	f	82	-	#	-	-	#	-	-	-	-	-	-	-	-
mut	895	f	82	-	-	-	-	-	-	-	-	-	-	-	-	-
wt	896	f	82	-	-	-	-	-	-	-	-	-	-	-	-	-
mut	901	f	63	-	-	-	-	-	-	-	-	-	-	-	-	-
wt	905	f	63	-	-	-	-	-	-	-	-	-	-	-	-	-
wt	924	f	61	-	-	-	-	-	-	-	-	-	-	-	-	-
mut	926	f	61	-	-	-	-	-	-	-	-	-	-	-	-	-

-: no abnormality detected / not present
x: phenotype present
#: sudden jumping

9.3.3 Suppl. results – Gene expression analysis

Table 6: Results from microarray analysis of Braf^{cko} mice

Symbol	Name	Accession number	fold change	p-value
downregulated				
C330006P03Rik	RIKEN cDNA C330006P03 gene	AK049142	-3.04	<0.001
Cyp26b1	cytochrome P450, family 26, subfamily b, polypeptide 1	NM_175475.2	-2.76	<0.001
Dusp6	dual specificity phosphatase 6	NM_026268.1	-2.46	<0.001
Pla2g4e	phospholipase A2, group IVE	NM_177845	-2.46	0.023
Htr5b	5-hydroxytryptamine (serotonin) receptor 5B	NM_010483.2	-2.37	<0.001
Crhbp	corticotropin releasing hormone binding protein	NM_198408.1	-2.35	<0.001
Npy	neuropeptide Y	NM_023456.2	-2.27	<0.001
Egr4	early growth response 4	NM_020596.1	-2.24	0.010
Cort	cortistatin	NM_007745.2	-2.22	0.003
Egr1	early growth response 1	NM_007913.2	-2.13	0.008
Rasd1	RAS, dexamethasone-induced 1	NM_009026.1	-2.11	<0.001
Dusp6	dual specificity phosphatase 6	NM_026268.1	-2.09	0.001
Wnt9a	wingless-type MMTV integration site 9A	NM_139298	-2.05	0.039
Ky	kyphoscoliosis peptidase	NM_024291	-2.03	<0.001
Nptx2	neuronal pentraxin 2	NM_016789.2	-2.01	<0.001
Scg5	secretogranin V	NM_009162.2	-1.97	0.003
Dusp5	dual specificity phosphatase 5	NM_001085390	-1.90	0.021
Oxr1[#]	oxidation resistance 1	NM_130885.1	-1.90	<0.001
Hcrtr1	hypocretin (orexin) receptor 1	NM_198959.1	-1.88	<0.001
Zfpm2[#]	zinc finger protein, multitype 2	NM_011766.2	-1.87	<0.001
Dusp4	dual specificity phosphatase 4	NM_176933	-1.86	0.006
Etv5	ets variant gene 5	NM_023794	-1.85	<0.001
Mboat2	membrane bound O-acyltransferase domain containing 2	NM_026037.2	-1.83	0.023
Efcab6	EF-hand calcium binding domain 6	NM_029946.3	-1.82	<0.001
3110047M12Rik[#]	RIKEN cDNA 3110047M12 gene	AK014186	-1.81	<0.001
Sst	somatostatin	NM_009215.1	-1.80	<0.001
Cort	cortistatin	NM_007745.2	-1.73	0.018
Dusp4	dual specificity phosphatase 4	NM_176933.3	-1.72	0.002
Gpnmb	glycoprotein (transmembrane) nmb	NM_053110.2	-1.72	0.009
Oxr1[#]	oxidation resistance 1	NM_001130166	-1.72	<0.001
Thsd4	thrombospondin, type I, domain containing 4	NM_172444.1	-1.71	0.015
Per2	period homolog 2 (Drosophila)	NM_011066.1	-1.69	0.011
Klk8	kallikrein related-peptidase 8	NM_008940.1	-1.68	0.018
9630021O20Rik	RIKEN clone 9630021O20	AK079321	-1.67	0.040
Synj2	synaptojanin 2	AK038038	-1.66	0.022
C2cd4b	C2 calcium-dependent domain containing 4B	XM_134869.3	-1.66	0.048
Cacna2d1	calcium channel, voltage-dependent, alpha2/delta subunit 1	NM_009784.1	-1.66	0.002
Midn	midnolin	NM_021565.1	-1.64	0.001
Fjx1	four jointed box 1 (Drosophila)	NM_010218.1	-1.62	0.049
Csrnp1	cysteine-serine-rich nuclear protein 1	NM_153287.2	-1.61	0.003
Tnfrsf12a	tumor necrosis factor receptor superfamily, member 12a	NM_013749.1	-1.61	0.009
Zranb3	zinc finger, RAN-binding domain containing 3	NM_027678	-1.60	0.005
2900060B14Rik	RIKEN cDNA 2900060B14 gene	NR_027901	-1.60	0.001
Ryr1	ryanodine receptor 1, skeletal muscle	NM_009109	-1.59	0.006
Tac1	tachykinin 1	NM_009311.1	-1.58	0.006
Trib2	tribbles homolog 2 (Drosophila)	NM_144551.3	-1.58	0.017
LOC329646	hypothetical gene LOC329646	XM_287235.2	-1.56	0.012
Cd59a	CD59a antigen	NM_007652.2	-1.56	0.019
Igfbp4	insulin-like growth factor binding protein 4	NM_010517.2	-1.55	<0.001
Oxr1	oxidation resistance 1	NM_130885.1	-1.55	0.019
Igfbp4	insulin-like growth factor binding protein 4	NM_010517.2	-1.53	0.002
Zbtb7	zinc finger and BTB domain containing 7a	NM_010731.1	-1.53	0.011
Fibcd1	fibrinogen C domain containing 1	NM_178887.2	-1.53	0.034
Masp1	mannan-binding lectin serine peptidase 1	NM_008555	-1.52	0.006
Slc38a5	solute carrier family 38, member 5	NM_172479.1	-1.52	0.003
Camk1g	calcium/calmodulin-dependent protein kinase I gamma	NM_144817.1	-1.52	0.004
2900060N12Rik	RIKEN cDNA 2900060N12 gene	NM_183095.1	-1.51	0.019
Cck	cholecystokinin	NM_031161.1	-1.51	0.003
Car4	carbonic anhydrase 4	NM_007607.1	-1.51	0.034
Chd4	chromodomain helicase DNA binding protein 4	NM_145979.1	-1.51	0.023
Arhgef10	Rho guanine nucleotide exchange factor (GEF) 10	NM_172751.1	-1.50	0.023

Zap70	zeta-chain (TCR) associated protein kinase	NM_009539.2	-1.49	0.011
Zyx	zyxin	NM_011777.1	-1.48	0.008
Shc3	src homology 2 domain-containing transforming protein C3	NM_009167.1	-1.48	0.040
Gm336	predicted gene 336	XM_140607.1	-1.47	0.015
Etv1	ets variant gene 1	NM_007960.1	-1.46	0.012
Mtap2	microtubule-associated protein 2	AK079618	-1.46	0.037
Spred1	sprouty protein with EVH-1 domain 1, related sequence	NM_033524	-1.45	0.004
Calb1	calbindin 1	NM_009788	-1.45	0.023
Pde1a	phosphodiesterase 1A, calmodulin-dependent	NM_016744.1	-1.44	0.034
Tpd52l1	tumor protein D52-like 1	NM_009413.1	-1.44	0.009
Bcl6	B-cell leukemia/lymphoma 6	NM_009744.2	-1.44	0.023
Hs3st1	heparan sulfate (glucosamine) 3-O-sulfotransferase 1	NM_010474.1	-1.43	0.006
A630022G20Rik	RIKEN clone A630022G20	AK041581	-1.43	0.008
Ppapdc2	phosphatidic acid phosphatase type 2 domain containing 2	NM_028922	-1.42	0.010
Fam19a1	family with sequence similarity 19, member A1	NM_182808.1	-1.42	0.010
Pex5l	peroxisomal biogenesis factor 5-like	AK044552.1	-1.42	0.020
Asap2	ArfGAP with SH3 domain, ankyrin repeat and PH domain 2	NM_001004364	-1.42	0.014
A130009M03Rik	RIKEN clone A130009M03	AK037351	-1.42	0.033
Osbpl3	oxysterol binding protein-like 3	NM_027881.1	-1.41	0.025
Bdnf	brain-derived neurotrophic factor	AY057913	-1.41	0.036
Cdh10	cadherin 10	NM_009865	-1.41	0.009
Camk1g	calcium/calmodulin-dependent protein kinase I gamma	NM_144817	-1.40	0.019
Bach2	BTB and CNC homology 2	NM_007521.2	-1.40	0.011
Tpd52l1	tumor protein D52-like 1	NM_009413.1	-1.39	0.016
Etv1	ets variant gene 1	NM_007960.1	-1.38	0.033
Zfpm1	zinc finger protein, multitype 1	NM_009569.1	-1.38	0.019
A630020C08Rik	RIKEN clone A630020C08	AK041540	-1.37	0.022
Tuft1	tuftelin 1	NM_011656.1	-1.37	0.023
Ttc39b	tetratricopeptide repeat domain 39B	NM_025782.2	-1.37	0.048
Fam19a1	family with sequence similarity 19, member A1	NM_182808	-1.36	0.022
Stard8	START domain containing 8	NM_199018.1	-1.36	0.045
Zfp326	zinc finger protein 326	NM_018759.1	-1.36	0.034
Scn3b	sodium channel, voltage-gated, type III, beta	NM_153522.1	-1.36	0.019
Neto2	neuropilin (NRP) and tolloid (TLL)-like 2	NM_001081324	-1.35	0.019
C030027H14Rik	RIKEN cDNA C030027H14 gene	AK021106	-1.35	0.042
Rhobtb1	Rho-related BTB domain containing 1	XM_125637	-1.34	0.039
Sgk1	serum/glucocorticoid regulated kinase 1	NM_011361	-1.34	0.042
Gria3	glutamate receptor, ionotropic, AMPA3 (alpha 3)	NM_016886.1	-1.34	0.027
Itpr1	inositol 1,4,5-triphosphate receptor 1	NM_010585.2	-1.34	0.021
Sept6	septin 6	NM_019942.2	-1.34	0.019
Homer1	homer homolog 1 (Drosophila)	NM_147176.1	-1.34	0.049
Anks1b	ankyrin repeat and sterile alpha motif domain containing 1B	NM_181398.2	-1.33	0.049
Pramef8	PRAME family member 8	NM_172877.1	-1.33	0.016
Lmo2	LIM domain only 2	NM_008505.3	-1.32	0.049
Fam98c	family with sequence similarity 98, member C	NM_028661.1	-1.32	0.044
Bhlhe40	basic helix-loop-helix family, member e40	NM_011498.2	-1.31	0.017
Tns1	tensin 1	XM_355214.1	-1.31	0.027
Mast4	microtubule associated serine/threonine kinase family member 4	XM_283179.2	-1.31	0.042
Exph5	exophilin 5	NM_176846	-1.31	0.030
Elmo2	engulfment and cell motility 2, ced-12 homolog (C. elegans)	NM_080287.2	-1.31	0.042
Magi1	membrane associated guanylate kinase, WW and PDZ domain containing 1	AK031353	-1.31	0.042
Dcbld1	discoidin, CUB and LCCL domain containing 1	NM_025705	-1.31	0.034
Cds1	CDP-diacylglycerol synthase 1	NM_173370.3	-1.30	0.048
Tmem25	transmembrane protein 25	NM_027865.1	-1.30	0.038
Lypla2	lysophospholipase 2	NM_011942.1	-1.30	0.026
C030007I01Rik	RIKEN cDNA C030007I01 gene	AK021055	-1.30	0.036
9330154F10Rik	RIKEN cDNA 9330154F10 gene	AK020373	-1.30	0.034
D15Wsu169e	DNA segment, Chr 15, Wayne State University 169, expressed	NM_198420.1	-1.29	0.031
A830055N07Rik	RIKEN cDNA A830055N07 gene	AK034366	-1.29	0.048
Trappc6b	trafficking protein particle complex 6B	XM_127025.2	-1.28	0.049
Rlbp1	retinaldehyde binding protein 1	NM_020599.1	-1.28	0.048
Psmd8	proteasome (prosome, macropain) 26S subunit, non-ATPase, 8	NM_026545.1	-1.27	0.049
LOC383514	similar to Lix1 protein (LOC383514)	XM_357101.1	-1.27	0.048
	upregulated			
Oprl1	opioid receptor-like 1	NM_011012.2	1.26	0.048

Dgat2	diacylglycerol O-acyltransferase 2	NM_026384.2	1.27	0.049
Magi3	membrane associated guanylate kinase, WW and PDZ domain containing 3	NM_133853	1.29	0.040
Syn2	synapsin II	AK043584	1.30	0.047
D530007H06Rik	RIKEN clone D530007H06	AK052561	1.30	0.042
Mycl1	v-myc myelocytomatosis viral oncogene homolog 1, lung carcinoma derived (avian)	NM_008506.2	1.31	0.030
Pak4	p21 protein (Cdc42/Rac)-activated kinase 4	NM_027470.2	1.32	0.022
Cdca7l	cell division cycle associated 7 like	NM_146040.1	1.33	0.019
9530019H20Rik	RIKEN cDNA 9530019H20 gene	NM_177308.2	1.33	0.047
Mbd4	methyl-CpG binding domain protein 4	NM_010774.1	1.33	0.033
Ehd1	EH-domain containing 1	NM_010119.3	1.34	0.016
Cygb	cytoglobin	NM_030206.1	1.34	0.017
C630001G18Rik	RIKEN cDNA C630001G18 gene	AK048185	1.35	0.013
D230046F09Rik	RIKEN clone D230046F09	AK052106	1.38	0.022
Neurod2	neurogenic differentiation 2	NM_010895	1.39	0.023
Lypd1	Ly6/Plaur domain containing 1	NM_145100.2	1.39	0.035
Cxcl12	chemokine (C-X-C motif) ligand 12	NM_021704.1	1.40	0.049
Cacna1g	calcium channel, voltage-dependent, T type, alpha 1G subunit	NM_009783.1	1.41	0.026
Abcb10	ATP-binding cassette, sub-family B (MDR/TAP), member 10	NM_019552.1	1.41	0.034
Slc24a4	solute carrier family 24 (sodium/potassium/calcium exchanger), member 4	NM_172152	1.41	0.014
C030009J22Rik	RIKEN cDNA C030009J22 gene	AK044617	1.41	0.019
Ncrna00081	non-protein coding RNA 81	NR_027828	1.41	0.022
Igfbp5	insulin-like growth factor binding protein 5	NM_010518	1.43	0.016
2900084I15Rik	RIKEN cDNA 2900084I15 gene	AK013819	1.43	0.006
Prss12	protease, serine, 12 neurotrypsin (motopsin)	NM_008939.1	1.43	0.022
Smoc2	SPARC related modular calcium binding 2	NM_022315.1	1.48	0.019
Ntng2	netrin G2	NM_133500	1.48	0.002
Spata13	spermatogenesis associated 13	XM_147847.4	1.50	0.009
B930095M22Rik	RIKEN cDNA B930095M22 gene	AK047590	1.50	0.006
Lpl	lipoprotein lipase	NM_008509.1	1.50	0.041
Slc24a4	solute carrier family 24 (sodium/potassium/calcium exchanger), member 4	NM_172152.1	1.54	0.003
Gpc3	glypican 3	NM_016697.2	1.54	0.002
Fam101b	family with sequence similarity 101, member B	XM_203453	1.54	0.023
Prss12	protease, serine, 12 neurotrypsin (motopsin)	NM_008939.1	1.54	0.006
Nos1	nitric oxide synthase 1, neuronal	NM_008712	1.59	0.013
Gpr68	G protein-coupled receptor 68	NM_175493.2	1.63	0.047
Wnk4	WNK lysine deficient protein kinase 4	NM_175638	1.67	0.005
Rasl10a	RAS-like, family 10, member A	NM_145216.2	1.73	0.002
Cartpt	CART prepropeptide	NM_013732.3	1.75	<0.001
Rnf170	ring finger protein 170	NM_029965	1.81	<0.001
Ctdspl2	CTD small phosphatase like 2	NM_212450	1.99	0.026

#: transcripts also regulated in control experiment (CaMKIIα-Cre vs. wild-type)

Table 7: Results from conservation studies

Gene symbol	Binding site (BS)	BS in mouse promoter location*	# of species	Orthologs#	Conserved BS/Module	fold change	Promoter ID	Transcript ID
Sst	CREB1	−55 bp	10	Hs, Mm, Rn, Bt, Cfa, Pt, Mmu, Ssc, Mdm, Dr	2§	−1.80	GXP_82140	NM_009215
Nos1	CREB1	−21 bp	8	Hs, Mm, Rn, Bt, Cfa, Eca, Mmu, Ssc	2§	+1.59	GXP_435815	NM_008712
	CREB1	−31 bp	3	Mm, Rn, Cfa	2§			
	CREB1	−129 bp	7	Hs, Mm, Rn, Bt, Eca, Mmu, Ssc	1			
	CREB1	+129 bp	4	Mm, Cfa, Gga, Mdm	1			
Gria3	CREB1	−885 bp	8	Hs, Mm, Bt, Cfa, Eca, Pt, Mmu, Mdm	1	−1.34	GXP_229843	AK046158
Dusp4	CREB1	−459 bp	8	Hs, Mm, Rn, Cfa, Eca, Pt, Mmu, Dr	1	−1.86	GXP_270699	NM_176933
	ETS / SRF	+17 bp	7	Hs, Mm, Rn, Cfa, Eca, Pt, Mmu	1			
Egr1	CREB1	−145 to −76 bp	6	Hs, Mm, Bt, Cfa, Gga,	2	−2.13	GXP_423205	NM_007913
	ETS / SRF	−422 to −82 bp	4	Hs, Mm, Bt, Cfa, Dr	4			
D15Wsu169e	CREB1	−74 bp	6	Hs, Mm, Rn, Bt, Pt, Mmu	1	−1.29	GXP_295561	AK035479
	ETS / SRF	−96 bp	2	Mm, Rn	1			
Spata13	CREB1	+16 bp	6	Hs, Mm, Rn, Eca, Pt, Mmu	1	+1.50	GXP_2042397	based on mapping of ENSCAFT00000039298
Spata13	ETS / SRF	−510 bp	2	Mm, Rn	1	+1.50	GXP_1452970	ENSMUST00000022566
Zfp326	ETS	−113 bp	5	Hs, Mm, Bt, Pt, Mmu	1	−1.36	GXP_152119	AK017693
Bdnf (transcript variant 3)	CREB1	−45 bp	4	Hs, Mm, Eca, Pt	1	−1.41	GXP_892129	NM_001048141
Dusp5	CREB1	−238 bp	3	Mm, Bt, Ssc	1	−1.90	GXP_313715	NM_001085390
	ETS / SRF	−271 bp	4	Hs, Mm, Bt, Ssc	1			
Egr4	CREB1	−234 to −166 bp	3	Mm, Bt, Pt	2	−2.24	GXP_303501	NM_020596
Cacna1g	CREB1	−32 bp	3	Mm, Bt, Mmu	1	+1.41	GXP_1791781	AK296513
Cacna1g	ETS / SRF	−192 to	2	Mm, Rn	2x	+1.41	GXP_410659	AK142458

*: position relative to transcription start site (TSS)
#: Hs, Homo sapiens (human); Mm, Mus musculus (mouse); Rn, Rattus norvegicus (rat); Cfa, Canis lupus familiaris (dog); Bt, Bos taurus (cattle); Eca, Equus ferus caballus (horse); Pt, Pan troglodytes (chimpanzee); Mmu, Macaca mulatta (rhesus monkey); Ssc, Sus scrofa (wild boar); Gga, Gallus gallus (chicken); Mdm, Monodelphis domestica (short-tailed opossum); Dr, Danio rerio (zebrafish)
§: binding sites both on sense and antisense strand
x: sequences aligned in the region of the ETS binding site

9.3.4 Suppl. results – Summary of behavioural analysis

Table 8: Summary of behavioural tests in the modified hole board test

Modified hole board	Braf^{cko} (C. Hitz)	Braf^{icko} early induced	Braf^{icko} late induced	Braf$^{flox/flox}$ AAV-Cre dorsal	Braf$^{flox/flox}$ AAV-Cre ventral
line crossing (frequency)	-	↓ p=0.07	n.t.	-	-
line crossing (latency)	↑ *	-	n.t.	-	-
rearings box (frequency)	↓ ***	↓ **	n.t.	-	-
rearings box (latency)	↑ *	↑ ***	n.t.	↑ *	-
hole exploration (frequ.)	↓ p=0.07	↓ **	n.t.	-	-
hole exploration (latency)	-	-	n.t.	-	-
hole visit (frequency)	-	n.t.	n.t.	-	-
hole visit (latency)	-	n.t.	n.t.	-	-
board entry (frequency)	-	↓ **	n.t.	-	-
board entry (latency)	↓ *	↑ *	n.t.	-	-
board entry (total durat. %)	-	↓ **	n.t.	-	-
rearing board (frequency)	↓ ***	-	n.t.	-	-
rearing board (latency)	↑ **	-	n.t.	-	-
risk assessment (frequ.)	-	-	n.t.	-	-
risk assessment (latency)	-	-	n.t.	-	-
group contact (frequency)	↑ **	n.t.	n.t.	-	-
group contact (latency)	↑ p=0.07	n.t.	n.t.	-	-
group contact (total dur. %)	-	n.t.	n.t.	-	-
grooming (frequency)	↑ p=0.08	↓ *	n.t.	-	-
grooming (latency)	↓ *	↑ ***	n.t.	-	-
grooming (total durat. %)	↑ **	-	n.t.	-	-
defecation (frequency)	↑ *	-	n.t.	-	-
defecation (latency)	↓ **	-	n.t.	-	-
unfam. obj. explor. (frequ.)	↓ ***	↓ **	n.t.	-	↑ *
fam. obj. explor. (frequ.)	↓ ***	-	n.t.	-	-
unfam. obj. explor. (lat.)	↑ ***	↑ ***	n.t.	-	-
fam. obj. explor. (lat.)	↑ ***	↑ *	n.t.	-	-
unfam. obj. explor. (tot. %)	↓ ***	-	n.t.	-	↑ p=0.07
fam. obj. explor. (tot. %)	-	-	n.t.	-	-
object index	↓ ***	↓ *	n.t.	-	-
total distance moved	-	↓ *	n.t.	-	-
mean velocity	↑ ***	-	n.t.	-	-
maximum velocity	↑ ***	-	n.t.	-	-
turns (frequency)	↓ p=0.07	↓ **	n.t.	-	-
mean turn angle (degrees)	-	-	n.t.	-	-
angular velocity	↓ *	-	n.t.	-	-

Absolute meander	-	-	n.t.	-	-
board entry (max. duration)	-	-	n.t.	-	-
mean distance to wall	↓ ***	↓ **	n.t.	-	-
mean distance to board	↑ ***	↑ ***	n.t.	-	-

Table 9: Summary of behavioural tests in the elevated plus maze

Elevated plus maze	Braf^{cko} (C. Hitz)	Braf^{icko} early induced	Braf^{icko} late induced	Braf$^{flox/flox}$ AAV-Cre dorsal	Braf$^{flox/flox}$ AAV-Cre ventral
sex	m + f	m + f	m + f	m	m
weight	↓ ***	↑ ***	(f) ↑ ***	-	-
# entries to CA	↓ **	-	(f) ↓ **	-	-
# entries to OA	-	↓ **	-	-	-
# entries to ends of OA	-	-	-	-	-
latency to centre	↑ ***	(f) ↑ *	↑ ***	-	-
latency to OA	↑ ***	-	↑ ***	-	-
latency to ends of OA	-	-	-	-	-
total duration centre [%]	-	↑ **	-	-	-
total duration OA [%]	↑ ***	↑ **	-	-	-
distance moved total	-	↓ p=0.05	(f) ↓ ***	-	-
distance moved CA	↓ *	-	↓ *	-	-
distance moved OA	↑ *	↑ *	-	-	-
mean velocity CA	-	↑ ***	(f) ↓ **	-	-
mean velocity OA	-	-	↓ ***	-	↓ p=0.07
maximum velocity CA	-	↓ p=0.08	(f) ↓ **	↓ *	-
maximum velocity OA	-	-	↓ *	-	-

Table 10: Summary of behavioural tests in the light/dark box

Light/dark box	Braf^{cko} (C. Hitz)	Braf^{icko} early induced	Braf^{icko} late induced	Braf$^{flox/flox}$ AAV-Cre dorsal	Braf$^{flox/flox}$ AAV-Cre ventral
dark box (frequency)	-	n.t.	n.t.	-	-
dark box (total duration)	↓ ***	n.t.	n.t.	-	-
rearings DB (frequency)	↓ ***	n.t.	n.t.	↑ **	-
rearings DB (latency)	↑ ***	n.t.	n.t.	-	-
grooming DB (frequency)	-	n.t.	n.t.	-	-
grooming DB (total durat.)	-	n.t.	n.t.	-	-
tunnel (frequency)	-	n.t.	n.t.	-	-
tunnel (latency)	-	n.t.	n.t.	-	-
tunnel (total duration)	↓ p=0.07	n.t.	n.t.	-	-
rearings tunnel (frequency)	↓ **	n.t.	n.t.	-	-
rearings tunnel (latency)	↑ p=0.07	n.t.	n.t.	-	-

grooming tunnel (frequ.)	-	n.t.	n.t.	-	-
grooming tunnel (t. durat.)	-	n.t.	n.t.	-	-
light box (frequency)	-	n.t.	n.t.	-	-
light box (latency)	-	n.t.	n.t.	-	-
light box (total duration)	↑ ***	n.t.	n.t.	-	-
light box entries (%)	-	n.t.	n.t.	-	-
rearings LB (frequency)	-	n.t.	n.t.	-	-
rearings LB (latency)	↑ *	n.t.	n.t.	-	-
grooming LB (frequency)	-	n.t.	n.t.	-	-
grooming LB (total durat.)	-	n.t.	n.t.	-	-
total number rearings	↓ *	n.t.	n.t.	-	-
rearings DB (%)	-	n.t.	n.t.	↑ *	-
rearings tunnel (%)	-	n.t.	n.t.	↓ **	-
rearings LB (%)	-	n.t.	n.t.	-	-
first rearing (latency)	↑ ***	n.t.	n.t.	-	-
distance moved (total)	↑ *	n.t.	n.t.	-	-
velocity (mean)	-	n.t.	n.t.	-	-
velocity (maximum)	-	n.t.	n.t.	-	-

Table 11: Summary of behavioural tests in the forced swim test

Forced swim test	Braf^{cko} (C. Hitz)	Braf^{icko} early induced	Braf^{icko} late induced	Braf$^{flox/flox}$ AAV-Cre dorsal	Braf$^{flox/flox}$ AAV-Cre ventral
sex	m + f	m + f	m + f	m	m
swimming total	↓ ***	-	↓ ***	-	-
floating total	-	-	↑ ***	-	-
struggling total	(f) ↑ ***	-	-	-	-
swimming 1st min	↓ **	↓ p=0.08	-	-	-
swimming 2nd min	↓ ***	-	↓ **	-	-
swimming 3rd min	↓ ***	-	↓ ***	-	-
swimming 4th min	↓ *	-	↓ ***	-	-
swimming 5th min	↓ *	-	↓ *	-	-
swimming 6th min	-	-	↓ p=0.05	-	-
floating 1st min	↑ **	↑ **	↑ *	-	-
floating 2nd min	↑ p=0.07	-	↑ *	-	-
floating 3rd min	↑ p=0.08	-	↑ **	-	-
floating 4th min	-	-	↑ **	-	-
floating 5th min	↓ **	-	↑ *	-	-
floating 6th min	↓ *	-	-	-	-
struggling 1st min	-	-	-	-	-
struggling 2nd min	↑ *	-	-	-	-
struggling 3rd min	↑ p=0.05	-	-	-	-

struggling 4th min	↑ *	-	-	-	-
struggling 5th min	↑ ***	↑ *	-	-	-
struggling 6th min	↑ **	-	-	-	-

Table 12: Summary of behavioural tests in the accelerating rotarod

Accelerating rotarod	**Braf^{cko} (C. Hitz)**	**Braf^{icko} early induced**	**Braf^{icko} late induced**	**Braf$^{flox/flox}$ AAV-Cre dorsal**	**Braf$^{flox/flox}$ AAV-Cre ventral**
sex	m + f	m + f	m + f	m	m
weight	↓ ***	↑ ***	↑ ***	-	-
latency to fall, trial 1	↓ ***	-	↓ ***	↑ *	-
latency to fall, trial 2	↓ ***	↓ ***	↓ ***	-	-
latency to fall, trial 3	↓ ***	↓ ***	↓ ***	-	-
mean latency to fall	↓ ***	↓ ***	↓ ***	-	-
passive rotations	-	-	↓ ***	-	-

9.3.5   Suppl. results – Analysis of circadian rhythm

Actograms – Male controls
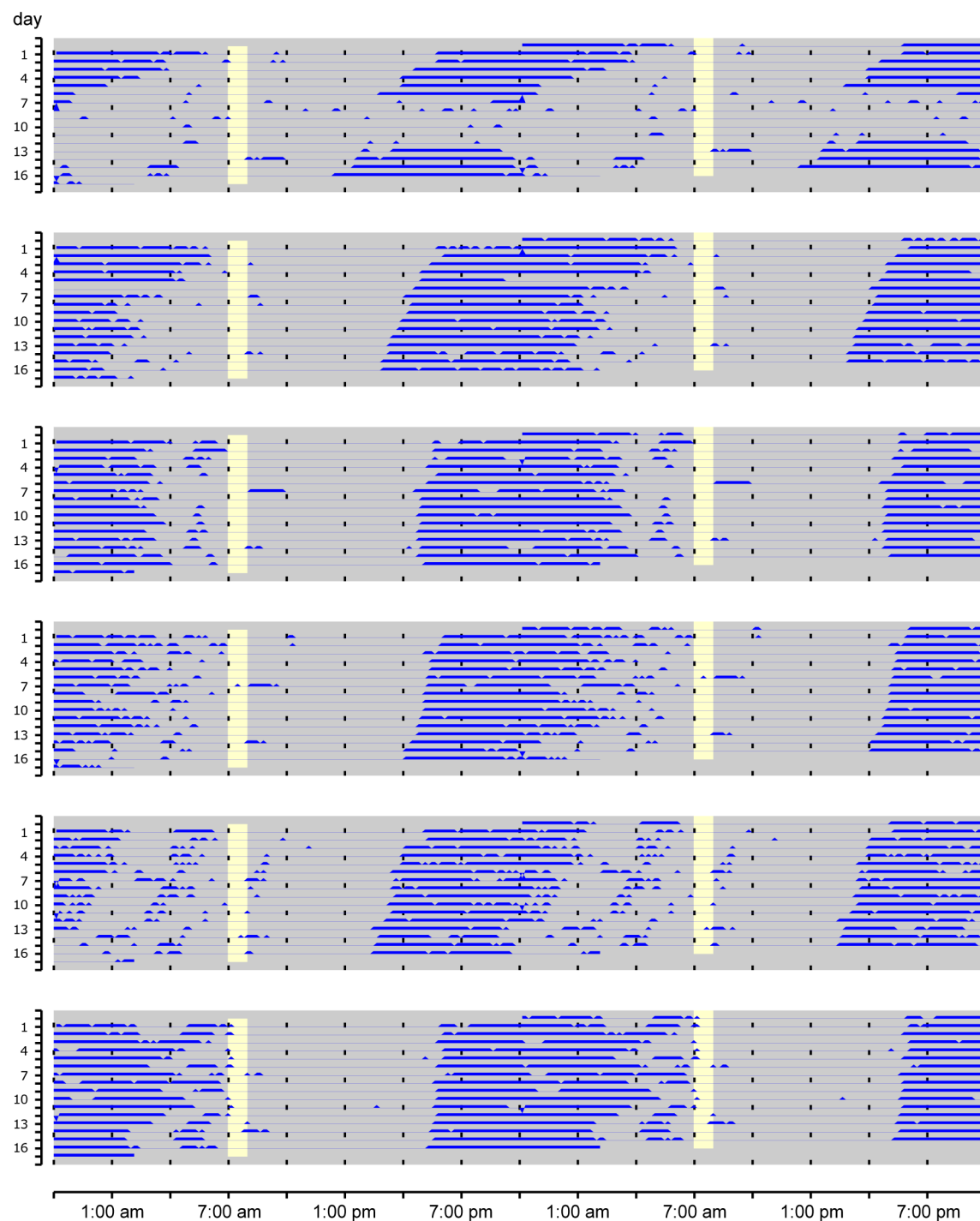
Fig. 36: Actograms of male Braf^cko controls

Actograms – Male mutants:
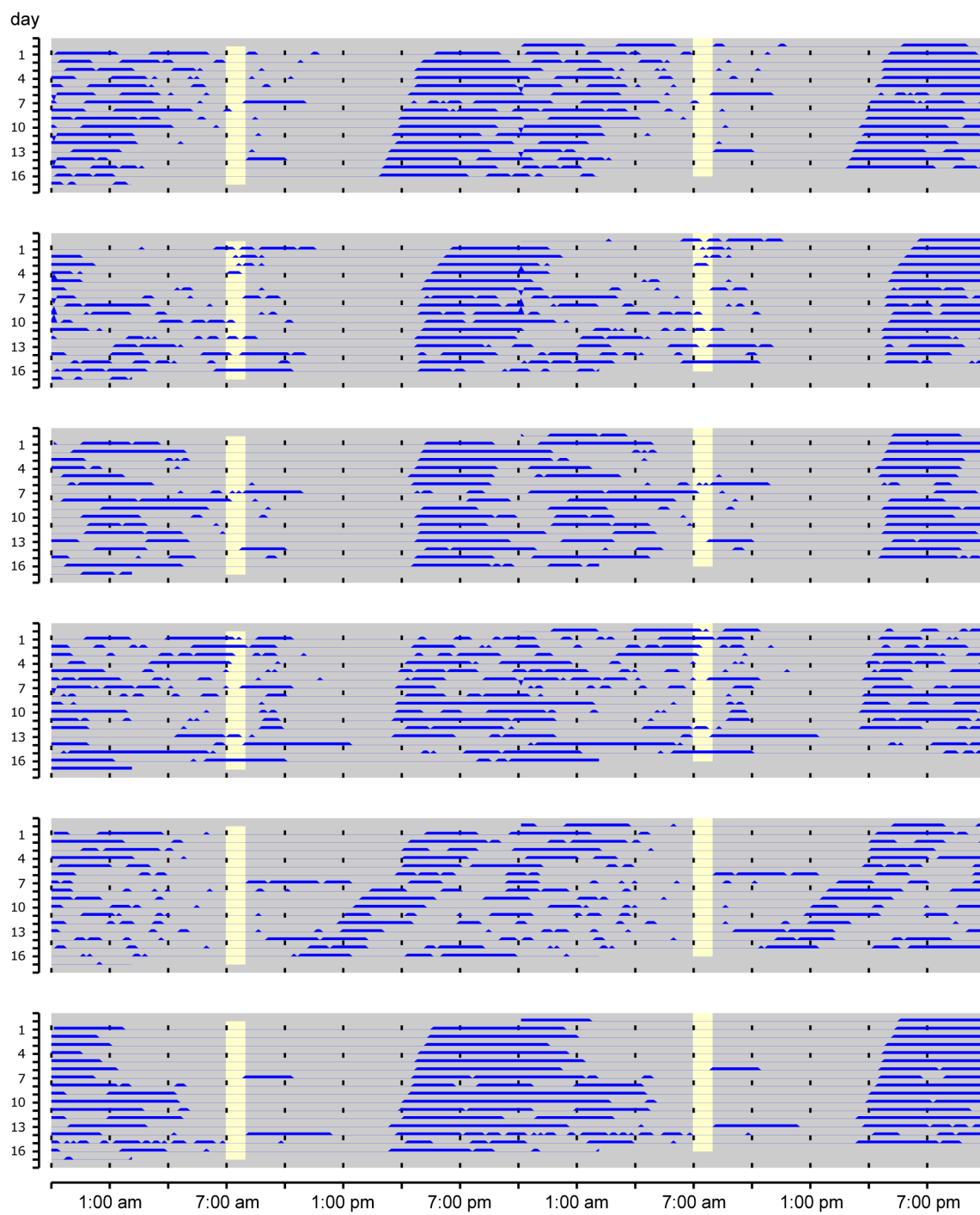
Fig. 37: Actograms of male Braf[cko] mutants

Actograms – Female controls:
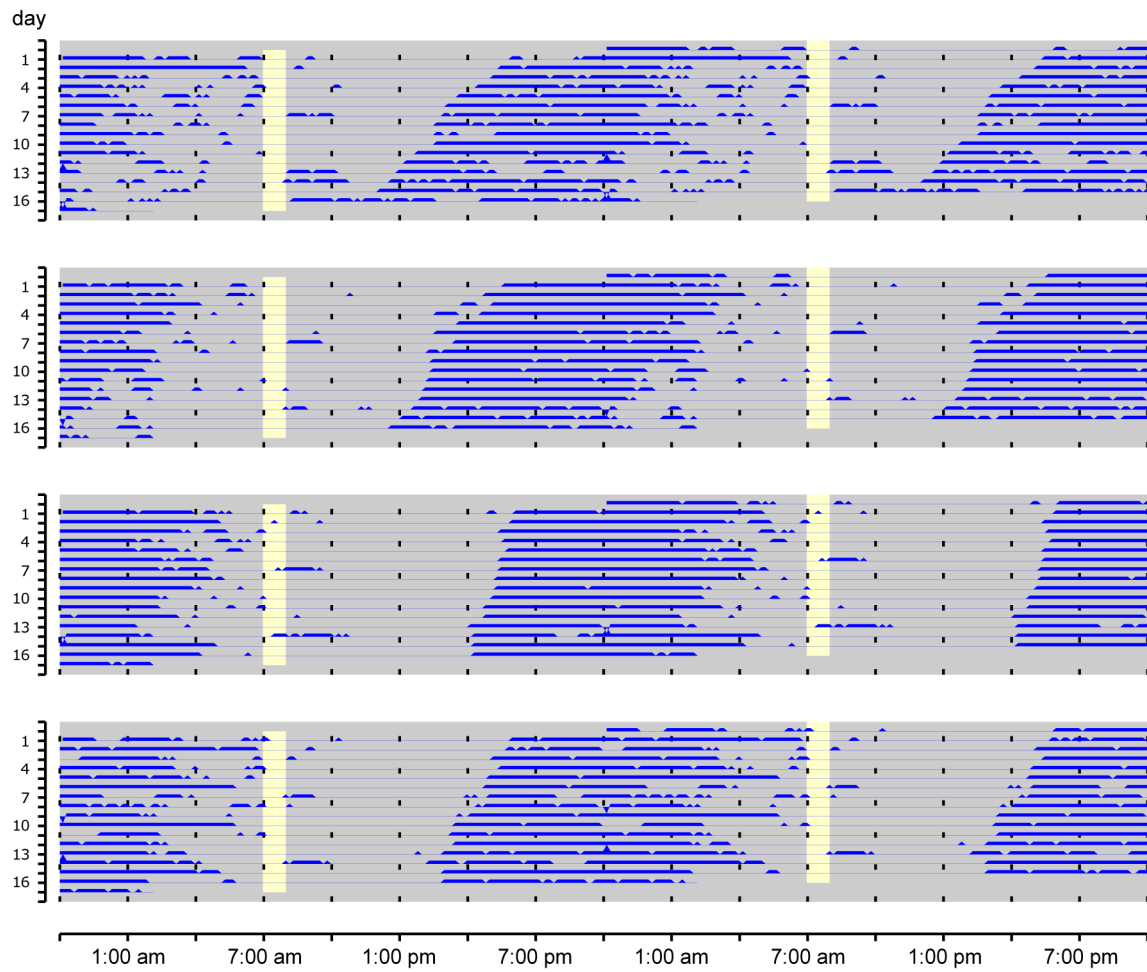
Fig. 38: Actograms of female Braf[cko] controls

Actograms – Female mutants:
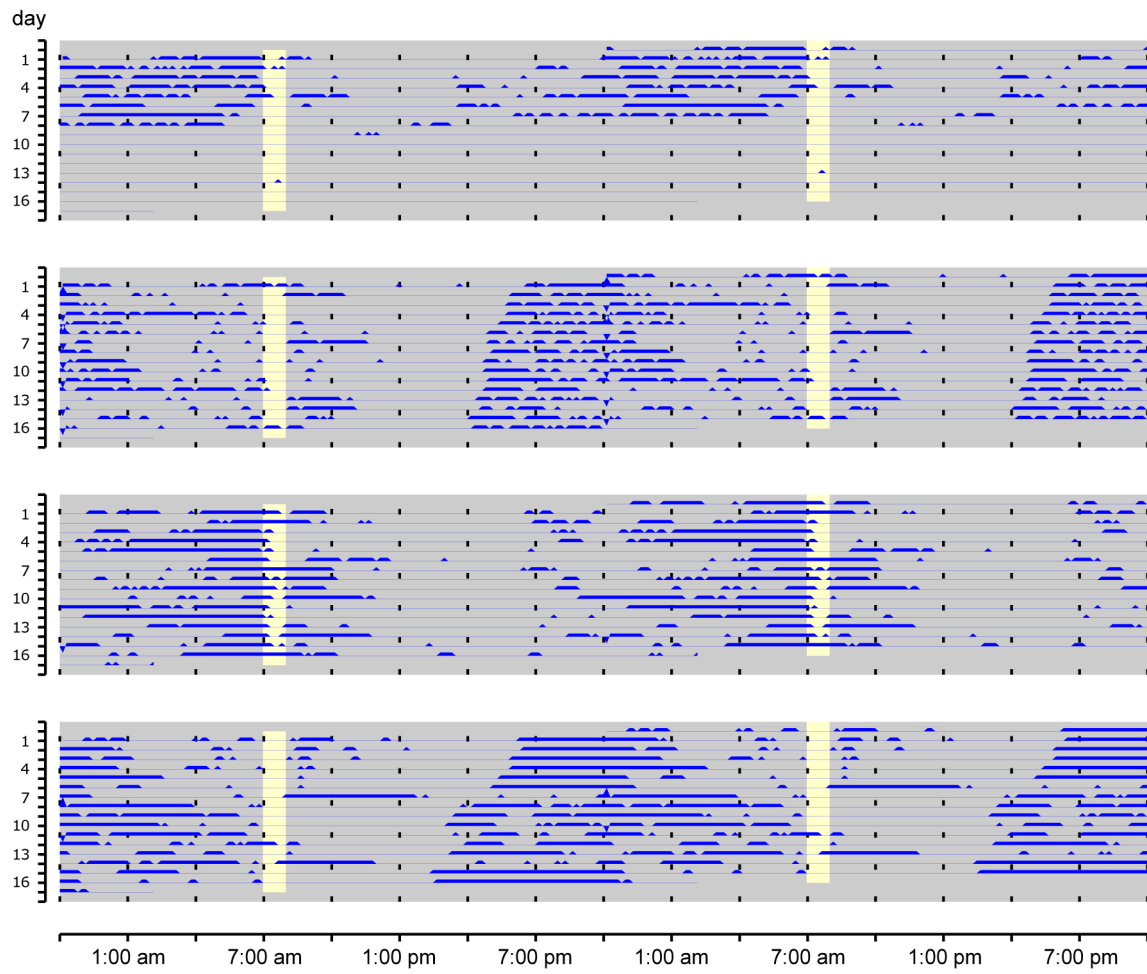
Fig. 39: Actograms of female Braf^{cko} mutants

Periodograms – Males:

Controls:
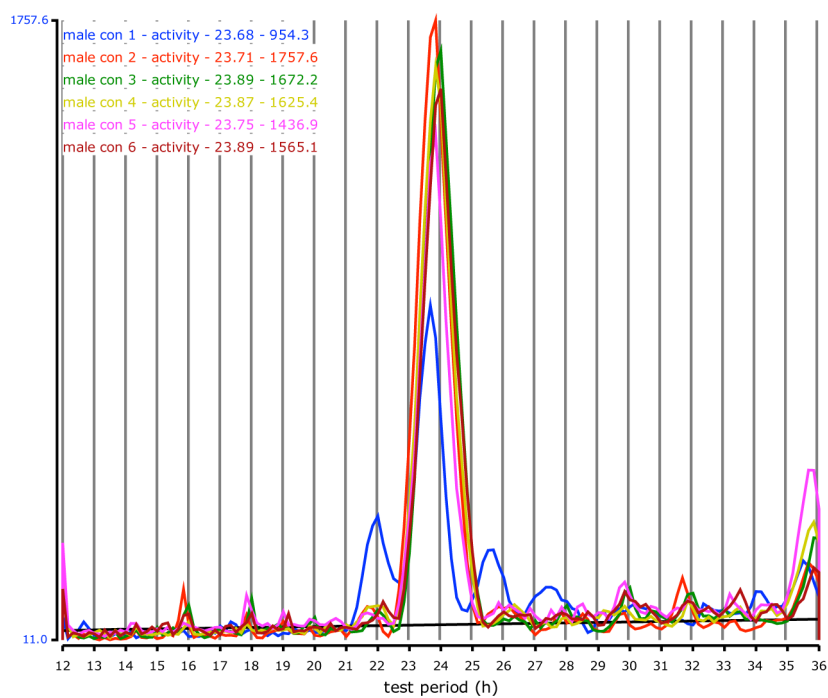
Mutants:
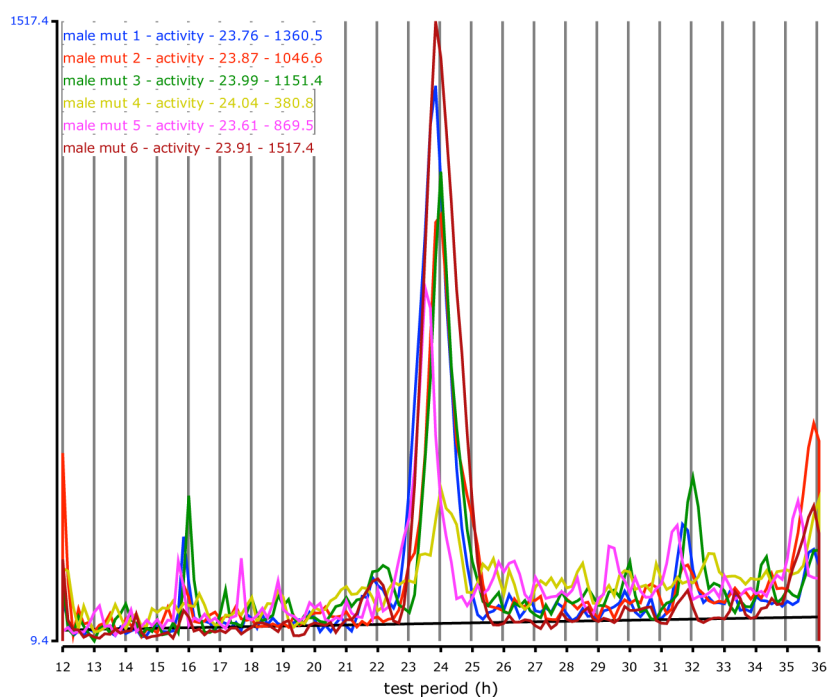
Fig. 40: Periodograms of male Braf^{cko} mice
Upper panel: controls
Lower panel: mutants

Periodograms – Females:

Controls:
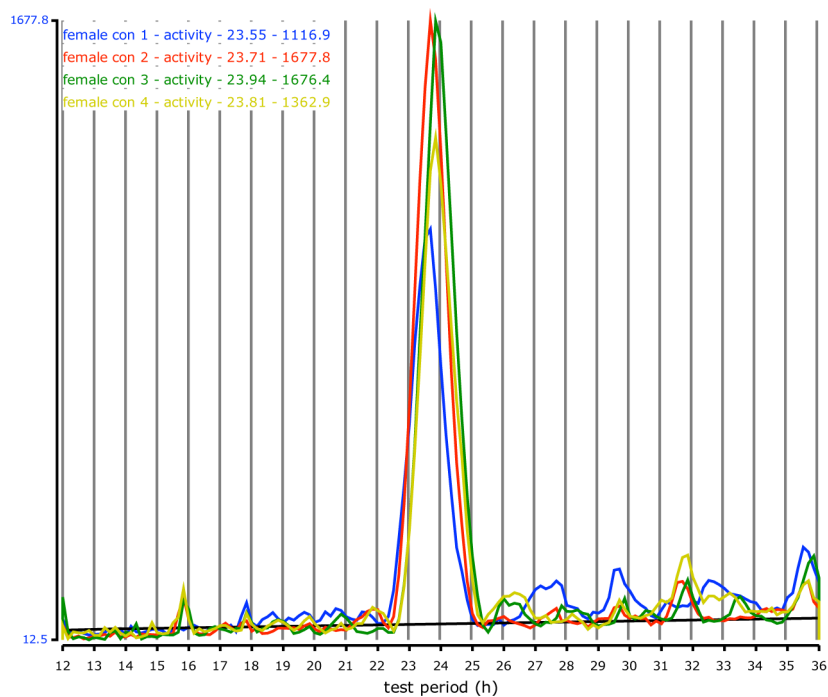
Mutants:
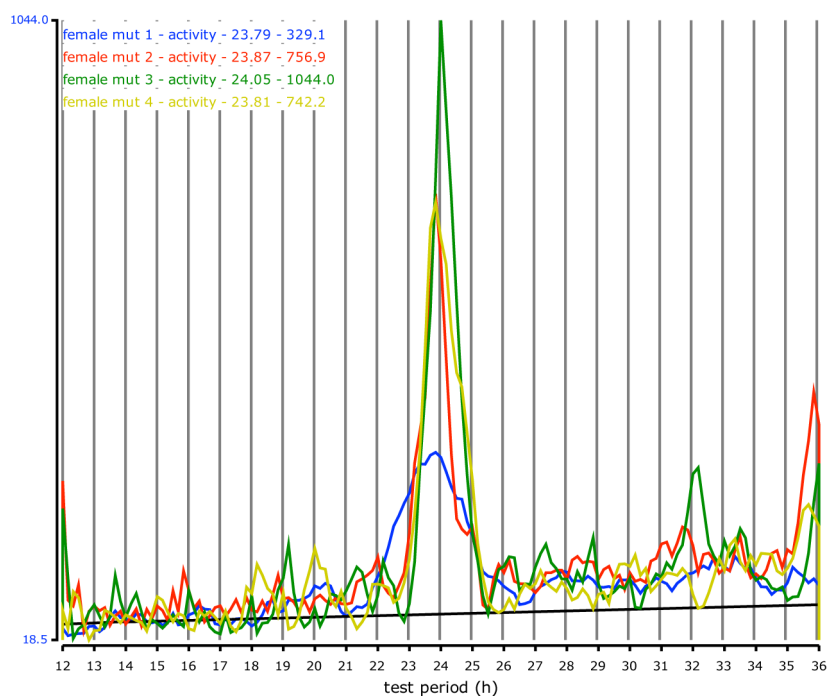
Fig. 41: Periodograms of female Braf^{cko} mice
Upper panel: controls
Lower panel: mutants

Composite graphs – Male controls:
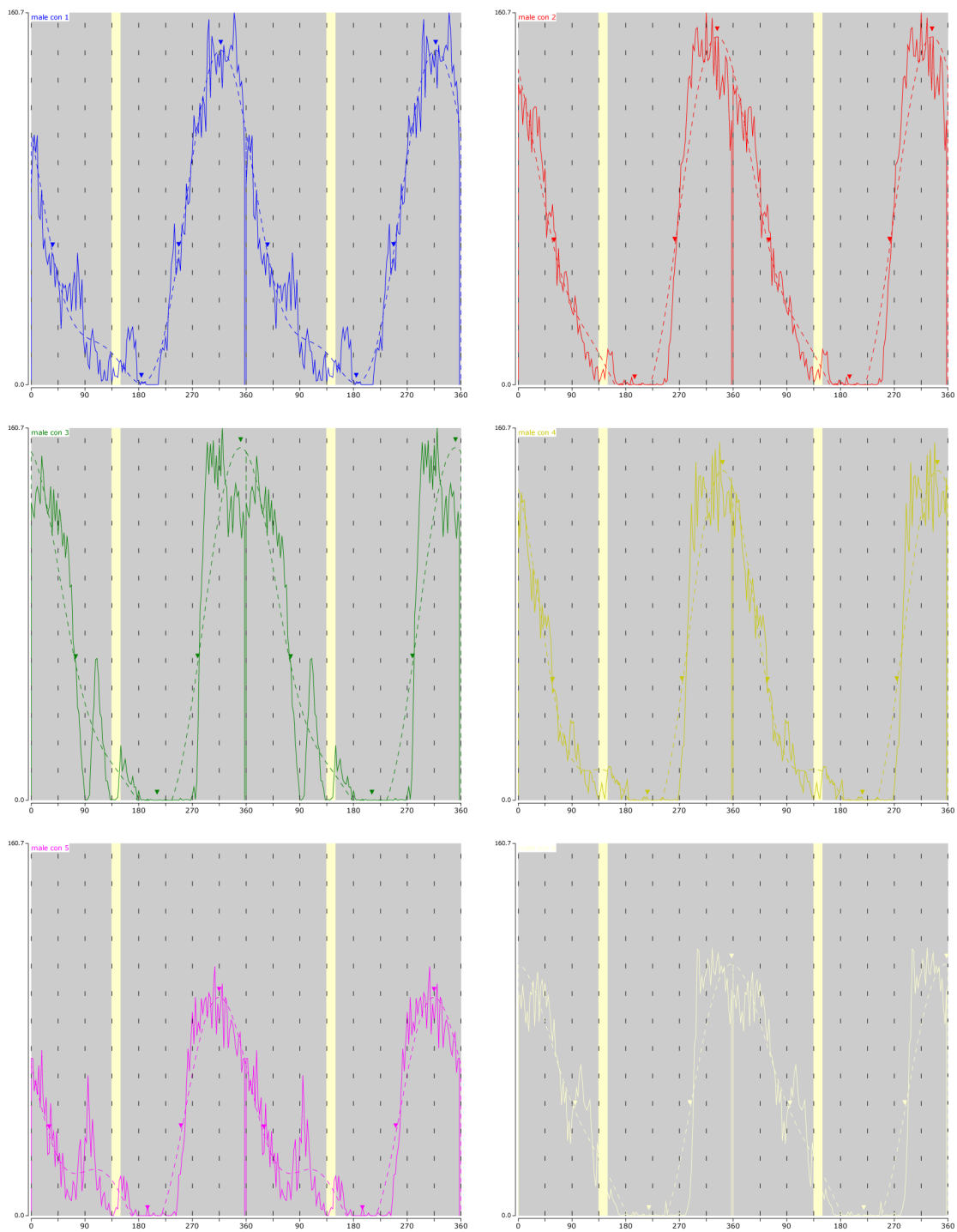
Fig. 42: Composite graphs of male Braf[cko] controls

Composite graphs – Male mutants:
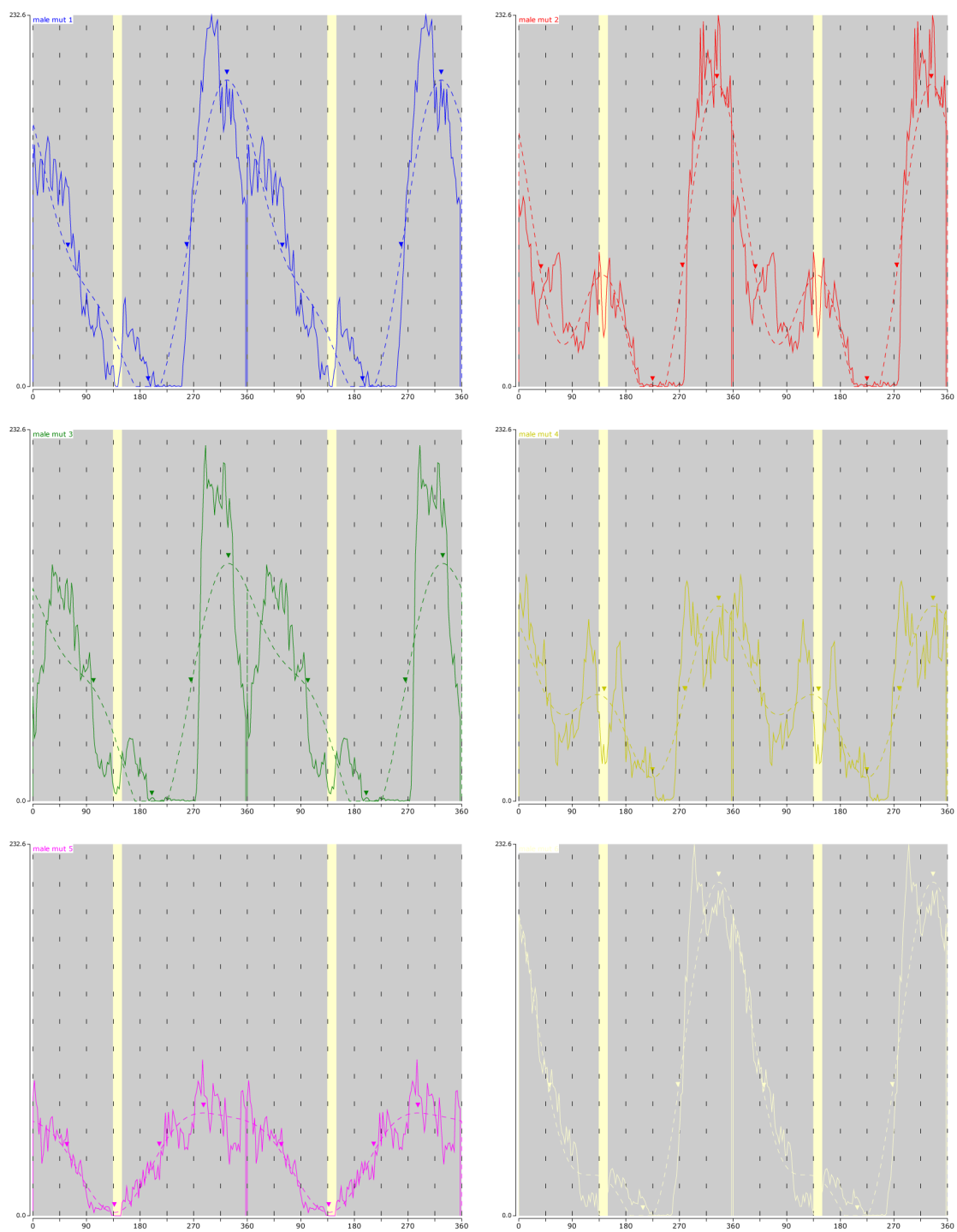
Fig. 43: Composite graphs of male Braf^{cko} mutants

Composite graphs – Female controls:
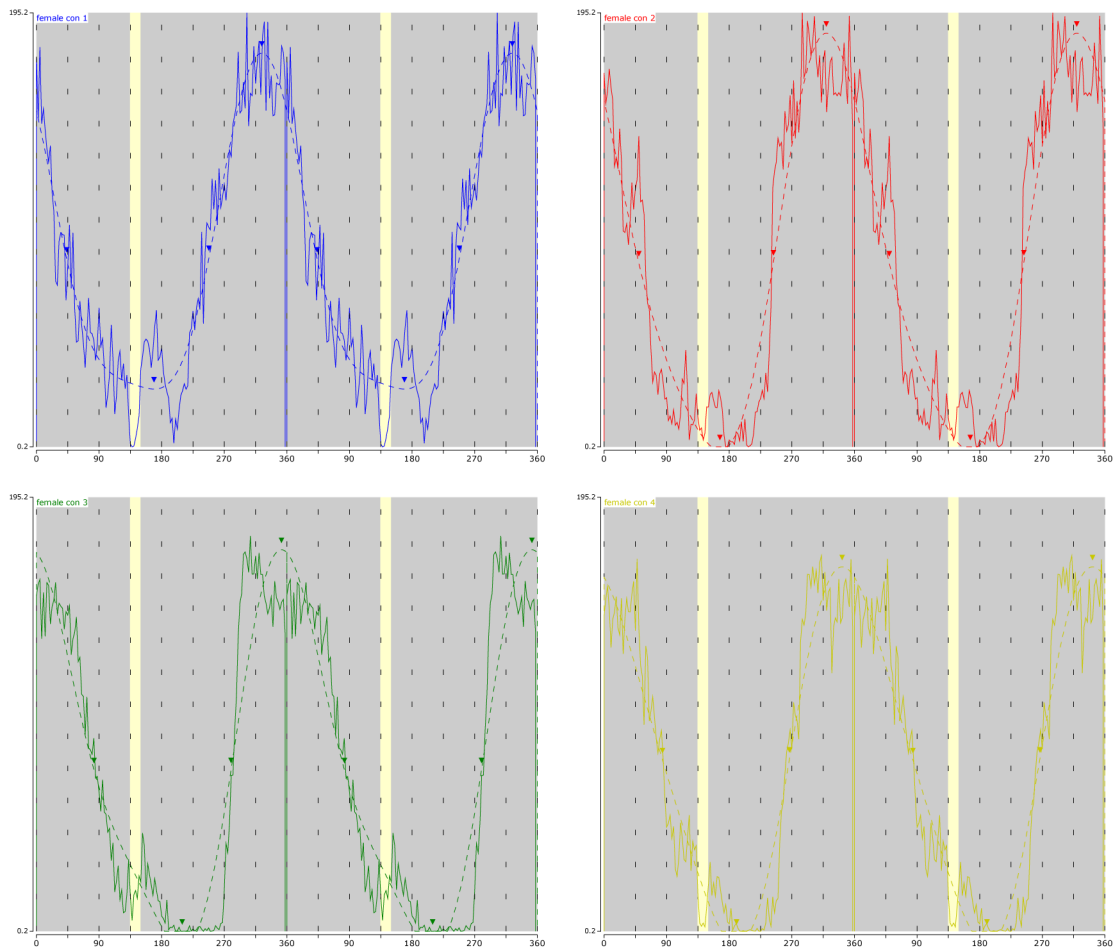
Fig. 44: Composite graphs of female Braf[cko] controls

Composite graphs – Female mutants:
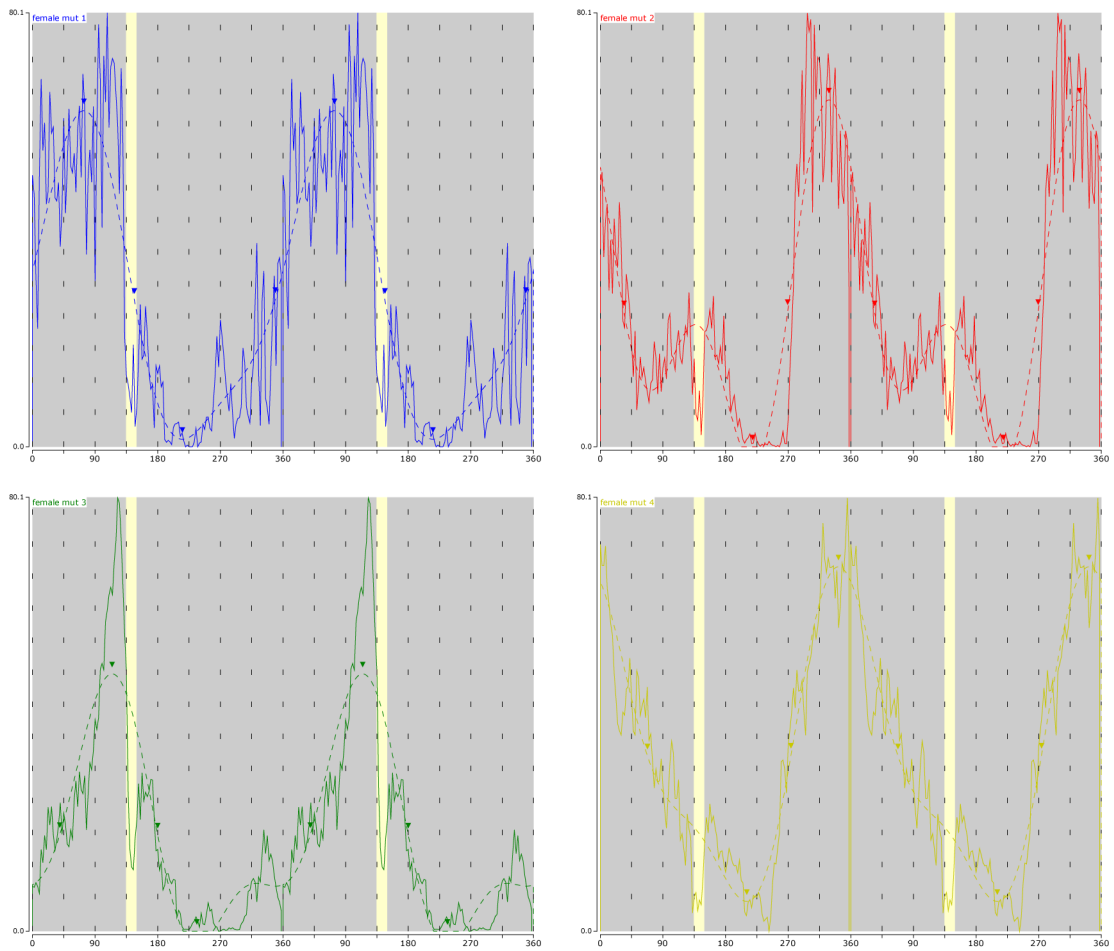
Fig. 45: Composite graphs of female Braf^{cko} mutants

Danksagung

Mein Dank richtet sich auch an alle Tierpflegerinnen und Tierpfleger des GMCs, des Oktogons und des C-Streifens, die sich immer ausgezeichnet um meine Mäuse gekümmert haben.

Ich danke außerdem allen anderen Mitarbeitern des IDG für die freundliche Arbeitsatmosphäre, die Hilfsbereitschaft und die stetige Unterstützung, die die Arbeit hier am Institut so angenehm gemacht haben.

Meiner Frau Tina, meiner Familie und meinen Freunden danke ich ganz herzlich für die Unterstützung, den Zuspruch und die Geduld, die sie mir während meines Studiums und meiner Promotion entgegengebracht haben. Vielen Dank, dass ihr mir geholfen habt, diesen Weg erfolgreich zu beschreiten.

Was wir wissen, ist ein Tropfen, was wir nicht wissen, ein Ozean.

Sir Isaac Newton (1643-1727)

Benedikt Wefers
Maria-Wagenhäuser-Str. 18
85570 Markt Schwaben

Telefon: 08121 / 88 30 800
Mobil: 0179 / 10 74 085
Benedikt@FamilieWefers.de

LEBENSLAUF

Persönliche Daten

geboren am 25.01.1981 in München
verheiratet

Berufliche Tätigkeit

11/2006 – 07/2010	**Helmholtz Zentrum München – Deutsches Forschungszentrum für Gesundheit und Umwelt**, Institut für Entwicklungsgenetik **Erstellung einer Dissertation mit dem Thema:** „The ERK/MAPK signalling in emotional behaviour – studies in *Braf* knockout and gain-of-function mutant mice"
01/2004 – 10/2010	**Sequiserve** (molekularbiologisches Labor, DNA-Sequenzierservice)

Ausbildung

10/2001 – 10/2006	**Ludwig-Maximilians-Universität München, Studium der Biologie** **Abschluss: Diplom, Gesamtnote: 1,3** mit Schwerpunkt Genetik und den Nebenfächern Zoologie, Pharmakologie/Toxikologie und Immunologie **Erstellung einer Diplomarbeit mit dem Thema:** „Etablierung und Optimierung von AAV-shRNA-Vektoren zur Untersuchung von Gen-Knockdown *in vitro* und *in vivo*" (extern am Helmholtz Zentrum München)
09/1991 – 07/2000	**Franz-Marc-Gymnasium Markt Schwaben** Abschluss: Allgemeine Hochschulreife, Note 2,1

Erste Berufserfahrungen

10/2000 – 08/2001	**Jugendherberge Regensburg** (Zivildienst)
07/2000 – 09/2000	**Rohde & Schwarz München**, Abteilung Logistik
09/1997 – 08/2000	**Müller-Brot GmbH**, Filiale Poing

Benedikt Wefers
Maria-Wagenhäuser-Str. 18
85570 Markt Schwaben

Telefon: 08121 / 88 30 800
Mobil: 0179 / 10 74 085
Benedikt@FamilieWefers.de

Weiterbildung	Helmholtz Zentrum München „Leitlinien der Zellkultur-praxis"
	Helmholtz Zentrum München „Clear Writing for Science Publications"
	Helmholtz Zentrum München „Protection and Commercialization of Intellectual Property"

Sprachkenntnisse	**Deutsch:**	Muttersprache
	Englisch:	präsentationssicher
	Französisch:	gute Kenntnisse

IT-Kenntnisse	**Microsoft Office:** sehr sicherer Umgang mit allen gängigen Tools
	Invitrogen VectorNTI 10: sicherer Umgang
	Ariadne Genomics Pathway Studio 6: sicherer Umgang
	Genomatix BiblioSphere: Grundkenntnisse
	Adobe Photoshop CS3 und Illustrator CS3: sicherer Umgang
	Endnote X2: sicherer Umgang
	SPSS Statistics 18: Grundkenntnisse

Ehrenämter

01/2000 – 12/2009	Jugendgruppenleiter im DPSG-Pfadfinderstamm „Windrose" Anzing/Poing
Seit 11/2006	Kassier im DPSG-Stamm „Windrose" Anzing/Poing
Seit 05/2010	1. Vorstand des Förderkreises e.V. des DPSG Stammes „Windrose" Anzing/Poing

Benedikt Wefers

Maria-Wagenhäuser-Str. 18

85570 Markt Schwaben

Telefon: 08121 / 88 30 800

Mobil: 0179 / 10 74 085

Benedikt@FamilieWefers.de

Publikationen

Di Benedetto B., Wefers B., Wurst W., Kühn R. (2009). Local knockdown of ERK2 in the adult mouse brain via adeno-associated virus-mediated RNA interference. Mol Biotechnol 41(3), 263-9.

Wefers B., Hitz C., Hölter S., Trümbach D., Hansen J., Weber P., Pütz B., Deussing J., Hrabé de Angelis M., Roenneberg T., Zheng F., Alzheimer C., Silva A., Wurst W., Kühn R. (2011). Altered emotional behavior of neuron-specific BRAF-deficient mice. J Neurosci, *submitted*

Patente

WO/2008/148522 A3: *Method to identify modulators of B-Raf protein kinase and their use for the treatment of anxiety and depression*. Angemeldet am 03.06.2008, veröffentlicht am 11.12.2008, Anmelder: Helmholtz Zentrum München – Deutsches Forschungszentrum für Gesundheit und Umwelt (GmbH), Erfinder: Hitz C., Hölter S., Kühn R., Wurst W., Wefers B.

Markt Schwaben, den 31.10.2010